TU Graz

Graz University of Technology

Michael Eßl BSc.

Design of a Distributor for Fibre Suspensions

MASTER'S THESIS

to achieve the university degree of

Diplom-Ingenieur

Master's degree program: Chemical and Process Engineering

submitted to

Graz University of Technology

Supervisor

Ass.Prof. Dipl.-Ing. Dr.techn. Stefan Radl

Institute of Process and Particle Engineering

Graz, September 6th 2017

Copyright © Michael Eßl, Graz University of Technology, Institute of Process and Particle Engineering.

OpenFOAM® is the name given to software produced by OpenCFD Ltd. and released free and open source to the general public.

See http://www.openfoam.com/legal/trademark-policy.php.

All rights reserved. No part of the material protected by this copyright notice may be reproduced or utilized in any form or by any means, electronically or mechanically, including photocopying, recording or by any information storage and retrieval system without written permission from the author.

EIDESSTATTLICHE ERKLÄRUNG

Ich erkläre an Eides statt, dass ich die vorliegende Arbeit selbstständig verfasst, andere als die angegebenen Quellen/Hilfsmittel nicht benutzt, und die den benutzten Quellen wörtlich und inhaltlich entnommenen Stellen als solche kenntlich gemacht habe. Das in TUGRAZonline hochgeladene Textdokument ist mit der vorliegenden Masterarbeit identisch.

AFFIDAVIT

I declare that I have authored this thesis independently, that I have not used other than the declared sources/resources, and that I have explicitly indicated all material which has been quoted either literally or by content form the sources used. The text document uploaded to TUGRAZonline is identical to the present master’s thesis.

Datum / Date	Unterschrift / Signature

Abstract

The purpose of the developed apparatus is to distribute cellulose pulp suspensions to a fractionation device. The key objective of the newly designed apparatus is to ensure an equal (i) mass flow and (ii) fibre length distribution at every outlet port, while minimizing energy demand, as well as maximizing reliability and ease of maintenance. Following a comparison of the state of the art in the field of paper making machinery, the approach of a forward distributor was chosen. The newly designed distributor consists of two mayor sections: A step diffusor, in which the pulp is deflocculated, followed by a splitter in which the suspension is distributed to the outlets. The key parameters affecting the distribution were investigated, which were the geometry, the fibre concentration and the mass flow rate. The results showed an acceptable mass flow distribution without an unwanted prefractionation of the suspension. The pressure drop, and hence the energy consumption, was in a satisfying range as well.

Detailed information about the flow conditions inside the distributor were obtained by means of single phase computational fluid dynamic simulations. The simulations were performed considering (i) two different turbulence models, as well as (ii) different grid sizes and (iii) flow resistances at the outlet ports. Unfortunately, the simulation results showed a poor agreement with experimental data.

Kurzfassung

Der in dieser Arbeit entwickelte Apparat dient der Aufteilung von Fasersuspensionen für einen Fraktionierapparat. Dabei muss, unter Berücksichtigung von minimalem Energieaufwand sowie größtmöglicher Zuverlässigkeit und Wartbarkeit, die (i) gleichmäßige Verteilung des Massenstromes auf die einzelnen Auslässe, sowie (ii) eine gleichbleibende Faserlängenverteilung an den Auslässen gewährleistet werden. Auf Basis einer Recherche des aktuellen Standes der Technik für Verteiler in Papiermaschinen wurde das Konzept eines progressiven Verteilers gewählt. Der neu entwickelte Verteiler besteht aus zwei Hauptbaugruppen. Als Erstes ein Stufendiffusor, welcher der Entflockung dient, gefolgt von einer Verteileinrichtung, welche den Massenstrom auf die Auslässe aufteilt. Der Einfluss der Geometrie, der Faserkonzentration und des Massenstromes auf die Aufteilung wurde untersucht. Die Ergebnisse zeigten eine zufriedenstellende Aufteilung ohne dabei eine ungewollte Fraktionierung der Suspension zu verursachen. Der auftretende Druckverlust und damit der Energieverbrauch für den Betrieb lag ebenfalls in einen zufriedenstellenden Bereich.

Um einen detaillierte Einblick in den Strömungszustand im Verteiler zu erhalten wurde eine numerische Strömungssimulation durchgeführt. Es wurde der Einfluss (i) zweier Turbulenzmodelle, sowie (ii) Modifikationen der Gitterauflösung und (iii) der Strömungswiderstände an den Auslässen auf die berechnete Strömung untersucht. Die Simulationsergebnisse zeigten im Vergleich mit den experimentellen Daten eine unakzeptable Abweichung.

Acknowledgement

At first I want to thank my parents who gave me the possibility to study at the TU Graz and provided all the necessary "boundary conditions".

As next in line I want to thank my supervisor Ass.Prof. Dipl.-Ing. Dr.techn. Stefan Radl who was very supportive and patient with me and helped whenever I needed him.

I also want to thank the *FLIPPR* consortium for enabling this thesis and their financial support.

Big thanks go also to all my friends and fellow students who I met here in Graz and who supported me with their knowledge and for all the fun we had together.

I also want to thank my colleges and the staff at the institute who made my stay at the office as pleasant as possible.

Special thanks go to the TUG Racing Team whose workshop I used for the manufacturing of the distributor. I also really enjoyed the time as an active team member in 2011/12 when we were building the race car and I still benefit from the skills I gained during that time. Especially my know-how in designing and construction as well as the skills in machining and of course laminating CFRP parts came in handy for the execution of this thesis.
"Thank U Guys and Keep On Racing!"

Table of Content

List of Figures

List of Tables

Abbreviations

avg.	average
CAD	Computer Aided Design
CFD	Computational Fluid Dynamics
DNS	Direct Numerical Simulation
DSLR	Digital Single Lens Reflex
FLIPPR	Future Lignin and Pulp Processing Research
HDF	Hydrodynamic Filtration Device
I/O	Input / Output
IPPT	Institute of Process and Particle Engineering at TU Graz
IPZ	Institute of Paper, Pulp and Fibre Technology at TU Graz
LES	Large Eddy Simulation
PISO	Pressure Implicit with Splitting of Operator
OpenFOAM®	Open Source Field Operation and Manipulation
RANS	Reynolds-Averaged Navier-Stokes equations
SGS	Sub Grid Scale
SIMPLE	Semi-Implicit Method for Pressure-Linked Equations

Nomenclature

Latin Symbols

A	cross section	m^2
Co	Courant number	-
d_h	hydraulic diameter of channel	m
g	gravitational acceleration	$m\ s^{-2}$
H	height of channel	m
k	turbulent kinetic energy, exponents for pressure drop model	$m^2\ s^{-2}$
m, n, r	exponents for pressure drop model	-
L	length of channel	m
$p,\ \Delta p$	pressure , pressure difference	$m^2\ s^{-2}$
Re	Reynolds number	-
S_{ij}	strain rate tensor	s^{-1}
u_i	velocity component	$m\ s^{-1}$
$\bar{u}$	average velocity	$m\ s^{-1}$
U	perimeter of a single wetted channel	m
$\lvert u \rvert$	velocity magnitude of one cell	$m\ s^{-1}$
$\dot{V}$	volumetric flow rate	$m^3\ s^{-1}$
w_i	mass fraction	kg_i / kg_{total}
W	width	m

Greek Symbols

∂t	time step size	s
∂x	cell size in the direction of the velocity	m
ρ	fluid density	$kg\ m^{-3}$
ν	kinematic viscosity	$m^2\ s^{-1}$
μ	dynamic viscosity	$kg\ m^{-1}\ s^{-1}$
σ	standard deviation	-
ς	pressure loss coefficient	-
τ_{ij}	stress tensor	$kg\ m^{-1}\ s^{-2}$

Indices

bin	bin for outlet mass flow measurement
dist	distributor
fib	fibre
i	outlet port index, index tensor notation
j	index tensor notation
k	index tensor notation
in	inlet
IP	inlet profile
lam	laminar
out	outlet
sus	pulp suspension
turb	turbulent

1. Introduction

1.1. Context

Operating under the *Horizon 2020* Program of the European Union, the *Bio-Based Industries Joint Undertaking* (BBI) makes investments of €3.7 billion from 2014-2020. The amount is raised in a Public-Private Partnership (PPP) between the EU and the Bio-based Industries Consortium (i.e. split approximately 1/4 to 3/4). The project aims to significantly reduce Europe's dependency on fossil-based products and help the EU meet climate change targets. Therefore the key is to develop new bio refining technologies [1].

This work was done in cooperation with the *Future Lignin and Pulp Processing Research* project (FLIPPR). FLIPPR is a research project of Austrian universities and a consortium of the pulp and paper industry, which follows the idea of a wood-based bio refinery concept. The main goal of the project is the comprehensive utilization of wood. One subgoal in that matter is the development of new products made from cellulose fibres as well as the improvement of existing ones [2].

The part of the FLIPPR project which is covered by the *Institute of Process and Particle Technology* (IPPT) is the fractionation of fibres and fines. Fines are defined as cellulose particles that pass through a 75 µm diameter circular hole. The fines have an influence on the sheet formation process, as well as a variety of mechanical and optical properties of the sheet [3]. Besides the influence on paper properties, new areas of application such as the utilization of fines as superabsorbent are investigated. In current industrial plants the fines are usually not separated from the fibre suspension, since the few currently available fines separation processes are often energy intensive (e.g., when using pressure screens).

In order to make the fractionation economically feasible it is desirable to design new reliable fractionation devices that operate at minimal energy consumption. At the moment of writing this thesis, such a new method is under development at IPPT which is called hydrodynamic fractionation device (HDF). The HDF device designed by König J. [4] consists of a straight channel with multiple junctions. By applying special flow conditions it is possible to separate the fines from the fibres and remove them at the junctions. The principal of this fractionation method showed viable results on a laboratory scale.

The next step towards industrial application is an increased throughput and separation efficiency. Since the geometry of the HDF is vital for the operation, it is not possible to simply scale the device. In order to increase the throughput, multiple HDF devices must operate in a parallel arrangement (i.e., a so-called "numbering up" strategy must be followed). This called for the need of a distributor which is designed during this thesis. The development of the full scale pilot scale plant is part of the FLIPPR² project [5], which at the time of writing this thesis has already started.

1.2. Content and Goals

The content of this work is the design, simulation, manufacturing and experimental validation of a distributor for cellulose fibre suspensions. First, a brief literature research is performed (see Chapter 2) where the state of art in distributing pulp suspensions is described. The two main parts of the thesis are the experimental section (see Chapter 3), and the simulation section (see Chapter 4). The conclusion and outlook form the final Chapter 5 and 6, which view the achievements of the present thesis in the context of current developments in the field.

The purpose of this thesis is to develop a distributor for pulp suspensions that facilitates the needs of the HDF device. The needs of the HDF device are translated into the following requirements for the distributor:

1. Equal mass flow at every outlet port
2. Equal fibre length distribution at every outlet port
3. Minimal energy consumption
4. Reliable and stable operation
5. Easy maintenance

These requirements lead to the research tasks for this thesis. At first the influence of the fibre concentration and the Reynolds number on the mass flow and fibre length distribution are investigated. The flocculation and deflocculation inside the distributor, as well as the blockage of outlet ports are observed. In order to minimize energy consumption the pressure drop should be as low as possible.

2. Theoretical Background

The first step of this work was the investigation of the current state of the art in the field of pulp suspension distributors. An already implemented application in the paper making industry which seemed similar to the requirements of the HDF is the headbox of a paper machine. The results of this literature research were a lot of patents [6]–[8] which mostly include the whole sheet formation process. By further investigation and personal talks [9] it was than confirmed that for this topic most of the knowledge is in the hand of the manufacturers of paper machines.

2.1. State of the Art

There are currently two different types of distributors used in paper machines. The first is a central pipe distributor Figure 2-1 which has an octopus-like shape. The distributor is integral with the pulsation damper which is used to cushion the pulsations from the pulp pump. The suspension enters the damper at the bottom where it is moderated by a damping plate. The distribution is carried out via many hoses which are mounted normal to the flow direction. To ensure equal pressure drop the hoses are of same length and diameter.

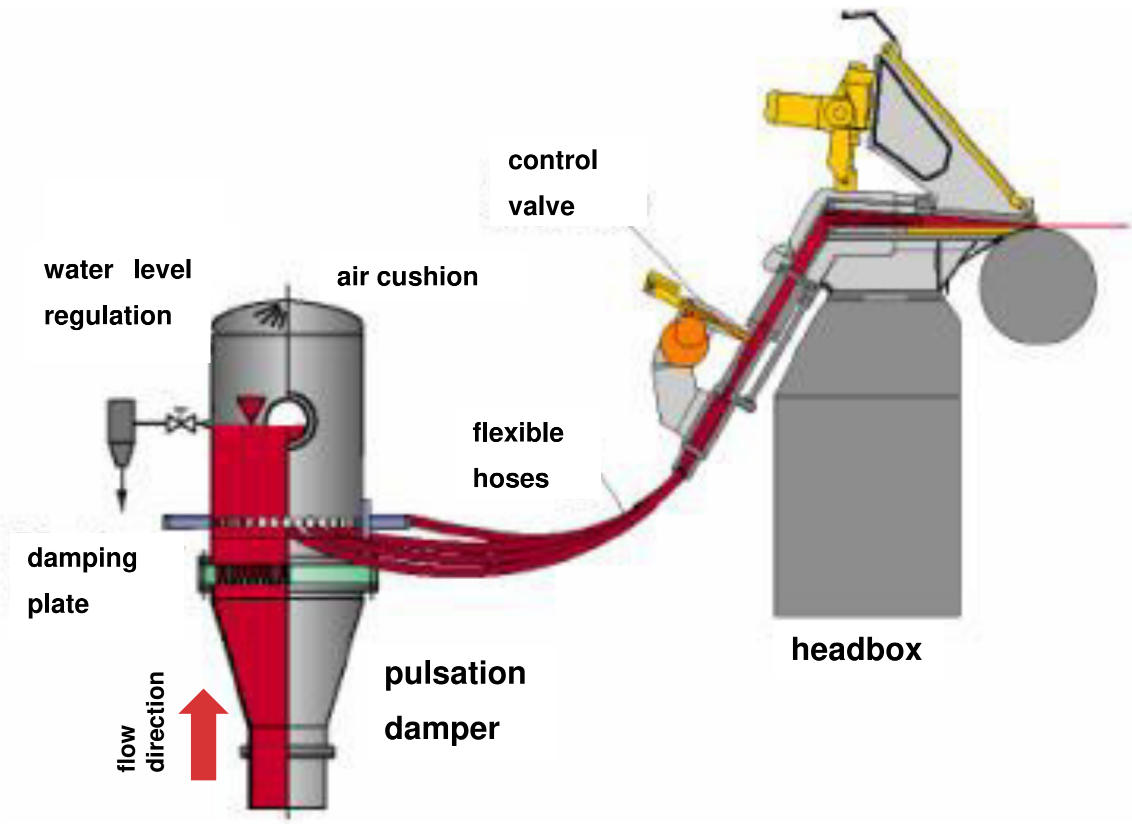

Figure 2-1: Central Pipe Distributor [10]

The second more common device is the cross flow distributor. In these devices the pulsation damper is a separate apparatus which is placed directly upstream. The main part of this distributor type is the conical main pipe. The pulp exits the main pipe via thousands of small channels which are placed normal to the flow direction in the main pipe. In order ensure equal mass flow distribution an equal pressure at every outlet must be maintained. The pitch of the conical main pipe is designed to achieve this condition. A CAD rendering is shown in Figure 2-2. To avoid ram pressure at the end of the conical pipe, and as a basic control mechanism a part of the pulp is recirculated.

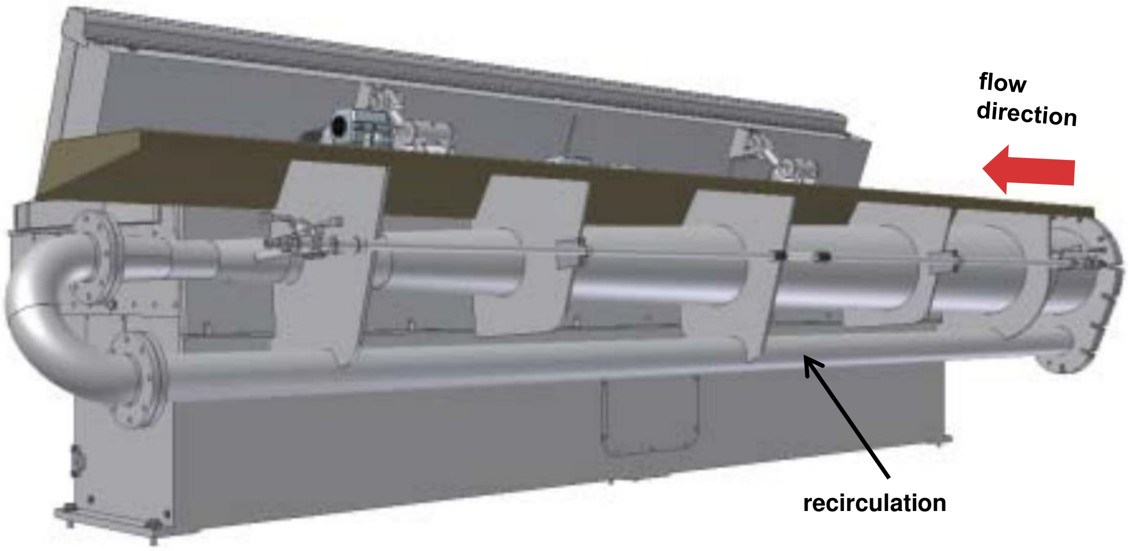

Figure 2-2: Cross Flow Distributor [10]

2.2. Step Diffusors and Turbulence Generators

In order to achieve an equal mass flow and fibre length distribution, it is vital to create a homogeneous suspension. To achieve this, the flocculation of fibres must be controlled and hence deflocculation methods are typically applied. The essential components of the floc-formation in dilute pulp suspension are according to Mason [11] the mechanical entanglement as a result of the independent rotation and translation of individual fibres. The flocs are classified in (i) transient flocs with low network strength which form and break up depending on the level of shear and the large rolling, and (ii) coherent flocs with large floc strength which form at low levels of shear. Another aspect of coherence besides mechanical forces caused by friction and entanglement are air bubbles trapped in the interstices of fibre networks which cause fibres to adhere from surface tension [12]. This has to be considered when performing the experiments to minimize the air transported with the pulp since it is not possible to de-aerate the suspension like it is done in paper machines.

For the rupture of flocs simple shear flow and pure extensional flow are considered. As Kao and Mason [13] found that in both cases dispersion occurred in a tensile mode. They showed that extensional flows having little (or no) rotation were superior to shear flows. This is also shown by simulations of Switzer and Klingenberg [14] who predict that an extensional flow disrupts flocs much faster with the drawback of remaining intact floc fragments. A simple shear flow acts more slowly, but it breaks up flocs completely. In industrial application there are two approaches. One is by rotating slotted drums, and the other is an extensional flow realised via step diffusors. A deflocculation by simple shear flow is not applied since it is difficult to generate at large scales.

In this work the method of expansion flow is chosen because of its simple and robust design and to avoid any sealing and additional energy consumption of rotating devices. The influence of the geometry of turbulence generator was investigated by Youn and Lee [15]. The compared geometries were a sudden expansion tube, an L-shaped conduit, and a saw blade shaped conduit as shown in Figure 2-3a. It was suggested that saw blade conduits would be suitable for head boxes requiring sufficient turbulence and flow stability at relatively short span. Since the cross section of the planed distributor has to expand this option is not realizable. However, it could be of interest for the HDF to de- and reflocculate the suspension between junctions to free fines who are trapped in the flocs.

a)

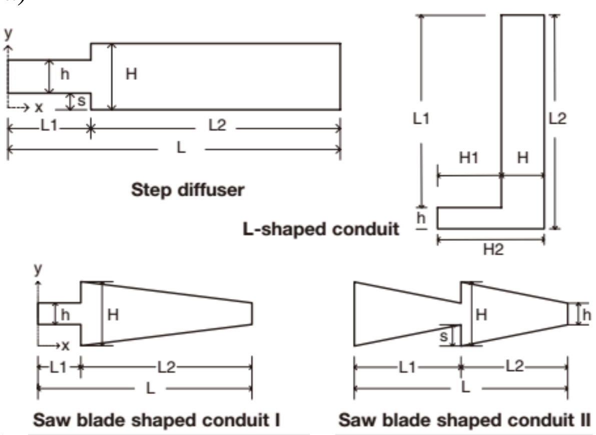

b)

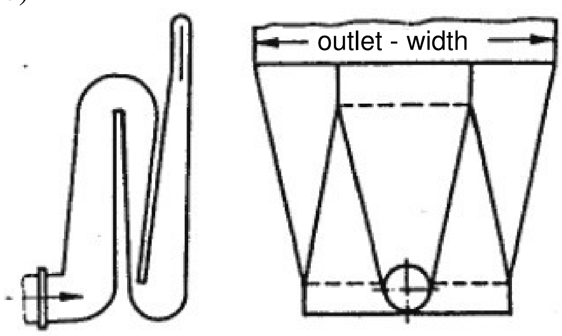

Figure 2-3: Tested geometries for turbulence generators from Youn and Lee [15] **a) The important parameter for the reattachment length is the expansion ratio** h/H **b) Concept of a pleated diffusor in order to save building space in pilot scale plant** [10]**.**

The chosen geometry is the sudden expansion tube. In order to avoid reflocculation the distributor consists of three consecutive single sided backward facing steps. The important parameter for the reattachment length is the expansion ratio. According to Youn and Lee the normalised reattachment length (L_r / S) after sudden expansion was within 6 to 8 [15]. This is also shown in numerical simulations of a single sided backward facing step carried out by Anwar-ul-Haque et al [16]. According to Youn and Lee [15] the Reynolds number had little effect on the normalised reattachment length which is an advantage for the planed application.

Another type of diffusor that was looked in was the pleated diffusor which was used in early headboxes of paper machines, see Figure 2-3b. The advantage of this type is a reduced requirement for building space, which is a crucial parameter for later pilot scale plants. Despite this advantage of a pleated diffusor this concept was discarded due to the complex geometry which prevents an easy adjustment, make optical access impossible, and would require expensive manufacturing techniques.

3. Experiments

One of the two main parts of the thesis was the design, the manufacturing and the operation of the distributor. This section describes the preparation and properties of the pulp (Chapter 3.1) followed by the experimental setup (Chapter 3.2), the experimental plan (Chapter 3.3) and the results (Chapter 3.4).

3.1. Fibres and Pulp

The prior treatment of the fibres, as well as the origin of the fibres (i.e., the tree species) has a big influence on their flow behaviour if suspended in water. In this work all experiments are carried out with the same pulp mixture from the same batch. This has been done to ensure a 1:1 comparability of the result. Specifically, the fibres used in the experiments are described as a soft wood chemical pulp (*Sulphite Ecocell*, 90% spruce, 10% beech, batch: 25-Nov-2016) which were provided by our industrial partner *SAPPI® (Gratkorn mill)*. Unfortunately, there was no detailed datasheet of the pulp treatment available, but according to verbal information [17] the fibres are unrefined.

3.1.1. Disintegration and Pre-Treatment

The fibres were provided in dry sheets with a grammage of ~1100 g / m². Therefore a pre-treatment by means of disintegration was necessary. The disintegration was carried out according to the procedure described in ISO 5263-1. This includes soaking the dry fibres in water for 4 hours and disintegration with the following parameters: 30 g of dry fibres, 2 litres of water and 30.000 revolutions. For every set of experiments needed a batch of 12 kg of pulp suspension. The disintegrated pulp was further diluted with deionized water to reach the desired quantity and fibre concentration.

3.1.2. Suspension Consistency

For consistency measurement the certified devices of our partner institute IPZ (Institute for Paper, Pulp and Fibre Technology) were used. The consistency of the pulp suspension is determined via a thermogravimetric analysis. First a circular paper filter (*Macherey Nagel*, type MN 615, 4 – 12 µm avg. retention capacity) is dried in an oven at 100 °C for 15 minutes. Following that, the filter and the suspension sample are weighed. Next the filter is placed in a Büchner Funnel and the suspension is dewatered by applying vacuum.

After dewatering the filter is folded in half to prevent any loss of fibres and dried in a vacuum drier for 10 minutes. Finally the filter with the fibres in it is weighed. The consistency was calculated with Equation 1.

$$C_{fibre} = \frac{m_{fibre+filter} - m_{filter}}{m_{suspension}}$$ **Equation 1**

3.1.3. Fibre Length Distribution

For a predictable and stable separation in the HDF, i.e., the device which follows downstream of the distributor, it is important to ensure a homogeneous distribution of the pulp suspension to all HDF inlets. In the context of this work the term "homogeneous" refers to (i) equal mass flow rate, (ii) equal fibre concentration as well as (iii) equal fibre length distribution in all outlets of the distributor.

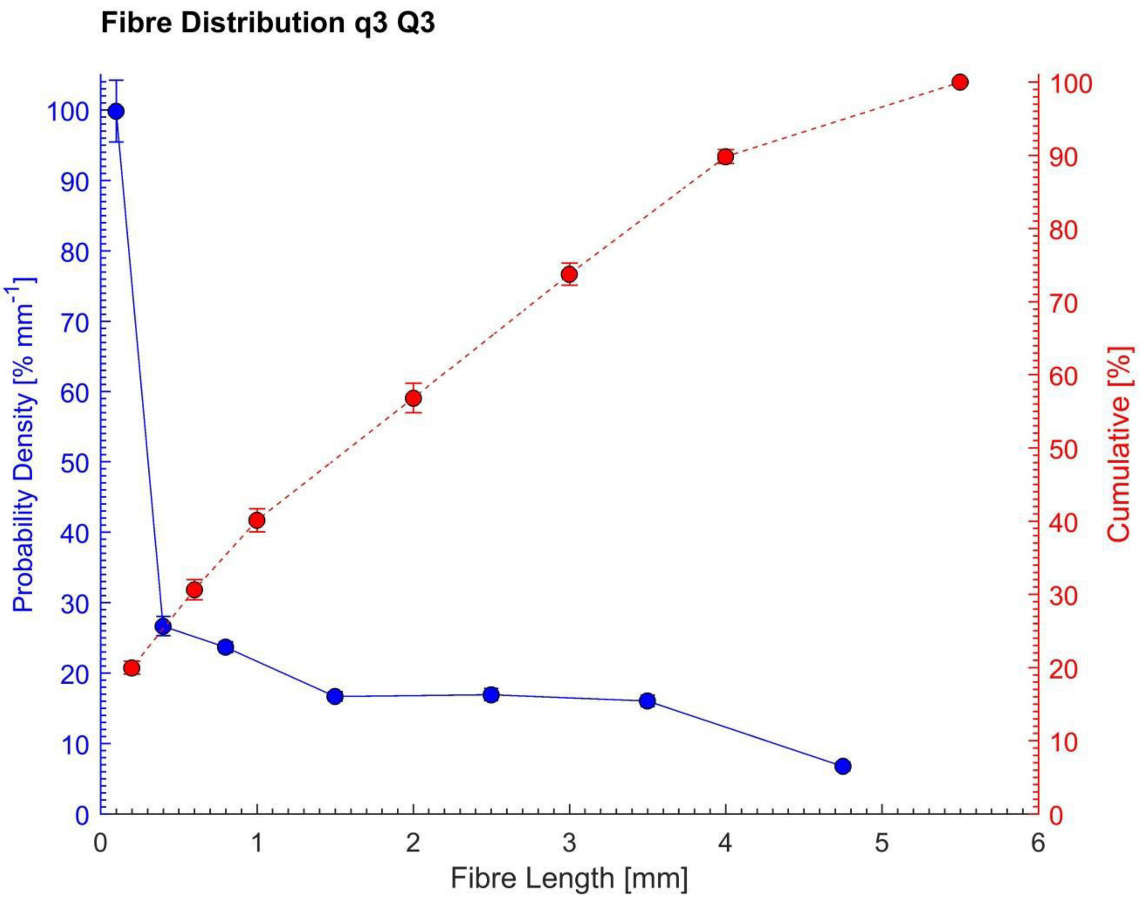

Figure 3-1: Cumulative (Q_3) and density-based (q_3) volume-weighted distribution of the raw fibre pulp suspension. The upper class limits (x_o) in millimetres are $[0; 0.2; 0.6; 1; 2; 3; 4; 5.5]$.

Unfortunately, it was not possible to draw samples from the inlet of the distributor during the experiments. Thus the fibre length distribution of the dry sheet raw material was measured. In order to compare the fibre length distribution at the inlet and the outlet the following procedure was applied. Nine samples from different locations on the sheet material were drawn and disintegrated as described in Chapter 3.1.1. The samples of the outlets were drawn during the experiments as described in Chapter 3.2.1. The measurement of the fibre length distribution was carried out with a hydrodynamic - optical device (*Lorentzen & Wettre FIBER TESTER PLUS*) [18] which was provided by our partners from IPZ. The device automatically dilutes the samples and pumps it through a small gap between two plates. Between the latter the fibres are aligned and images are taken using a digital camera. A built in routine extracts different properties of every particle from the recorded images. As a rule of thumb, every sample should be analysed until approximately 8000 fibres with a length $L_{fib} > 0.2mm$ are detected. During our tests on average 180.000 particles and 13.000 fibres per sample were analysed. The detailed settings and results of the measurements are summarized in Appendix E. For further data processing and calculation of the volume-weighted distribution the fibres are assumed as ideal cylinders. The distribution is classified by fibre length where the upper class limits (x_o) in millimetres are $\left[0; 0.2; 0.6; 1; 2; 3; 4; 5.5\right]$. The resulting distribution shown in Figure 3-1 is the average from the nine drawn samples.

The measured fines content of $w_{fines} = 20\%$ is untypically high for a chemical pulp suspension. This could be due to the optical measurement method and the assumptions made for calculating the distribution. To get exact measurements of the total fines content, an additional test with a Britt Dynamic Drainage Jar could be performed. However, since the total fines content was of lower priority for the present work, this aspect was not further investigated.

3.2. Experimental Setup

In order to keep the volume of pulp suspension low, the pulp was circulated in a closed loop. This is reflected by the experimental setup, for which an overview including the used devices is shown in Figure 3-2. First, the preconditioned suspension is poured into the collection vessel. This vessel is stirred via a magnetic stirrer at the bottom to prevent deposition of fibres. Following that, the suspension is pumped into the storage tank with a peristaltic pump. The Storage tank is also stirred, however, as opposed to the collection vessel with a blade stirrer from the top. The suspension than exits the storage tank at the bottom via a flexible rubber hose, enters the distributor at the inlet manifold and flows through the distributor. The five outlet streams are finally merged in the collection vessel. For optical analysis of the fibre motion and network formation, a DSLR- and high speed camera mounted on a movable stand are used.

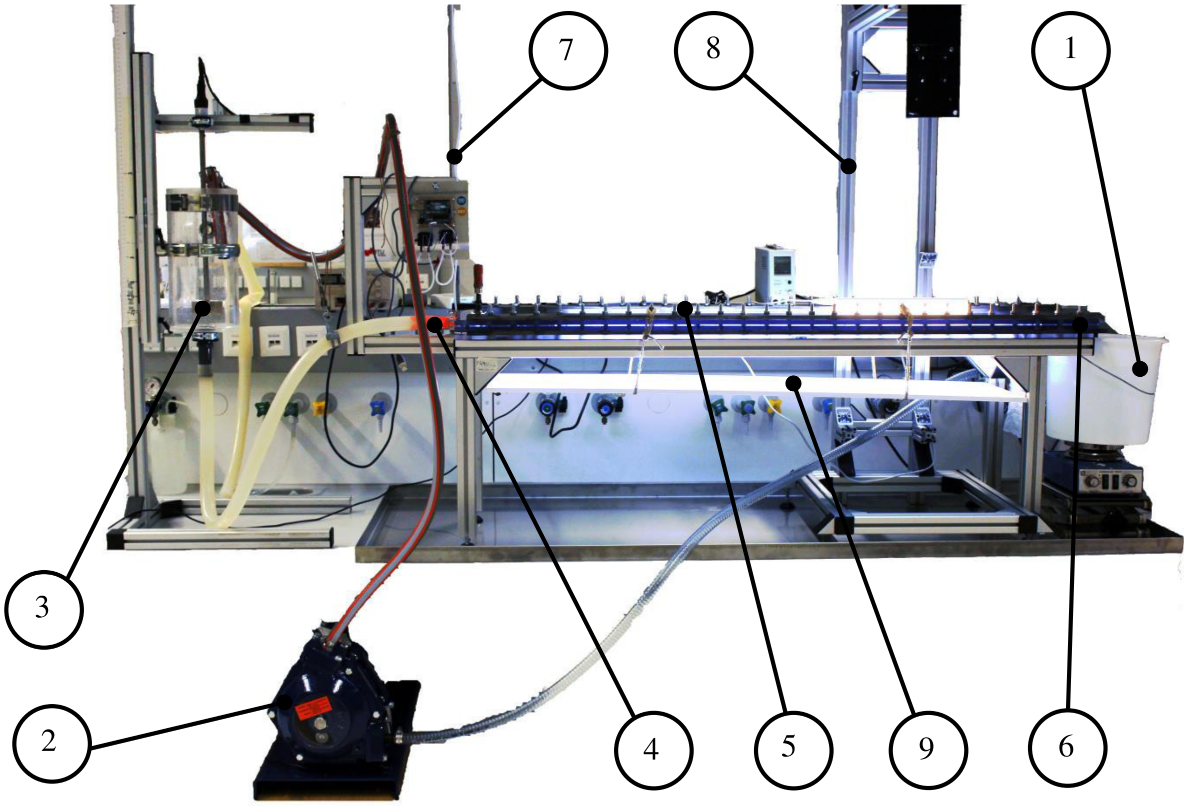

Figure 3-2: Experimental setup for distributor testing. The pulp suspension is pumped form the stirred collection vessel (1) via a peristaltic pump (2) into the stirred storage tank (3). The suspension enters the distributor as one stream (4), flows through the device (5) and exits as five streams (6). For pressure measurement between inlet and outlet, a vertical hose is attached to the hose near the inlet (7). For imaging, an adjustable camera support (8) and a LED–panel (9) are installed.

The distributor which is the main apparatus in the setup consists of four different sections. The side and top view of the distributor, including an illustration of the different sections, are shown in Figure 3-3. The first section is the inlet manifold. In the manifold the cross section gradually changes from a circular to rectangular shape. This is necessary to connect the hose with the inlet of the first diffusor. In the second section, the suspension enters a multi-stage step diffusor. The diffusor consist of an inlet section and three steps whereas every step has a height to length ratio of six. The third section is the splitter where the suspension is divided into five streams. The last section is the outlet where the streams are turned from the horizontal to the vertical direction. An overview of the dimensions is summarized in Table 3-1. The distributor can hold a volume of 0.42 litres of pulp suspension and has a weight of about 35 kg which made it hard to move and manipulate.

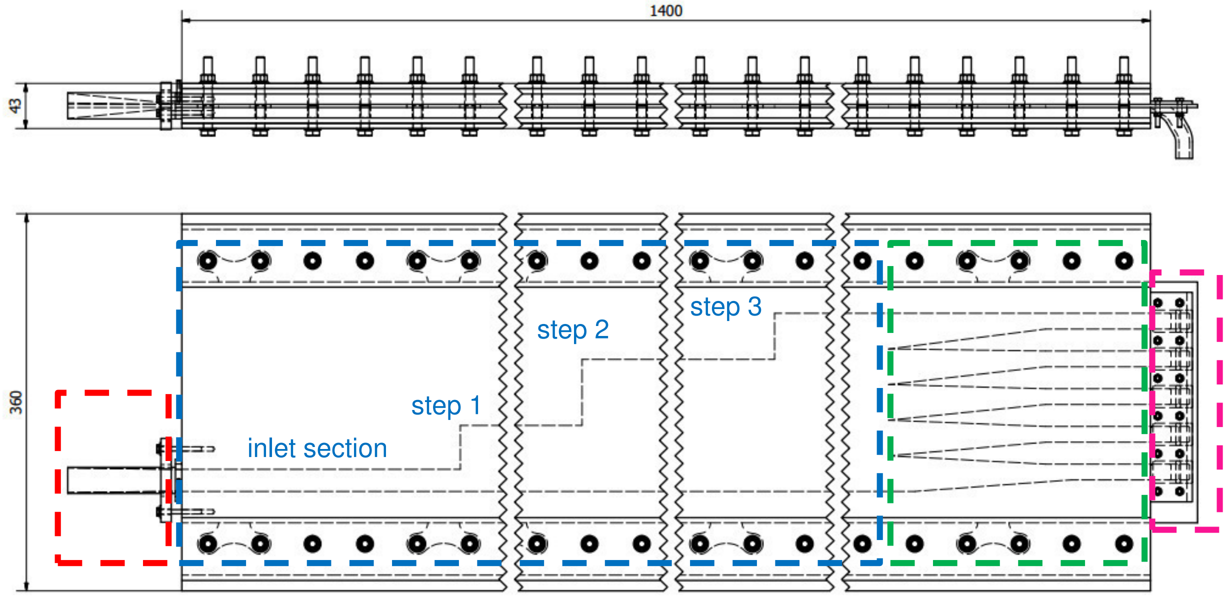

Figure 3-3: Side and top view of the distributor, including an indication of the different sections (red dashed line: inlet manifold, blue dashed line: step diffusors, green dashed line: splitter, pink dashed line: outlet).

Table 3-1: Dimensions of the step – diffusor and splitter.

geometrical part	cross section (W x H) [mm]	step height [mm]	step length [mm]
inlet section	21 x 3	0	200
step 1	63 x 3	42	252
step 2	126 x 3	63	378
step 3	170 x 3	44	264
splitter	variable	0	306
outlet 1-5	15 x 3	0	0

One main design specification of the experiment was the possibility of a sufficiently large geometry variation. For that reason a system with two plates and interchangeable inlays which are clamped together was chosen. This design allows an easy variation of (i) the channel height via the thickness of the inlays, (ii) the step diffusor design, as well as (iii) the splitter geometry by changing the shape of the inlays. In order to keep material consumption low, the inlays are cut into segments which are sealed to each other via a labyrinth seal. Sealing of the inlay and the top and bottom plate was done by non-setting compounds (e.g. *Hylomar*®). In order to enable imaging with cameras mounted outside of the channel, the whole apparatus has to be transparent. To facilitate that need, the top and bottom plates are made from Polycarbonate (PC) which was chosen due to its favourable mechanical properties. The inlays are made from Plexiglas® (PMMA) which has better properties when processed by a laser cutter. The clamps and bolts are made of steel. A top and cross section view of the assembly is shown in Figure 3-4.

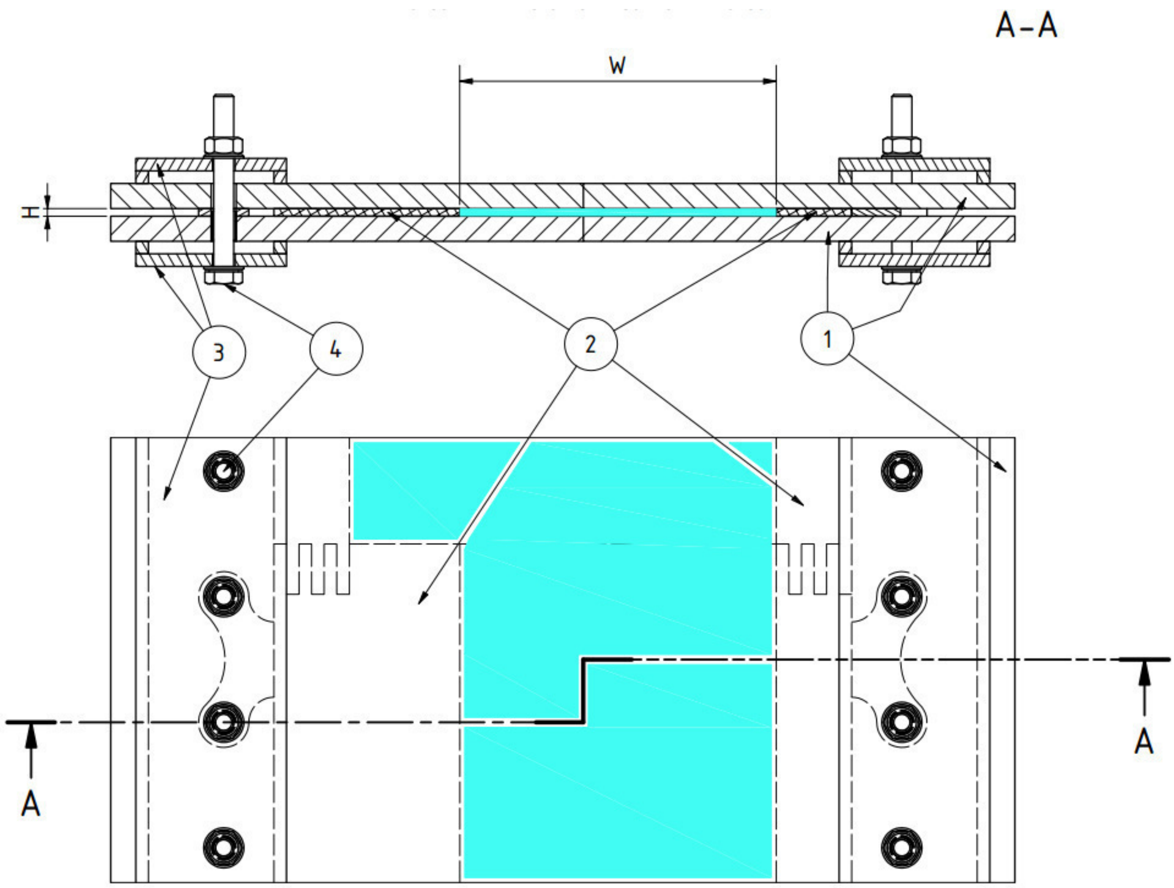

Figure 3-4: Cross-sectional and top view of the second step of the multi-stage diffusor. The main parts of the distributor are the upper and lower plates (1) which are made from transparent polycarbonate to enable imaging, the top and bottom clamps (3) which are held together by bolts (4), and the exchangeable plates which are made from acrylic glass and define the geometry of the distributor (2). The region which is indicated in light blue is the pulp suspension that flows through the diffusor. While the channel height (H) is constant throughout the whole distributor, the width (W) varies downstream.

3.2.1. Mass Flow Measurement

In order to minimize the influence of disturbances caused by the peristaltic pump and the fibres a simultaneous mass flow measurement at all five outlet ports is necessary. As shown in Figure 3-5 the measurement was performed by hand. The operator had to move the tray with the five equally sized bins in and out of the outlet streams. The time was measured by a stop watch, which was also done by the operator. The bins with suspension are separately weighed and the mass flow rate was calculated via:

$$\dot{m}_{sus_i} = \frac{m_{tot_i} - m_{bin}}{t} \qquad \textbf{Equation 2}$$

The disadvantage of this measurement technique is that the operator has a huge influence on the results. The biggest issue was the accurate timing because at higher flow rates (i.e., for situations characterized by outlet Reynolds numbers $\overline{Re}_{out} > 2500$) the measurements took only a few seconds. This might lead to deviations in the calculated mass flow rate caused by the time the operator needs to install and remove the bins. Fortunately, the important parameter for the mass flow in this work was the relative deviation between the outlets. For calculation the weighed mass is used, and therefore the drawback of the inaccurate time measurement is acceptable since this inaccuracy affects all bins equally.

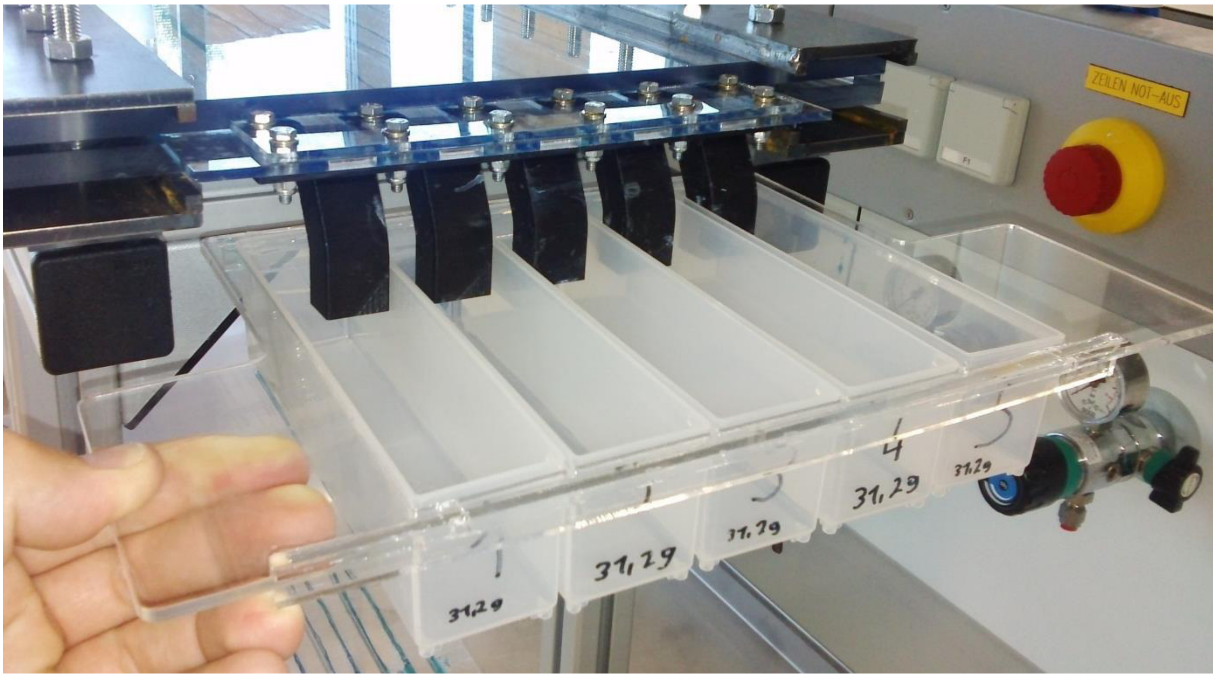

Figure 3-5: Measurement of the mass flow at the outlet of the distributor. The pulp suspension is simultaneously collected in five equally-sized bins. The bins are manually installed and removed.

3.2.2. Pressure Measurement

The pressure measurement is carried out via an evaluation of the geodesic height at the inlet manifold and the storage tank. The installation of the pressure measurement at the inlet manifold is illustrated in Figure 3-6. Before every measurement the hose connected to the manifold was detached, and the capillary was backwashed to remove fibres which deposited at the intersection of manifold and the capillary. For concentrations $w_{fib} > 0.1\%$ the intersection in the manifold started blocking so fast that even with backwashing it was not possible to perform a meaningful measurement. In addition to the pressure at the inlet, the water level of the storage tank is measured. These measurements have the drawback that (i) due to the donut-effect caused by the blade stirrer and (ii) the pulsations from the peristaltic pump especially in the range of $\overline{Re}_{out} = 1500 \div 2500$ (i.e. pump set point $40 \div 70\%$) led to a time-variant water level. Thus, the measured height in the storage tank has a deviation of approximately $\pm 10mm$.

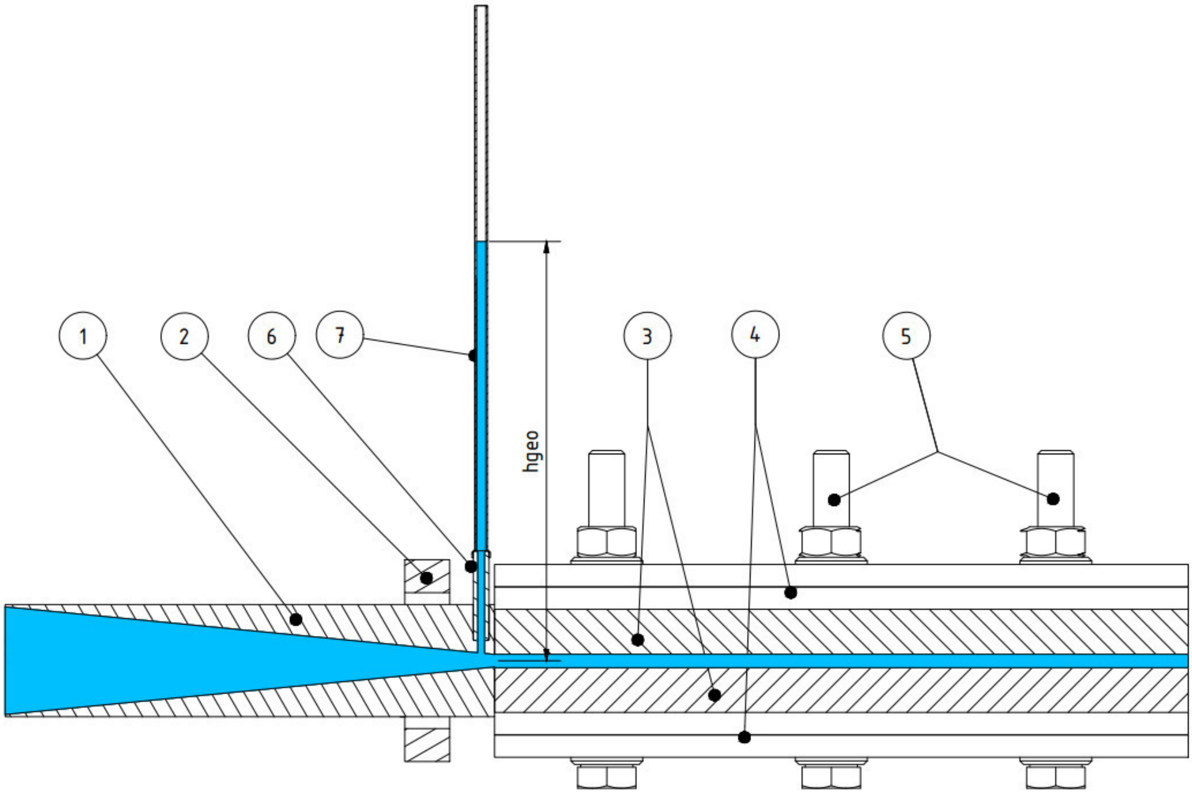

Figure 3-6: Pressure measurement at the inlet manifold (1). Manifold clamp (2), upper and lower plate of the distributor (3) which are hold together by the clamps (4) and bolts (5). The geodesic height is measured via a rubber hose (7) attached to a capillary (6). The pulp suspension is indicated in light blue.

The pressure was calculated from the measured heights by:

$$p = \rho \cdot g \cdot h_{geo} \quad with\ g = 9.81\, m/s^2 \ ;\ \rho = 1000\, kg/m^3$$ **Equation 3**

3.3. Experimental Plan

In order to evaluate the functionality and range of application of the distributor, three parameters were varied in the experiments:

- **Mass Flow**: this parameter was adjusted to ensure an outlet Reynolds number between $\overline{Re}_{out} = 500 \div 3500$, see Chapter 3.3.1.
- **Fibre Concentration**: varied from $w_{fib} = 0.01 \div 0.5\%_{mass}$, see Chapter 3.3.2.
- **Geometry:** Three different splitter designs were tested, see Chapter 3.3.3.

The experiments were carried out for all possible combinations of the above three parameters. During the experiments the mass flow rates at each outlet, as well as the pressure drop in the distributor were measured. Blockage of the outlet ports was visually observed.

3.3.1. Variation of the Mass Flow

The mass flow rate was adjusted by setting the rotational speed of the peristaltic pump. In addition, the height of the storage vessel was adjusted to match the pressure drop of the distributor. The correlation between mass flow rate and the set point of the peristaltic pump was examined in a separate experiment. The default inlet mass flow rate was that for five HDF channels operated at $Re_{HDF} = 1500$. In order to allow a possible extended application of the HDF in further experiments, the distributor was tested over the full range of Reynolds numbers, i.e., $Re_{HDF} = Re_{out,i} = 500 \div 3500$. It is expected that the mass flow rate will slightly differ between the outlet ports. Hence, the arithmetic mean outlet Reynolds number $\overline{Re_{out}}$ is chosen as reference to allow comparison of experiments with different geometries. Every set of experiments was started at $\overline{Re_{out}} = 3500$, and the flow rate was gradually reduced in steps that resulted in a change of the Reynolds number of 500. The Reynolds number is defined as:

$$Re = \frac{\bar{u} \cdot d_h}{\upsilon}$$ **Equation 4**

Here ν is the kinematic viscosity of water at 20°C ($\nu = 1.04 \cdot 10^{-6} m^2 s^{-1}$). With the hydraulic diameter d_h of the channel:

$$d_h = \frac{4 \cdot A}{U}$$ **Equation 5**

Here U is the perimeter of a single wetted outlet channel, and A is the cross section of the channel. The relation between the mean velocity $\bar{u}$ and mass flow rate $\dot{m}$ is:

$$\dot{m} = \dot{V} \cdot \rho = \bar{u} \cdot A \cdot \rho$$ **Equation 6**

The relation between Reynolds number and mass flow rate at the outlet is calculated by combining Equation 4, Equation 5 and Equation 6.

$$\dot{m}_{out,i} = \frac{Re_{out,i} \cdot \upsilon \cdot U \cdot \rho}{4}$$ **Equation 7**

The inlet mass flow rate is the sum of the outlet mass flow rates. The average outlet mass flow $\bar{\dot{m}}_{out}$ rate is calculated with the average outlet Reynolds number $\overline{Re_{out}}$.

$$\dot{m}_{in} = \sum_{i=1}^{5} \dot{m}_{out,i} = 5 \cdot \bar{\dot{m}}_{out} = 5 \cdot \frac{\overline{Re_{out}} \cdot \upsilon \cdot U \cdot \rho}{4}$$ **Equation 8**

3.3.2. Variation of the Consistency

As second parameter the fibre consistency was varied in four steps $w_{fib} = 0.01; 0.05; 0.1; 0.5\%$. In what follows, the notation “low consistency” relates to $w_{fib} = 0.01\%$, and “high consistency” to $w_{fib} = 0.5\%$.

The occurring effects at different concentrations such as network formation and break-up, agglomeration in the wake of the step diffusor, build up on the spikes of the splitter and blockage of outlet ports are observed and documented with pictures. The pictures are taken with a DSLR camera *CANON® EOS 700D* with an 18-55mm lens.

In this work the effects of the fibre concentration are just compared qualitatively, and no further classification based on quantitative information is done. The observed effects occurring at different fibre consistencies are shown in Figure 3-7.

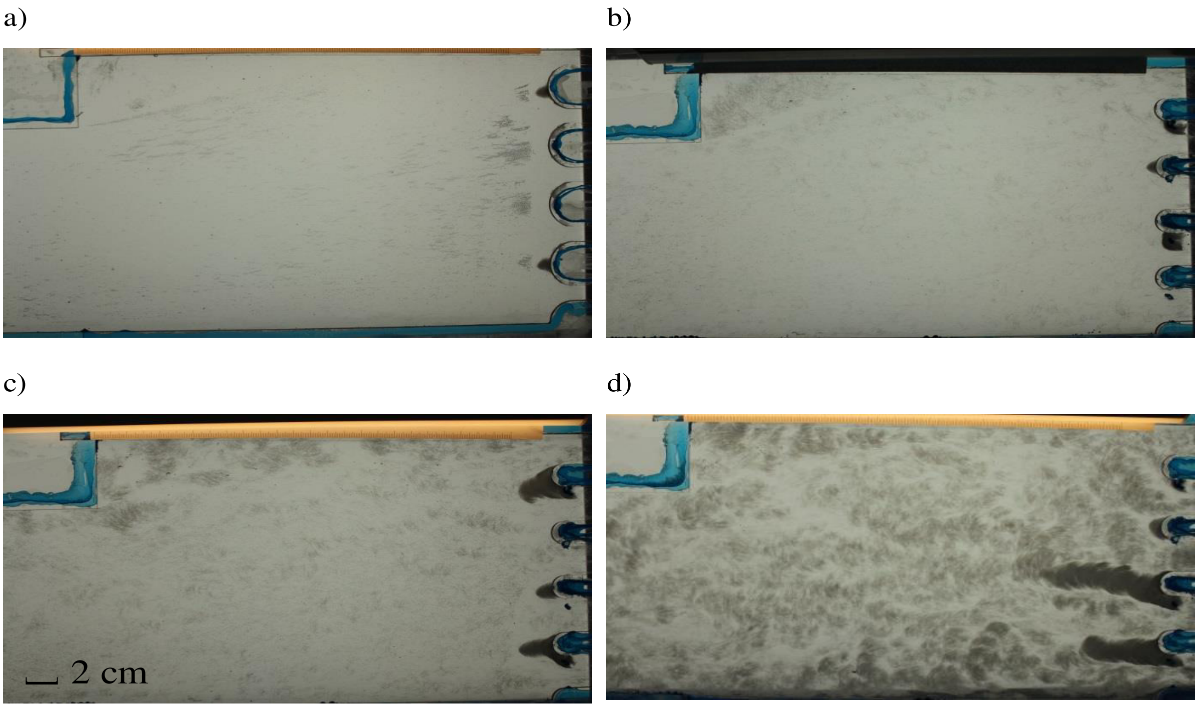

Figure 3-7: Visual investigation of pulp suspension flow at the third step of the multi-stage diffusor and the splitter inlet at $\overline{Re}_{out} = 3000$ for different fibre concentrations: a) $w_{fibre} = 0.01\%$ no flock formation, the fibres are hard to identify because many small air bubbles deposit on the upper plate; b) $w_{fibre} = 0.05\%$ air bubbles are washed out by the fibres, agglomeration of fibres in the wake of the third step, no floc formation; c) $w_{fibre} = 0.1\%$ initiation of network and floc formation, beginning build up on the spikes of the splitter; d) $w_{fibre} = 0.5\%$ enhanced network formation and large flocs agglomerate, large deposition on the spikes.

3.3.3. Variation of the Geometry

The third and most time consuming parameter to change was the geometry of the distributor. The first part downstream of the inlet into the distributor is a step diffusor with three backward facing steps. The steps are designed according to rules investigated by Anwar-ul-Haque et al. [16]. According to Youn [15] and Anwar-ul-Haque et al. [16] the reattachment length is $6 \div 8$ times the step height for $\overline{Re}_{out} > 3000$. In order to get a compact apparatus the ratio of step height to step length of the new developed distributor is set to six. This design bears the risk, that the flow will not reattach. In order to keep the experimental effort manageable the geometry of the step diffusor was not altered.

The geometrical variation was focused on the splitter which is the second part and follows after the step diffusor. The three different geometries (G1, G2 and G3) investigated in this work are depicted in Figure 3-8. In the following work the parts of the splitter that divide the stream are called “spikes” (note, in version G2 and G3 they are round and blunt, and do not look like a spike by a common definition). The idea of version G2 and G3 was to create geometry similar to the ones used in relaxation chambers in paper machines. Additionally, in version G3 the geometry in front of the outlet is shaped like a nozzle to increase the Reynolds number before decreasing it again towards the outlet. It was expected that the additional pressure drop caused by this nozzle would allow a more homogeneous mass flow distribution. The distance between the outlets was design according to the findings of Eßl [19].

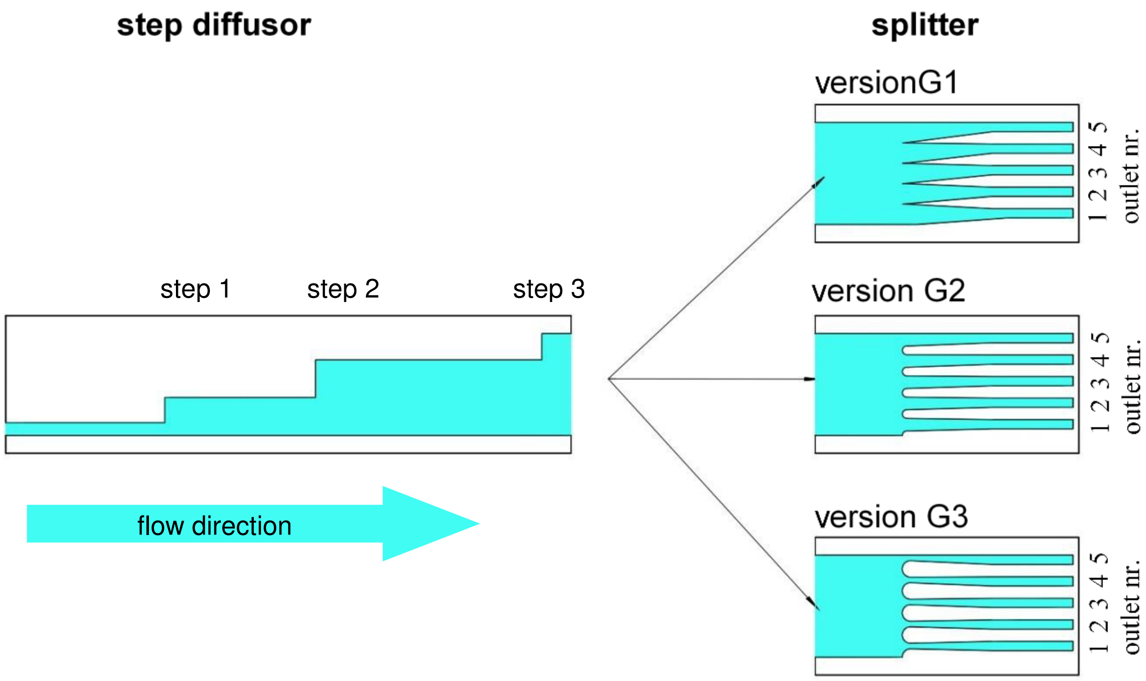

Figure 3-8: Variation of the splitter geometry. The fluid is marked in light blue.

3.4. Results of the Experiments

This section covers the findings of the experiments, as well as challenges encountered during the execution of the experiments.

3.4.1. Blockage of Outlet Ports

The main problem during the experimental work was the blockage of outlet ports. The mechanism of how blockages occur can be divided in four phases which are illustrated in Figure 3-9. First, small amounts of fibres deposit on the spikes of the splitter. In the next phase fibres aggregate at the spikes, and form a deposition. The depositions keep growing until they collapse towards one side of the spike. In case the fibre floc formed by the collapsed deposition is too large to fit through the outlet port, and this port is blocked. This mechanism was observed through all geometries, fibre concentrations and mass flow rates. Blockages caused by big flocs formed in the diffusor were not observed. This leads to the conclusion that the step diffuser works - in principle - well for deflocculation.

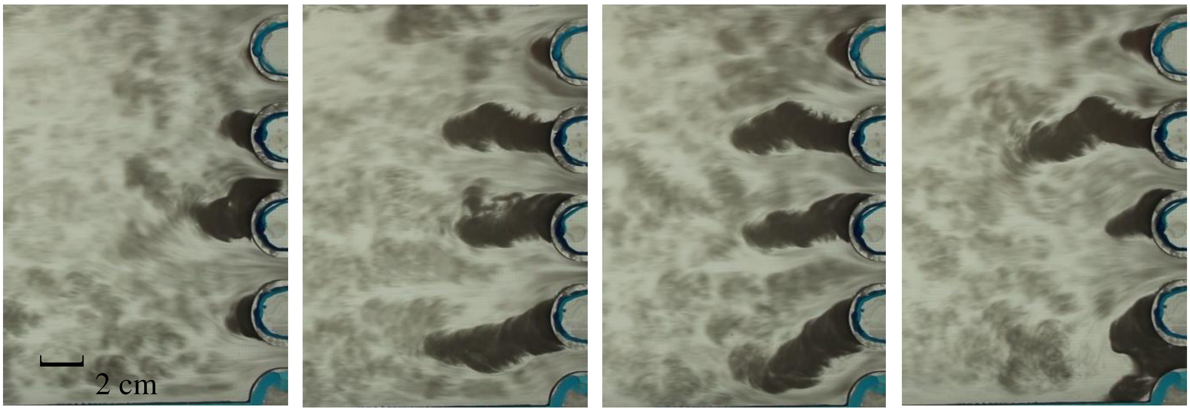

fibre deposition on spikes	formation of towering deposition	collapse of deposition	blockage of outlet port

Figure 3-9: Mechanism that leads to a blockage of outlet ports. Blockage occurring over time at outlet 1 in splitter geometry G3 at fibre concentration $w_{fib} = 0.5\%$ and $\overline{Re}_{out} = 2500$. This is the worst case scenario at high concentration. For all other geometries, Reynolds numbers and concentrations the mechanism of blockage is similar.

The occurrence of blockages is massively depending on the fibre concentration. At concentrations $w_{fib} < 0.01\%$ no blockages occurred. With increasing concentration the blockage occurred below a certain mass flow rate which is represented by the outlet Reynolds numbers in Figure 3-10.

A big issue was also the hindrance of fibre flow near the wall and the spikes of the splitter caused by excessive sealing agent squeezed out during assembly of the experimental device. This was especially observed with geometry G2. The duration until the outlets were blocked was not investigated in detail. However, as a guiding value at intermediate concentrations and low Reynolds number the blockage occurred within several minutes.

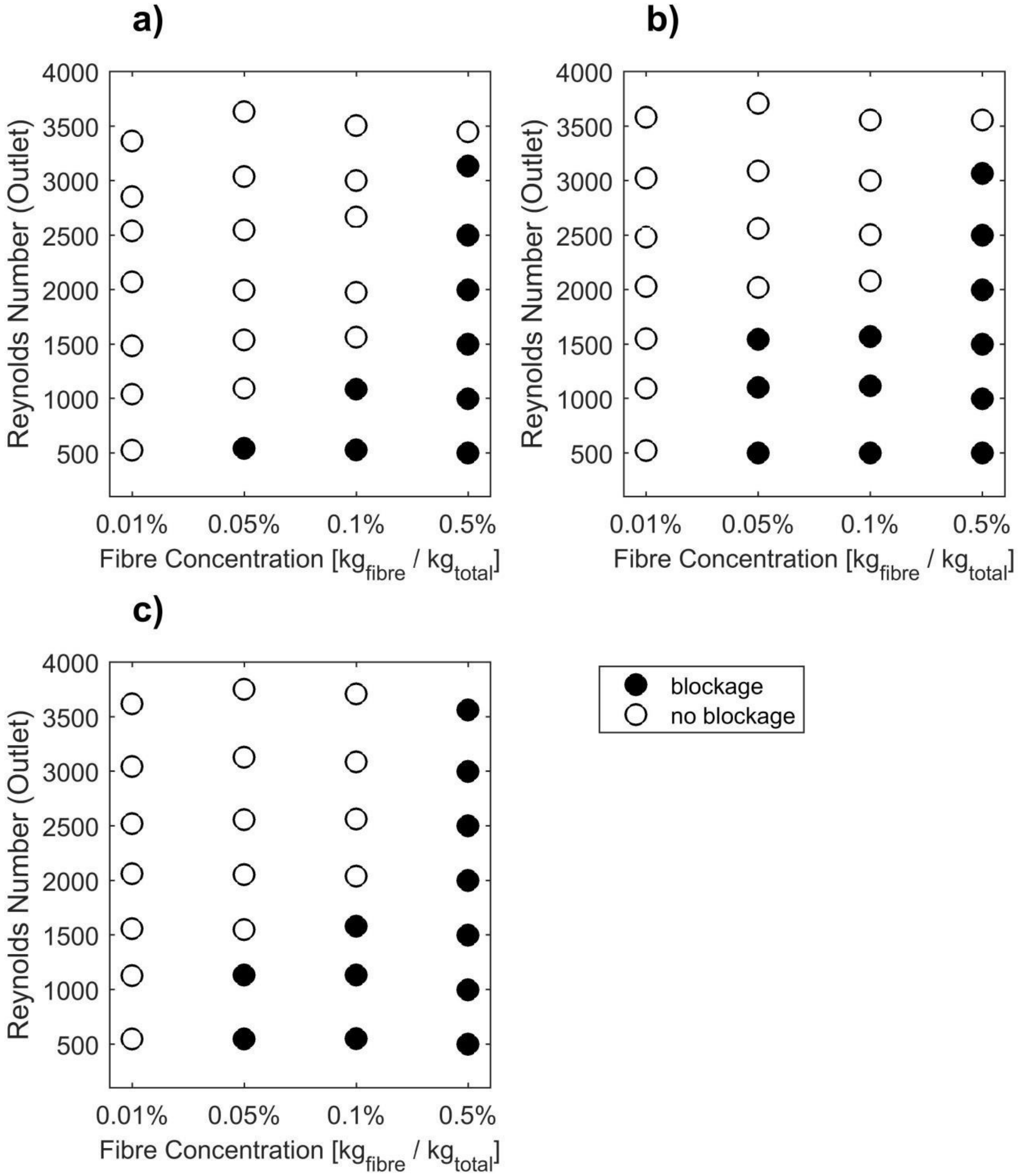

Figure 3-10: Blockage characteristics of the outlet ports for different distributor geometries at different fibre concentrations and outlet Reynolds numbers: a) geometry G1, which showed the best performance; b) geometry G2 had a lower performance compared to G1, which was mainly caused by excessive sealing agent in the splitter; c) G3 had the worst performance, at the highest concentration even at the highest possible mass flow rate blockages occurred.

Blockage occurred in two forms which in this work are called “soft” and “hard”. The classification is based on the required removal procedure of the blockage:

- **Soft blockages** occur at low fibre concentrations and low Reynolds numbers. The network is loose and located at the tip of the inlet section of the splitter. They are easy to remove via small variations in the inlet pressure, e.g., by squeezing the inlet hose.
- **Hard blockages** occur at high fibre concentrations and at low concentrations if they are not removed in time. They extend over the whole length of the outlet port for high Reynolds numbers. These blockages cannot be removed by a pressure pulse, but always necessitate backwashing with pure water. In severe cases a shutdown and a disassembly of the distributor is required to remove the blockage.

Table 3-2: Comparison and distinctive features of outlet port blockages

	soft blockage	**hard blockage**
Concentration	low	high
Reynolds Number	low $(500 \div 1000)$	intermediate $(2000 \div 2500)$
Location	at spikes and inlet section	whole channel
Network	loose	dense
Removal	easy, pressure pulse	hard, backwashing, disassembly

a) soft blockage b) hard blockage

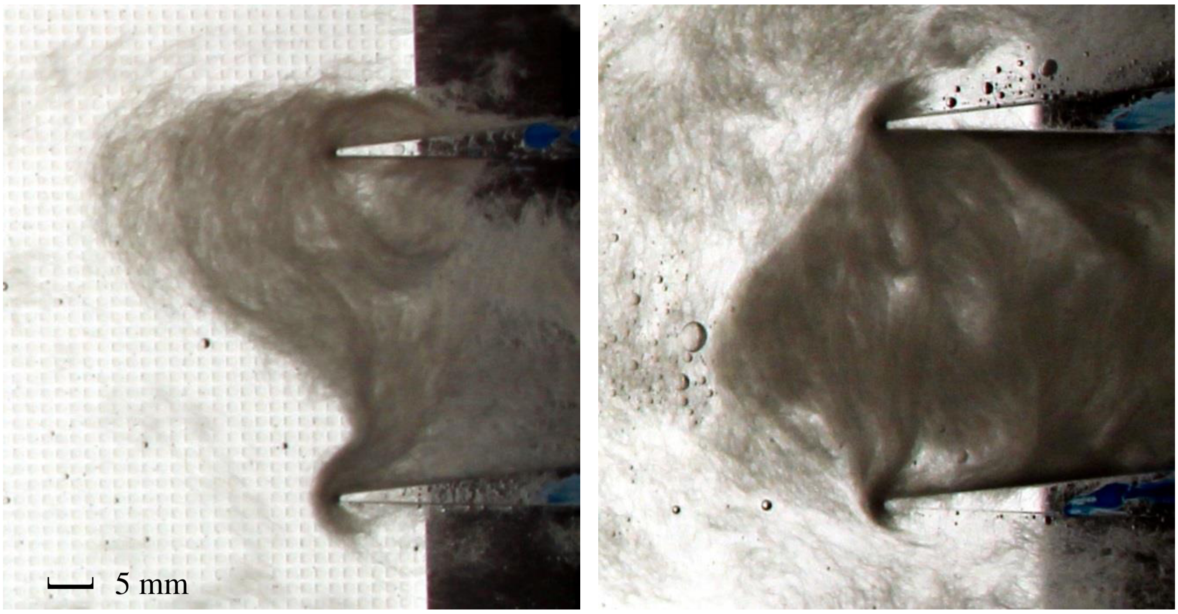

Figure 3-11: Different types of blockage of outlet ports: a) soft blockage: low fibre concentration and low Reynolds number, loose network, easy to remove, located at the spikes and at the inlet of the splitter; b) hard blockage: high fibre concentration, high Reynolds number, dense blockage of the whole outlet, hard to remove.

3.4.2. Mass Flow Distribution

The equal mass flow distribution is the core feature of the distributor and vital for the reliable operation of the HDF. Therefore, this was closely looked at. As described in Chapter 3.3, all three geometries and all four concentrations are tested at Reynolds Numbers from $\overline{Re_{out}} = 500 \div 3500$. For better comparison the relative deviation of the mass flow rates at the outlets is calculated via:

$$\Delta m_{rel} = \frac{m_i - \bar{m}}{\bar{m}} \cdot 100[\%]$$ **Equation 9**

Here $\bar{m}$ is the arithmetic mean mass flow rate determined from all five outlet ports.

The difference between absolute and relative mass flow rate is shown in Figure 3-12. When considering the absolute values of the mass flow rates, the first impression is that for higher Reynolds numbers the mass flow is more unequally distributed than at lower ones. However, when considering the relative deviation from the mean, it is clear that lower Reynolds numbers are more challenging with respect to an equal distribution of the suspension.

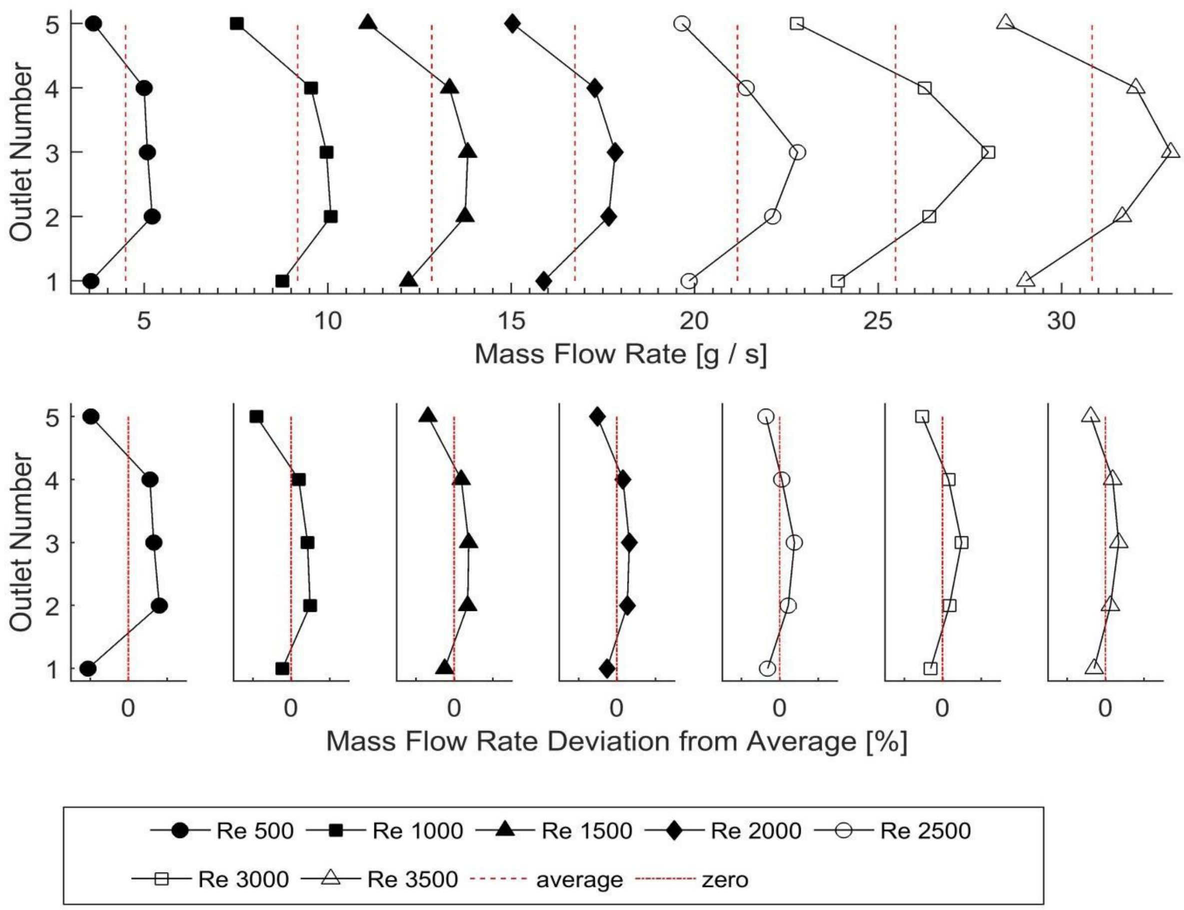

Figure 3-12: Absolute and relative mass flow distribution at the outlet ports of geometry G1 with pure water (no pulp) for different Reynolds Numbers. The lines are a guide for the eye.

The experiments showed that the flow rates between the outlets are distributed in an asymmetric parabolic shape. It is speculated that this asymmetry was caused by the asymmetric steps in the diffusor. Especially at outlet 1 the wall effect has a big influence on the flow rate. With increasing Reynolds number, a more even distribution of the (relative) mass flow rates was observed. The dependency of the mass flow rate from the geometry and pulp the concentration is depicted in Figure 3-13 for $\overline{Re}_{out} = 1000$ and Figure 3-14 for $\overline{Re}_{out} = 1500$.

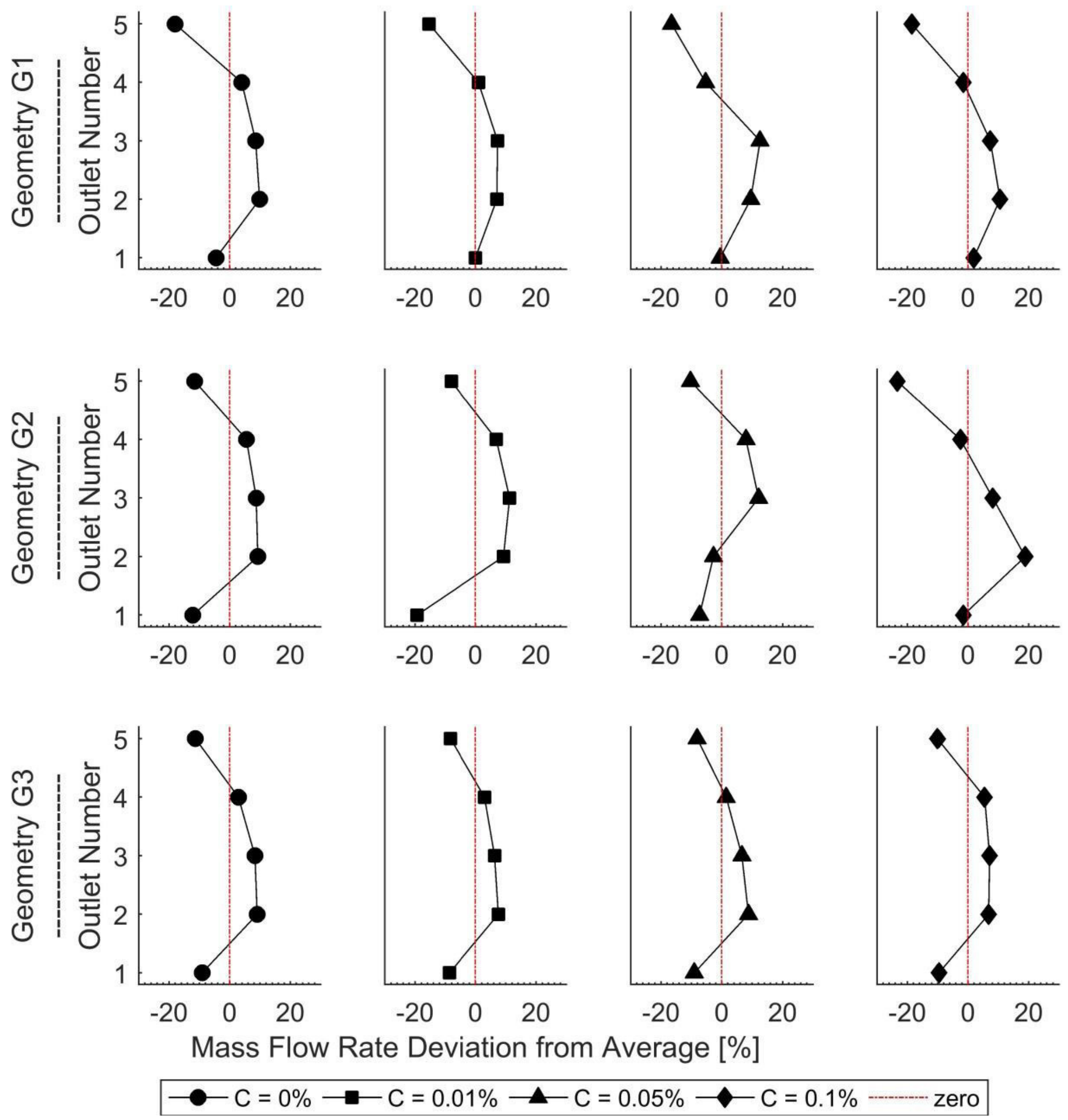

Figure 3-13: Deviation of mass flow rate from the arithmetic mean for various pulp concentrations and splitter geometries at $\overline{Re}_{out} = 1000$. The lines are a guide for the eye.

It is shown that outlets 1 and 5 were always below, and outlet 3 was always above average. The deviation of outlets 2 and 4 depend on the fibre concentration. In general, however, these two outlets tend to have flow rates that are above the average. In summary, it was observed that there is a small influence of the fibre consistency for $\overline{Re}_{out} = 1000 \div 1500$. The measured values of all experiments are collected in Appendix E.

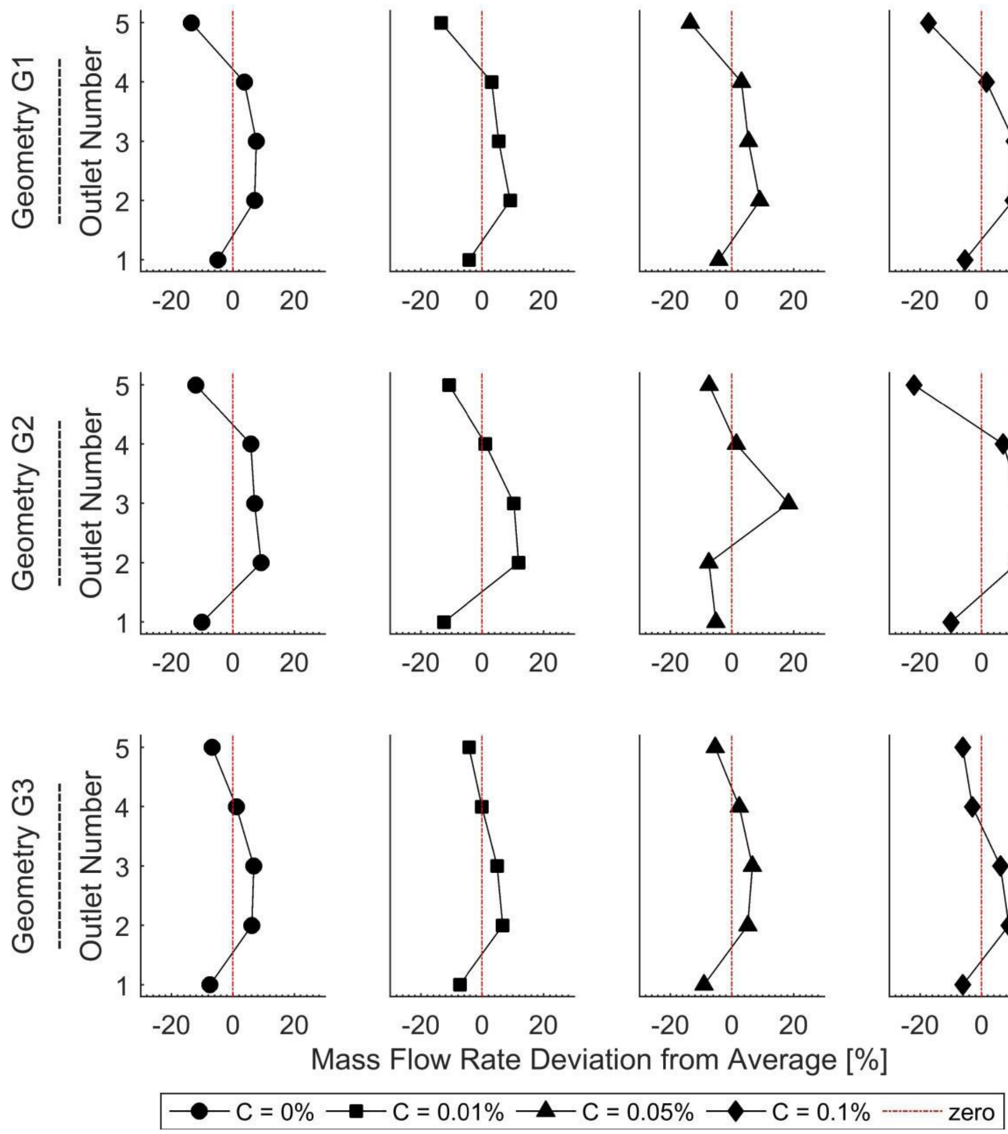

Figure 3-14: Deviation of mass flow rate from the arithmetic mean for variable concentrations and splitter geometries at $\overline{Re}_{out} = 1500$. The lines are a guide for the eye.

3.4.3. Fractionation Effects

The main purpose of the distributor is the continuous supply of a pulp suspension to the HDF. To ensure optimal operating conditions of the HDF, it is important to achieve an equal fibre length distribution in any channel. Any pre-fractionation in the distributor is unfavoured, because the fractionation should only be carried out in the HDF with close to identical conditions in each channel.

During the experiments samples of every outlet were taken and the volume-weighted fibre length distribution was measured as described in Chapter 3.1.3. The distributions are compared with each other, and with the distribution of the raw material. The samples were drawn for all geometries at $\overline{Re}_{out} = 1500$ and $w_{fib} = 0.1\%$. The distribution for geometry G2 is depicted in Figure 3-15. The mean standard deviation over all classes is $\bar{\sigma}_{out1\div5} = 2\%mm^{-1}$ for the q_3 distribution, which appears to be acceptable. Thus, there is no preferential accumulation of fibres in one of the outlets. Interestingly, compared to the raw material distribution the distribution of the outlets showed a significant offset. Specifically, it appears that small fibres (and fines) disappear during the experiment, and longer fibres form. The other geometries showed the same behaviour. This leads to the conclusion that fibres with a length below a certain threshold aggregate in the apparatus, or agglomerate with longer fibres and are therefore undetected by the fibre tester.

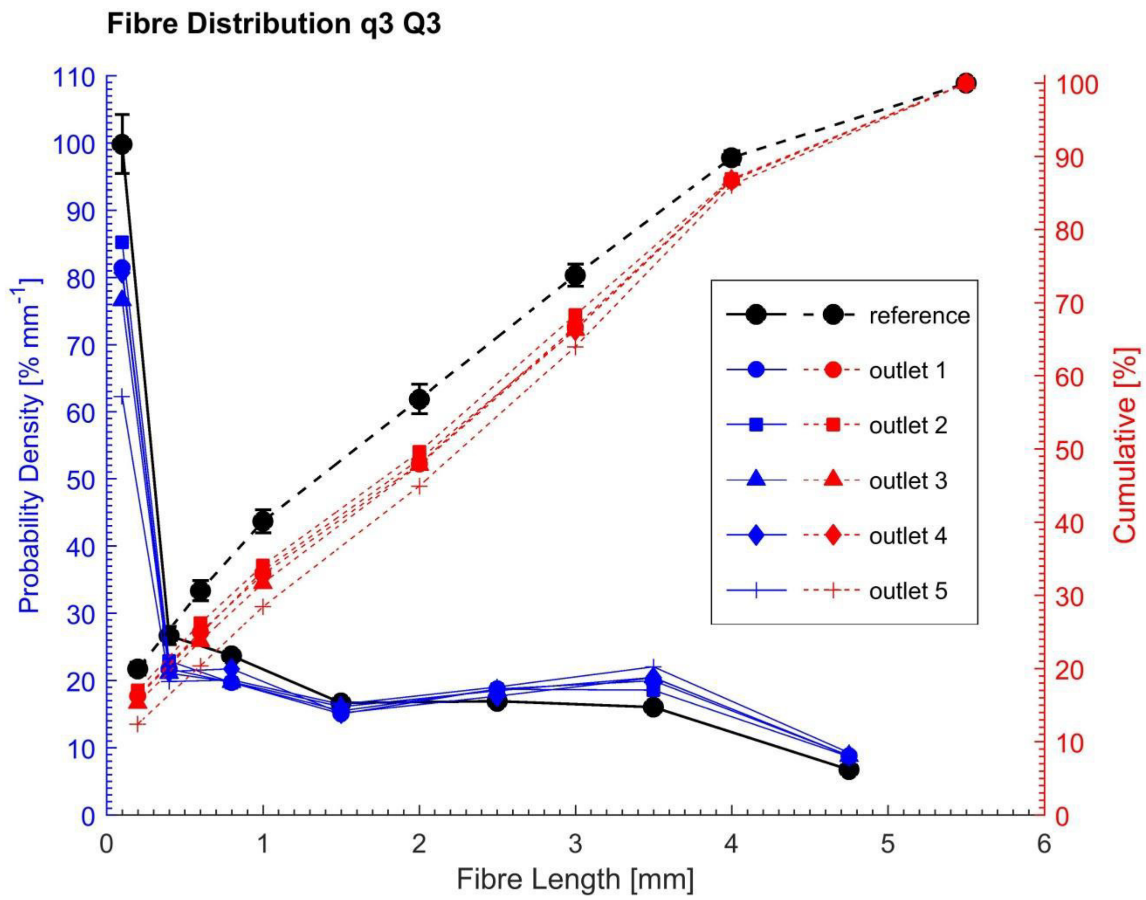

Figure 3-15: Cumulative (Q3) and density (q3) volume-weighted distribution of the pulp suspension at different outlet ports. The upper fibre class limits (x_o) are $[0; 0.2; 0.6; 1; 2; 3; 4; 5.5\ mm]$. The "reference" line refers to the raw material distribution. The samples were drawn with geometry G2 at $\overline{Re}_{out} = 1500$ and $w_{fib} = 0.1\%$.

3.4.4. Pressure Drop

One goal of the distributor was minimal energy consumption during operation, hence the pressure drop for the whole apparatus must be kept as low as possible. As described in Chapter 3.2.2 the pressure is measured via the geodesic height of the water level in the storage tank and a hose mounted at the inlet manifold. The pressure measurement at the inlet manifold was only applied for $w_{fib} = 0.01 \div 0.1\%$ since at a concentration of $w_{fib} = 0.5\%$ the measuring point was blocked immediately. Fortunately, and as shown in Figure 3-16, the fibre concentration had no significant influence on the pressure drop in the investigated range. The averaged normalized standard deviation of the pressure drop between experiments with different consistency is $\bar{\sigma}_w = 5\%$. Only at concentrations of $w_{fib} > 0.1\%$, or in case multiple outlet ports were blocked, an increased pressure drop was noticeable. The splitter geometry had a small influence on the pressure distribution as well. Geometry G1 had the smallest pressure drop, while the one of geometry G2 was on average 5% higher, and the one of geometry G3 was on average 13% higher. The measurements showed the majority of the pressure drop is generated by the hose connecting the storage tank and the distributor.

The general equation for the pressure loss in a straight pipe is modelled as follows[20]:

$$\Delta p \propto \frac{\bar{u}^n \cdot L \cdot \mu^k \cdot \rho^r}{H^m}$$ **Equation 10**

Here $\bar{u}$ is the mean flow velocity, L is the length of the pipe, μ is the dynamic viscosity, ρ is the density of the fluid and H is the diameter. For a fully developed turbulent pipe flow the exponents for *m,n,k,r* are 1,2,0,1, respectively. This leads to a quadratic dependency of the pressure drop with respect to the mean flow velocity. In case of a laminar flow the exponents are 2,1,1,0 which lead to a linear dependency.

Table 3-3: Pressure loss coefficients calculated from the experiment data of the inlet manifold

	G1	**G2**	**G3**
ζ_{turb}	0.238	0.305	0.436
ζ_{lam}	855	895	922

The investigated flow in the distributor is in the transitional flow regime, the geometry is complex and only the combined pressure drop of the step diffusor and the splitter was measured. Consequently, a simple combination of the above equations for the pressure loss was applied. For detailed calculations see Appendix C.

$$\Delta p_{dist} = \rho \cdot \left(\zeta_{turb} \cdot \overline{u}_{out}^2 + \zeta_{lam} \cdot \frac{\nu}{d_h} \cdot \overline{u}_{out} \right) \qquad \textbf{Equation 11}$$

Here $\overline{u}_{out}$ is the mean velocity at the outlets, d_h is the hydraulic diameter of the outlet channel and ν is the kinematic viscosity of water at 20°C ($\nu = 1.04 \cdot 10^{-6} m^2 s^{-1}$). The pressure loss coefficients ζ_{turb} and ζ_{lam} account for the whole pressure drop in the distributor including the exit losses. The coefficients are determined from fits of the measured values according to Equation 11. The results for the pressure drop from the inlet manifold to the outlets are summarized in Table 3-3. The measured values of all experiments are collected in Appendix E.

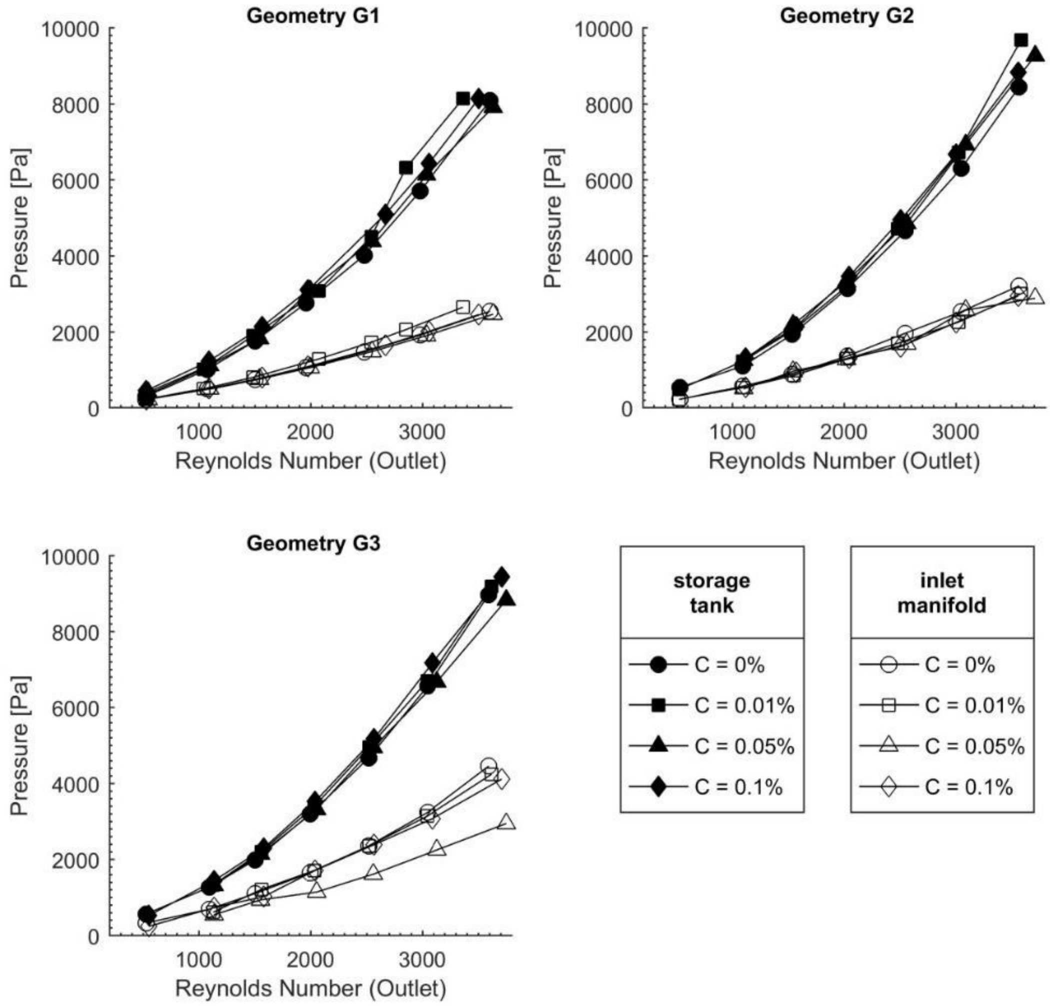

Figure 3-16: Pressure drop at different concentrations and outlet Reynolds numbers measured in the storage tank and at the inlet manifold. The concentration had no significant influence on the pressure drop. The influence of the geometry is noticeable and shows a clear tendency. As expected the pressure drop increases with decreasing gap between spikes of the splitter. The pressure drop data for geometry G3 at $w_{fib} = 0.05\%$ and measured at the inlet manifold seems corrupted, and therefore is treated as outlier.

4. Simulation

The second main part of the thesis was the CFD simulation of the flow in the distributor. This section describes the simulation setup (see Chapter 4.1), the applied boundary conditions (see Chapter 4.2), and the used turbulence models (see Chapter 4.3). The results for the basic configuration are shown in Chapter 4.4, followed by investigations of the influence of the grid size of the mesh (see Chapter 4.5). To consider a more realistic scenario, i.e., the final application of the distributor including the HDF, the effect of an additional pressure drop at the outlet was investigated (see Chapter 4.6). The comparison with the experiments (without suspended fibres) is shown in Chapter 4.7.

Since pulp suspensions are a material with many different properties to take into account, it is not possible at the moment to simulate the interaction between fibres and fluid in very detail. For that reason, and to keep the computational efforts manageable, only single phase simulations were performed. As show in the experimental section of the present thesis, for fibre concentrations $w_{fib} < 0.1\%$ the influence of the fibres on the flow field is negligible. Thus, for these systems the assumption of a single fluid appears reasonable in case one interested only in the flow characteristics (e.g., pressure drop and mass flow rates). Consequently, the OpenFOAM® software package is used to run single-phase simulations considering a Newtonian fluid behaviour.

4.1. Simulation Setup

For the simulation a three dimensional finite volume method is applied and therefore a spatial discretisation is necessary (i.e., mesh generation). The simulation domain was considered in its real-world size, i.e., no geometrical scaling was applied. The origin for the coordinate system is positioned at the middle of the channel height at the inlet of the splitter and at the wall of outlet 1. The dimensions of the domain are shown in Figure 4-1. For the standard case, i.e., the distributor with five outlets, the domain was split into 1.385.000 hexagonal cells. The cell size is gradually decreased towards the wall in the direction of the channel height. In flow direction the cell size is also decreased towards the steps of the diffusor. For all simulations it is assumed that density and viscosity are constant. It was decided to use the kinematic viscosity of pure water at 20°C ($\upsilon = 1.004 \cdot 10^{-6} m^2 \cdot s^{-1}$) for all simulations.

The settings for the nummerical solution of the problem are crucial for the accuracy, speed and stability of the simulation. To ensure a stable run and sufficient speed, only first order discretization schemes are used. The next settings in this manner concern the solver which depends on the time discretization. For the steadystate simulations with the RANS turbulence modell, a SIMPLE solver is used. The transient simulations with the LES turbulence modell require a PISO-based solver. Another aspect in the transient simulation is the size of the time-step (∂t). This simulation parameter is dynamically adjusted via a fixed Courant number, which is defined as [21]:

$$Co = \frac{\partial t \cdot |U|}{\partial x} \qquad \textbf{Equation 12}$$

Where the cell size ∂x is in the direction of the velocity and $|U|$ is the velocity magnitude through the cell. To ensure temporal accuracy and numerical stability the time-step is chosen to ensure $Co < 1$ in every cell. The total volume of the simulation domain is 0.39 litres. The exit condition is set after the double total volume has passed through the domain which was at approximately 12 seconds of run time. The detailed settings for mesh generation, solver, solution, time-step and I/O control are summarized in Appendix F.

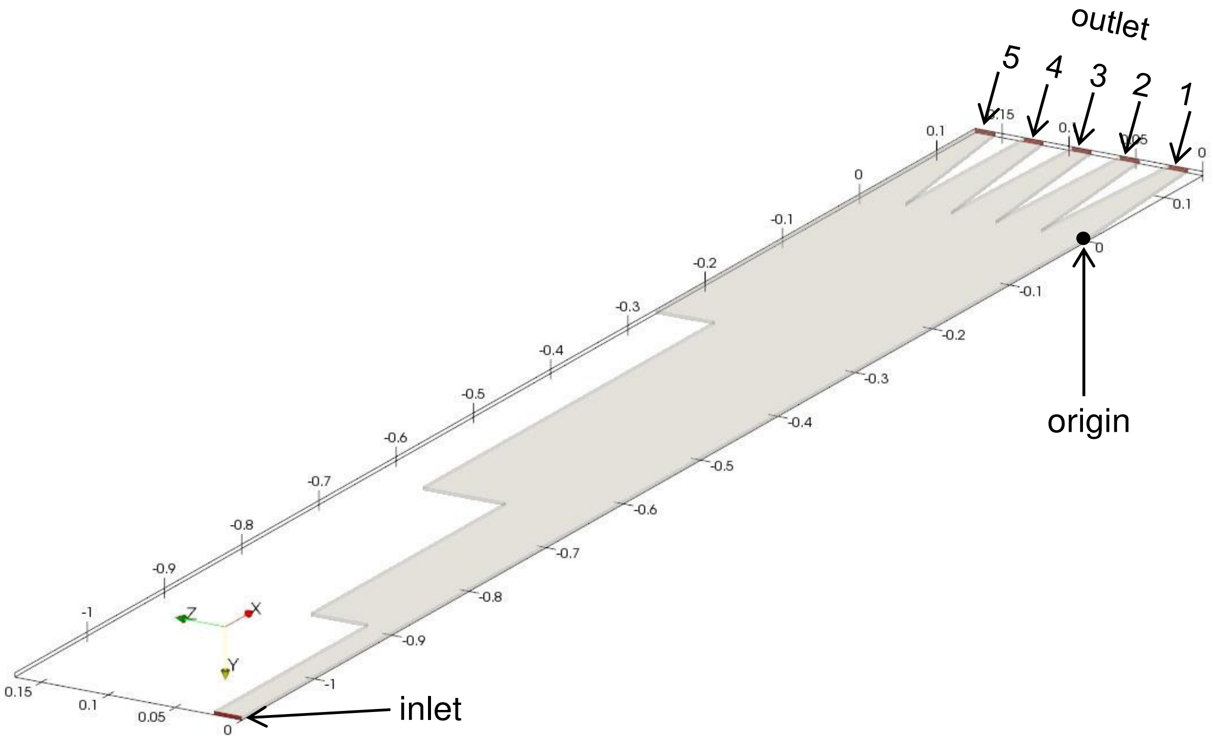

Figure 4-1: Dimensions and coordinates of the simulation domain, all inlet and outlet patches are marked in red. All other external faces are walls. The dimensions are given in meters. No geometrical scaling was applied.

4.2. Boundary and Initial Conditions

Since in the following simulations only the distributor without the auxiliary equipment is investigated, it is necessary to apply appropriate boundary conditions (BCs). The BCs are applied to all external faces of the simulation domain. The faces are grouped together to so-called patches, which specify where the fluid enters and exits the simulation domain, or which faces represent walls. For a stable, solvable and meaningful simulation there must be a sufficient number of conditions for every flow field and the settings should represent the conditions in the real device as precise as possible. Since the exact inlet flow conditions could not be determined during the experiments it was assumed that the flow conditions at the inlet are steady and fully developed. The velocity profile at the inlet was mapped from separate simulation using RANS with k–ω - SST turbulence model. The chosen types and values of the BC for pressure and velocity are summarized in Table 4-1. Besides pressure and velocity BCs for turbulent kinetic energy (k), turbulent viscosity (υ_t) and other fields used by the turbulence models are set. For all details related to the boundary condition setup see Appendix F.

Table 4-1: Pressure and velocity boundary conditions

		patch		
		inlet	**outlet 1-5**	**walls**
pressure	type	zeroGradient	fixedValue	zeroGradient
	value	-	uniform 0	-
velocity	type	fixedValue	inletOutlet	fixedValue
	value	nonUniformList	uniform (0 0 0)	uniform (0 0 0)

The fixedValue BC sets a time-invariant constant value for each face of the patch it is applied to. The zeroGradient BC sets the gradient normal to the patch to zero. The inletOutlet BC is a combined (derived) boundary condition which has two modes of operation. If the flow direction point out of the simulation domain the zeroGradient condition is applied, otherwise if due to pressure changes the patch would become an inlet the fixedValue condition is applied. This could occur in the unlikely event that an unfavourable velocity distribution leads to the occurrence of an area of negative pressure near an outlet port.

To ensure fast calculation the size of the simulation domain should be only as large as necessary. In order to avoid entrance effects the velocity profile at the inlet is assumed as steady state and fully developed. The velocity profile was generated by a separate simulation containing a straight channel with the same cross section as the distributor inlet. The obtained profile is shown in Figure 4-2, and was mapped to the inlet patches of the distributor simulations.

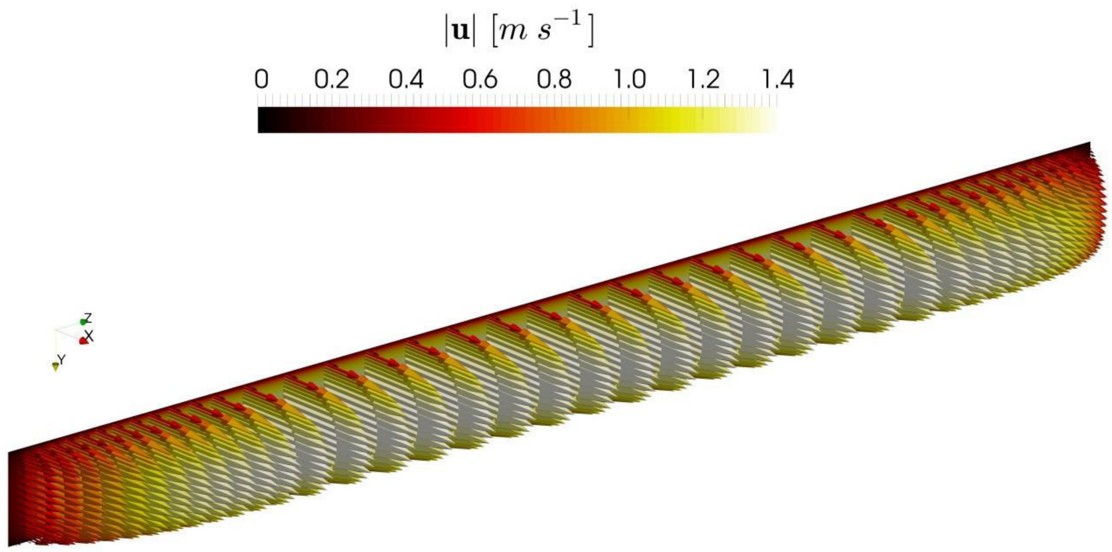

Figure 4-2: Velocity inlet profile of the distributor. This profile is used for simulations with $\overline{Re}_{out} = 1500$. The profile was generated by a separate simulation. The used geometry was a straight channel with the same cross section as the inlet of the distributor and a length of $L_{IP} = 1\,m$.

Besides the boundary conditions which were applied to the external faces, an initial value must be allocated to every cell and internal face. During this thesis the initial values of all flow properties are set to zero. These values change over time as the simulation advances whereas the values of the BCs used in this work are all time-invariant.

4.3. Turbulence models

In the simulation two different turbulence models were investigated. The goal was find the best model and simulation parameters that match the experimental results. This is especially of interest for the design of future distributor geometries. The basic difference in modelling the turbulent kinetic energy spectrum is shown in Figure 4-3.

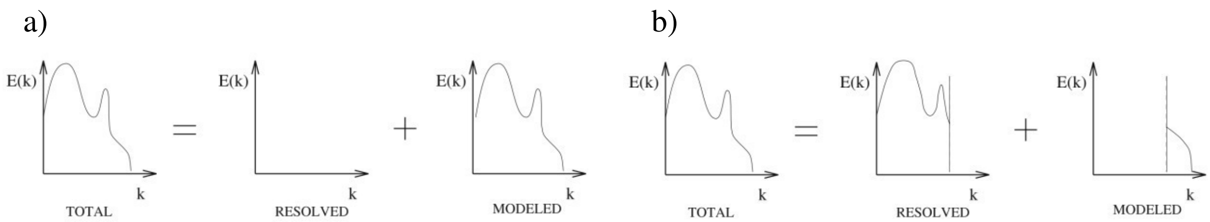

Figure 4-3: Decomposition of the energy spectrum (symbolic representation) of the solution associated with the a) Reynolds Averaged Numerical Simulation and the b) Large-Eddy Simulation [22]**.**

4.3.1. Reynolds Averaged Navier Stokes (RANS)

In typical engineering application it is sufficient to know a few quantitative properties of a turbulent flow [23]. The exact solution $\mathbf{u}$ splits into its statistical average $\bar{\mathbf{u}}$ and a fluctuation $\mathbf{u}'$ [22].

$$\mathbf{u}(\mathbf{x},t) = \bar{\mathbf{u}}(\mathbf{x},t) + \mathbf{u}'(\mathbf{x},t)$$ **Equation 13**

In steady state simulations, as they are carried out during this thesis, the values are averaged over time. Applying this concept to the incompressible Navier Stokes equations without body forces in tensor notation and Cartesian coordinates yields [23].

$$\frac{\partial(\rho \bar{u}_i)}{\partial t} + \frac{\partial}{\partial x_j}\left(\rho \bar{u}_i \bar{u}_j + \rho \overline{u_i' u_j'}\right) = -\frac{\partial \bar{p}}{\partial x_i} + \frac{\partial \bar{\tau}_{ij}}{\partial x_j} \; with\, \bar{\tau}_{ij} = \mu\left(\frac{\partial \bar{u}_i}{\partial x_j} + \frac{\partial \bar{u}_j}{\partial x_i}\right)$$ **Equation 14**

This procedure induces the additional terms $\rho \overline{u_i' u_j'}$ in the conservation equations which are called Reynolds stresses. Since it is impossible to derive a closed set of equations for these stresses one must introduce approximations which are called turbulence models. As the energy dissipation and transport of mass and momentum normal to the streamlines are mediated by the viscosity the effect of turbulence is modelled as an increased viscosity.

In this work the k–ω - SST model developed by Menter [24] is used because in simulation of Anwar-ul-Haque et al. [16] with similar geometries this model showed the best agreement with experimental data. The model is a blend of the k–ε model of Jones and Launder [25] and the k–ω model developed by Wilcox [26]. The basic idea behind the model is to retain the robust and accurate formulation of the k–ω model in the near wall region and take advantage of the free stream independence of the k–ε model in the outer part of the boundary-layer. In order to achieve this goal, the k–ε model is transformed into the k–ω notation. The original k–ω model is multiplied by a function F1 and the transformed k–ε model by a function (1 - F1) and both are summed [24]. The function F1 will be designed to be one in the near wall region (activating the k–ω model) and zero away from the surface (activating the k– ε model). The blending will take place in the wake region of the boundary-layer. For detailed equations see Appendix F. The simulations carried out with this model are further referred to as “RANS”.

4.3.2. Large Eddy Simulation (LES)

As second type Large Eddy simulations are performed. The method is an implication of Kolmogorov's theory of self-similarity which states that large scale eddies are dependent on the geometry, while small scale eddies are more universal [22]. In contrast to the RANS model only a part of the kinetic energy spectrum is modelled as shown in Figure 4-3. This is what is done in LES by calculating only the low-frequency modes in space directly. Therefore, it relies on the definition of large and small scales which are decomposed into resolved (filtered) and subgrid-scale (SGS) (residual) terms [22]. For example, any flow variable can be decomposed as:

$$\phi(x) = \overline{\phi}(x) + \phi'(x)$$ **Equation 15**

Here the spatial filtering (resolved) is:

$$\overline{\phi}(x) = \int_{\Omega} G_{\Delta}(x, y) \cdot \phi(y) \cdot dy$$ **Equation 16**

where $G_{\Delta}(x, y)$ is a non-linear flux function whose best possible approximation is the purpose of the LES. Using this procedure enables one to solve the large eddies explicitly. The small eddies are accounted implicitly by using a subgrid-scale model (SGS model).

When one applies this concept to the incompressible Navier-Stokes equation, one arrives at the filtered form [22]:

$$\frac{\partial \overline{u}_i}{\partial t} + \frac{\partial}{\partial x_j}\left(\overline{u}_i \cdot \overline{u}_j\right) = -\frac{\partial \overline{p}}{\partial x_i} + \nu \frac{\partial}{\partial x_j}\left(\frac{\partial \overline{u}_i}{\partial x_j} + \frac{\partial \overline{u}_j}{\partial x_i}\right) - \frac{\partial \tau_{ij}}{\partial x_j}$$ **Equation 17**

where $\overline{\phi}$ are the filter variables and τ_{ij} is the subgrid-scale stress defined by $\tau_{ij} \equiv \overline{u_i u_j} - \overline{u}_i \cdot \overline{u}_j$

For modelling the SGS stress the dynamic k-equation model developed by Chai and Mahesh [27] is used. The subgrid-scale stress and turbulent viscosity are defined as:

$$\tau_{ij} - \frac{2}{3} \cdot \rho \cdot k \cdot \delta_{ij} = -\mu_t \cdot S_{ij}^{*} \quad with \quad \mu_t = 2 \cdot C_s \cdot \Delta_f \cdot \rho \cdot \sqrt{k}$$ **Equation 18**

The turbulent kinetic energy of the subgrid-scale is:

$$k = \frac{1}{2} \cdot \left(\overline{u_i^2} - \overline{u}_i^2\right)$$ **Equation 19**

This model contains the Kronecker Delta function δ_{ij}, the filter size Δ_f, the filtered mean strain rate tensor S_{ij}^{*} and the model coefficient of the SGS stress (C_s) which is problem dependent and a function of time and space. Therefore, the coefficient is calculated dynamically using the resolved scales. The detailed description of the calculation of the stress coefficient and the kinetic energy is shown in Appendix F. The simulations carried out with this model are further referred to as “LES”.

4.4. Results of the Basic Simulations

This section shows the results for the simulation of the distributor geometry G1 with the basic settings as described in Chapter 4.1 and 4.2. These settings will be referred to as "base case". The influence of the two different turbulence models on the flow conditions as well as the structure of the flow is analysed in what follows.

4.4.1. Flow Structure

The big advantage of transient simulation is the possibility to investigate the development of the fluid structure over time. Unfortunately, this was only possible with the LES model, since the used RANS model only generates steady state solutions. The flow condition at different time instances is shown in Figure 4-4. It is clearly seen that the inlet section of the diffusor acts like a nozzle which leads to a free stream-like behaviour. The flow does not reattach at the walls of the steps, which is in contrary to expectations. This behaviour leads to an inhomogeneous mass flow distribution as will be shown in Chapter 4.7.2. Due to the time–invariant velocity profile at the inlet the flow conditions stabilize after five seconds, and assume a quasi-steady state behaviour afterwards.

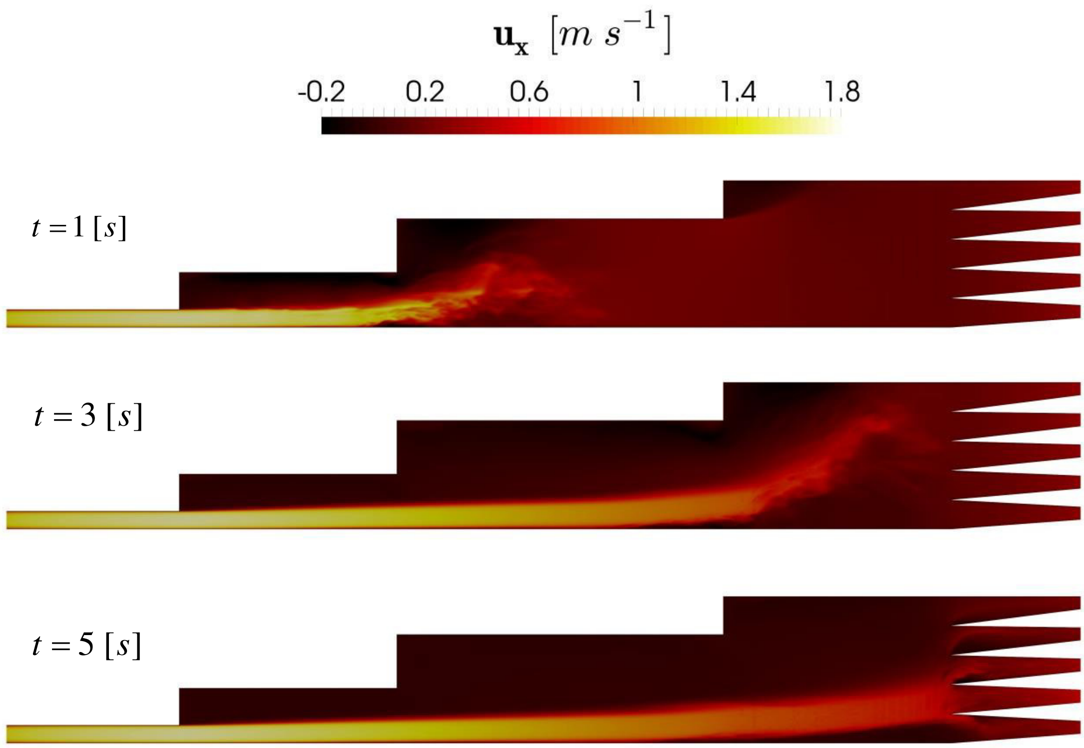

Figure 4-4: Flow structure in the distributor geometry G1 at different time instances using the LES turbulence model and base case settings at $\overline{Re_{out}} = 1500$. The data shown are instantaneous values in an *x*-*z* plane located at the centre of the channel height (i.e., at $y = 0$).

4.4.2. Comparison of the Velocity Distribution

The first flow quantity that was compared is the velocity distribution shown in Figure 4-5. It was observed that the RANS model predicted much higher energy dissipation than the LES model. The LES showed no reattachment of the flow after the steps of the diffusor, which is contrary to the observations made during the experiments. By taking a close look at the velocity gradient normal to the wall in the inlet section of the diffusor it was observed that the RANS simulations predict a steeper gradient than LES. Since the inlet profile was created with a RANS simulation (see Chapter 4.2) the velocity gradient did not match the one of the LES. This effect leads to an acceleration of the fluid in the middle of the inlet section towards the first step and even increases the free stream effect described in Chapter 4.4.1.

Looking at the mass flow it was seen that the RANS predicted a perfectly homogeneous distribution at the outlets, while the LES showed severe inhomogeneity. Both models could not represent the distribution found in the experiment. The direct comparison of the mass flow will be shown in Chapter 4.7.2.

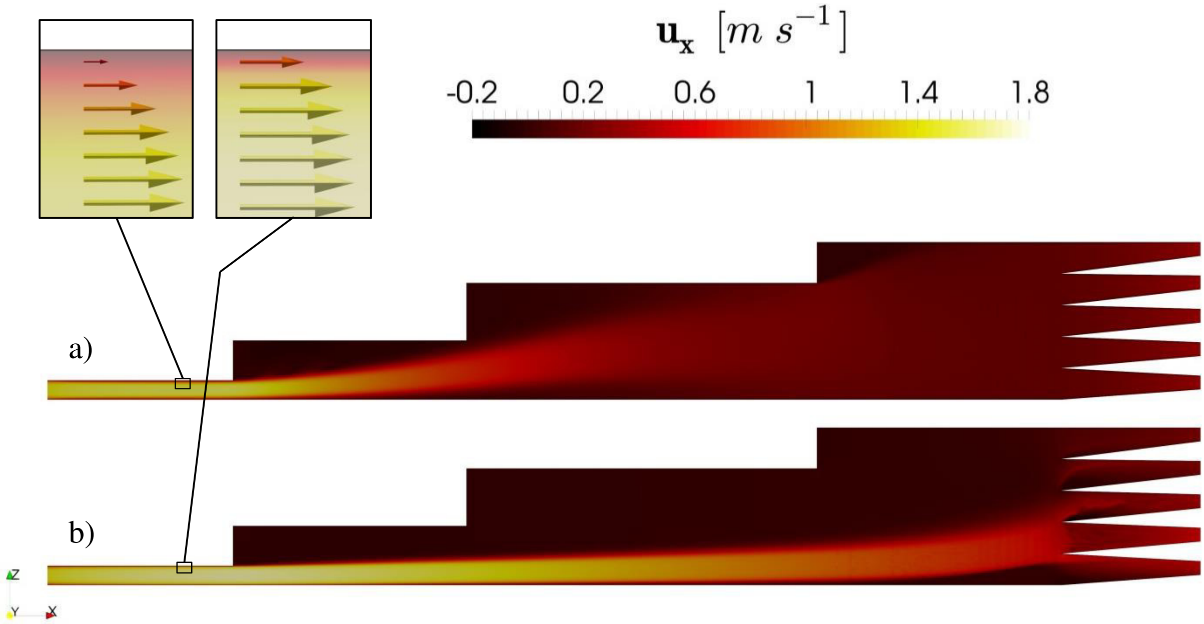

Figure 4-5: Comparison of the velocity distribution inside the distributor for the base case settings at $\overline{Re_{out}} = 1500$. The RANS model a) predicted a perfect distribution while and the LES model (shown is time-average data) b) shows a free stream-like behaviour. Both models could not sufficiently predict the mass flow distribution measured during experiments. The inserts show the velocity gradient normal to the wall caused by the near wall treatment of the turbulence model. The data shown are time averages (LES) in an *x*-*z* plane located at the centre of the channel height (i.e., at $y = 0$).

4.4.3. Comparison of the Pressure Distribution

As a second important flow metric the pressure distribution was investigated. The comparison of the RANS and LES model is shown in Figure 4-6. The pressure loss predicted by the RANS model is twice as high as the one predicted by the LES model. This is again caused by the higher dissipation predicted by the RANS model. The inhomogeneous velocity distribution in the LES, and the resulting elevated mass flow through outlet 2, lead to an increased pressure drop in that outlet port. When comparing the total pressure drop with the experimental result the LES model underpredicted by -20%, while the RANS model overpredicted by +77%. This was mainly caused by the difference in the velocity gradient normal to the wall in the inlet section of the distributor (see Chapter 4.4.2) since the pressure drop is proportional to the gradient. It is observed that in both models the mayor part of the total pressure drop is caused by the inlet section (i.e. $\Delta p_{in} \sim 84\% \cdot \Delta p_{dist}$). The detailed results and the comparison with the experimental results will be summarized in Chapter 4.7.3.

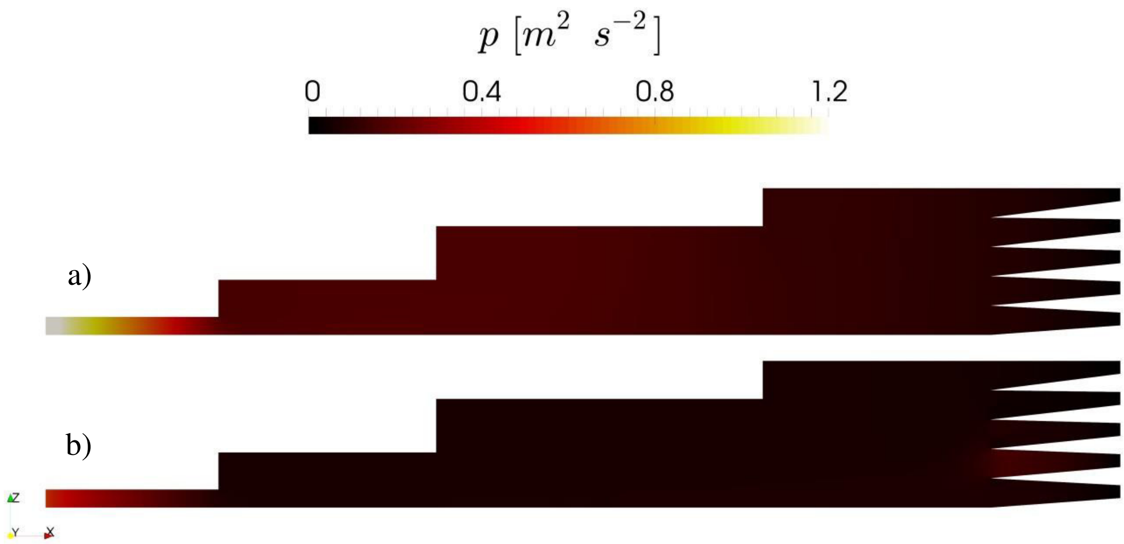

Figure 4-6: Comparison of the pressure distribution inside the distributor for the base case settings at $\overline{Re_{out}} = 1500$. The predicted values of the RANS model a) were twice as high as the ones found in the experiments while the LES model b) were slightly lower. The data shown are time averages (LES) in an *x*-*z* plane located at the centre of the channel height (i.e., at $y = 0$).

4.5. Influence of the Mesh Grid Size

Since the cell size is always a crucial parameter in finite volume simulations, a second simulation with a refined grid was performed and the influence on the flow field was investigated. In both cases the LES turbulence model with the same parameters is applied to ensure comparability. The refined grid showed a higher dissipation at the splitter inlet which leads to a more homogenous distribution. This is shown by the time averaged mass flow rates. The flow structure of both simulations is shown in Figure 4-7. The simulation with the refined grid size is further referred to as “+RES”. The detailed comparison of the results will be shown in Chapter 4.7.2 for the mass flow, and in Chapter 4.7.3 for the pressure distribution.

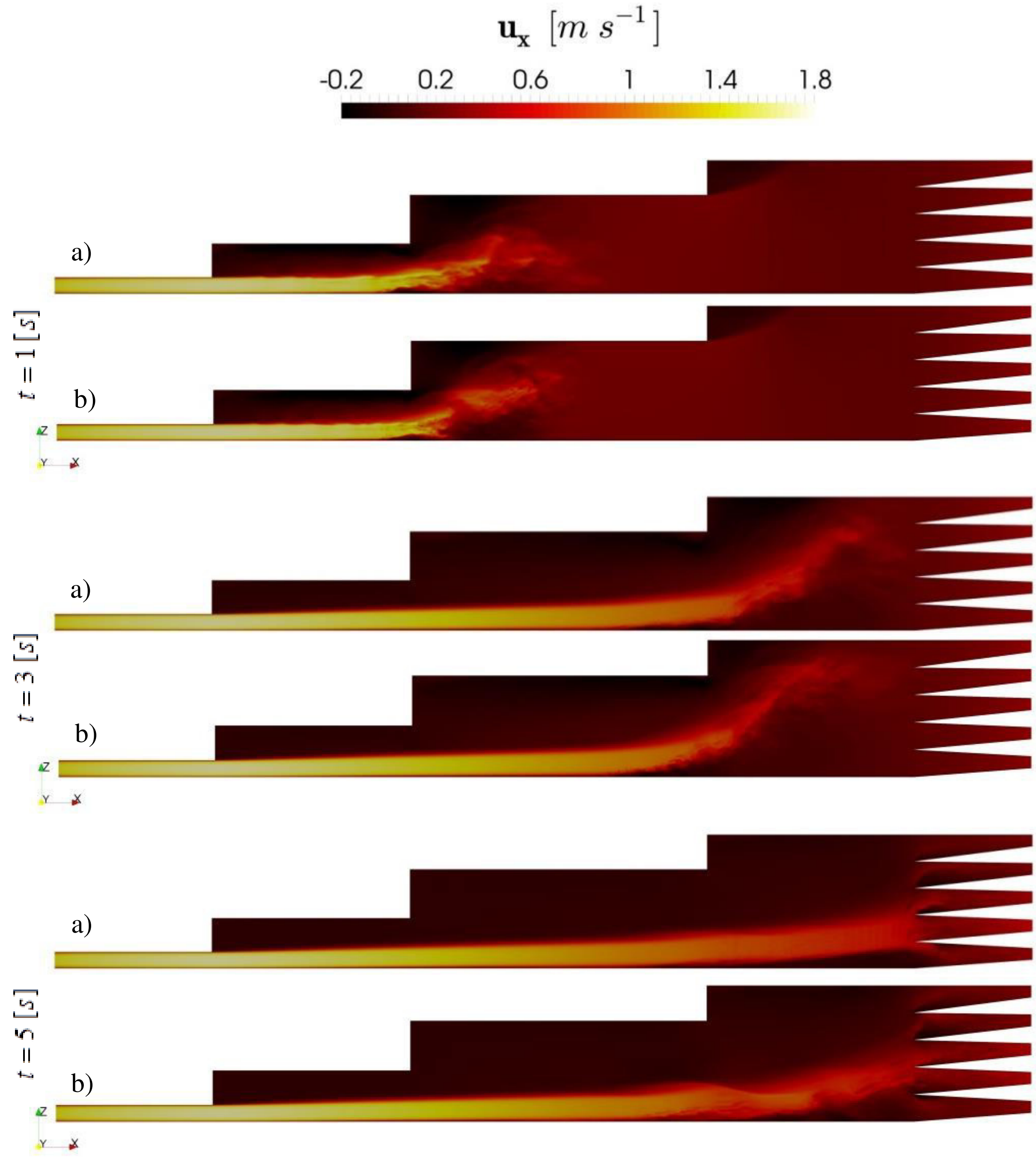

Figure 4-7: Comparison of the flow structure at different time instances of the distributor G1. a) base case domain with 1.4M cells; b) refined mesh domain with 4.3M cells at $\overline{Re}_{out} = 1500$. The refined mesh showed a higher dissipation although the comparison of the time-averaged mass flows showed no significant difference. The data shown are instantaneous values in an x-z plane located at the centre of the channel height (i.e., at $y = 0$).

4.6. Influence of the HDF Pressure Drop

One other influence that is crucial for the operation of the distributor is the additional pressure drop at the outlets caused by the HDF. A basic engineering rule states that this additional pressure drop should have a positive effect on the distribution [28]. For sufficiently high values of the pressure drop the mass flow should equalize due to the fact that the pressure differences in the distributor becomes small compared to that in the HDF. The influence on the mass flow distribution will be summarized in Chapter 4.7.2.

In order to keep the simulation effort low, the additional pressure drop of the HDF is modelled as a porous media at the outlet of the distributor. The value of the pressure drop was adjusted to match an HDF channel with ten separation side channels and a length of 2.5 meters. The model used for the additional pressure drop is the classical *Darcy-Forchheimer* type [29]:

$$-\frac{dp}{dx} = d \cdot \eta \cdot w + f \cdot \rho \cdot w^2 \qquad \textbf{Equation 20}$$

Here, d and f are the model coefficients, η and ρ are the dynamic viscosity and density of the fluid. The simulation carried out with these settings are referred to as “+HDF” in what follows.

The comparison of the velocity fields of the base case and the case with additional pressure drop is shown in Figure 4-8. In both cases an LES turbulence model is used since the RANS model already predicted an homogeneous distribution without additional pressure drop.

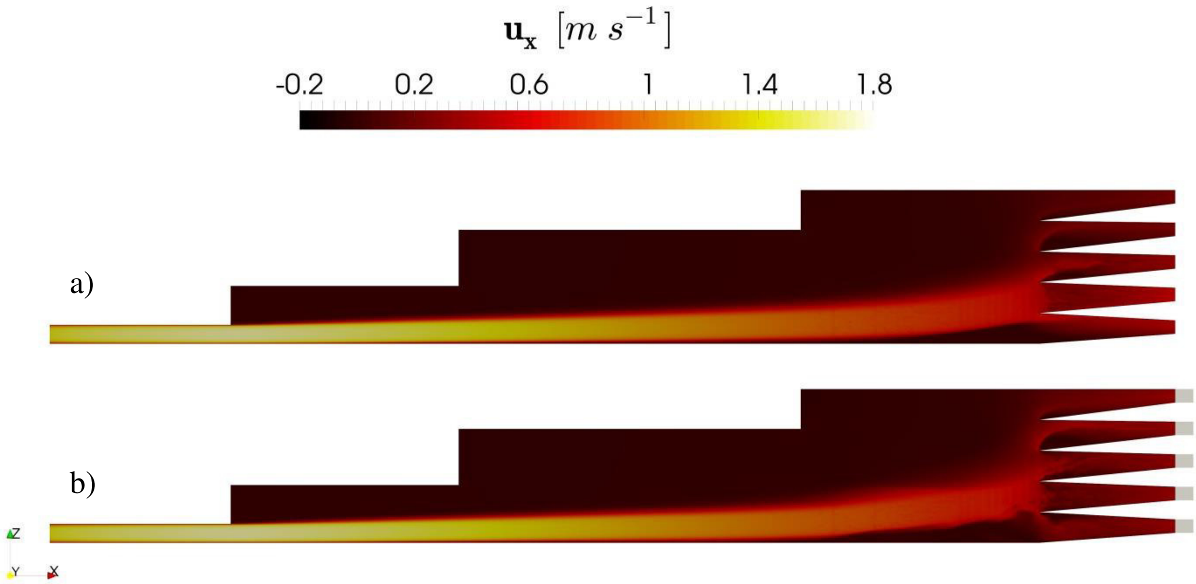

Figure 4-8: Comparison of the velocity flow field for the base case configuration (panel a) and the one with an additional pressure drop (panel b) at $\overline{Re_{out}} = 1500$. The pressure drop is realized via a porous zone at the outlet which is represented in grey in panel b. In both cases an LES turbulence model is used. The data shown are time averages in an *x-z* plane located at the centre of the channel height (i.e., at $y = 0$).

4.7. Comparison of Simulation and Experiment

In order to validate the simulation result a comparison with the experiment without fibres is executed. At first a qualitative comparison with the experiment is carried out (see Chapter 4.7.1), followed by a comparison of the mass flow distribution (see Chapter 4.7.2) and the pressure drop (see Chapter 4.7.3).

4.7.1. Qualitative Comparison with Experiment

At first the results are compared with images taken during the experiments to get a qualitative impression of the accordance of simulation and experiment. As criteria of comparison the air bubbles which deposit on the upper plate of the apparatus, and the wake formation due the diffusor steps were defined. It was assumed that the bubbles settled at the surface at a certain location if the velocity of the water in that location decreased under a distinctive value. Therefore it was possible to qualitatively identify regions with low and high velocities. These flow features are compared to the velocity distribution of the simulations. It was observed that the results from the RANS model matched the pattern quite well, while the LES model predicted a completely different flow field. A superposition of the images taken during the experiments and the flow fields generated from the simulation results are shown in Figure 4-9.

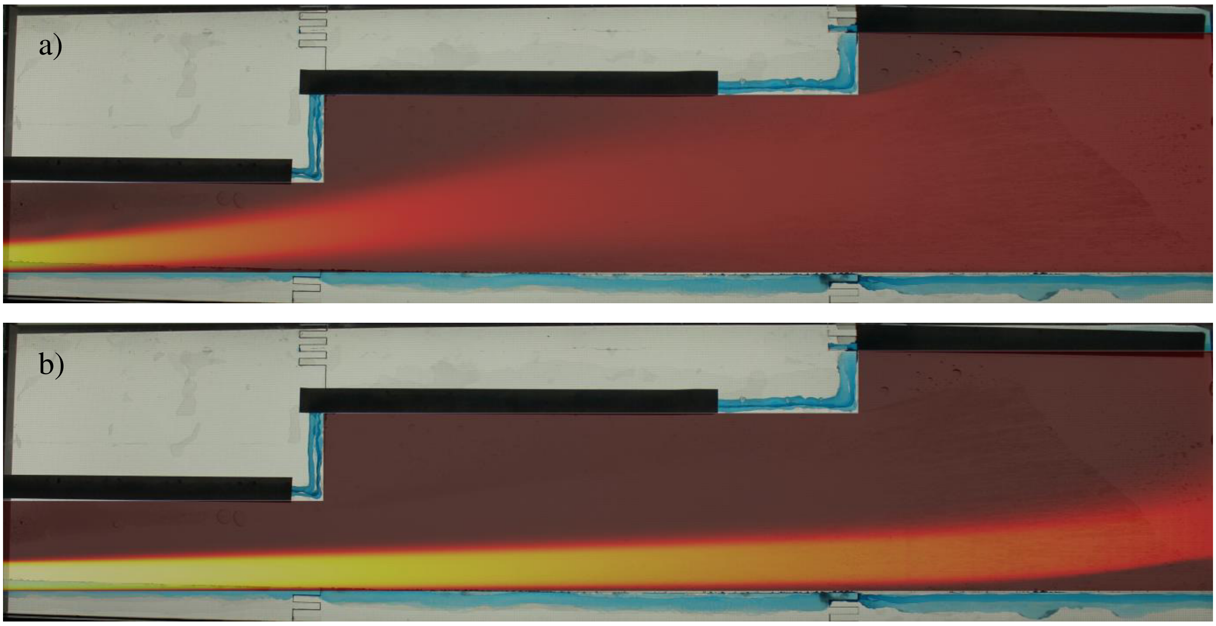

Figure 4-9: Superposition of a picture from an experiment $\left(geometry: G1;\ \overline{Re}_{out} = 1500;\ w_{fib} = 0\%\right)$ **with the velocity fields from the simulations in the step diffusor. The pattern of deposited air bubbles is chosen as criteria for comparison. The match of the RANS turbulence model a) is much better than the one from the LES b). The picture is the same in both cases.**

4.7.2. Comparison of the Mass Flow Distribution

The mass flow distribution of the experiment was compared with the simulations of the base case with different turbulence models, as well as the one with the refined grid and the simulation considering an additional pressure drop at the outlet. The mass flow distribution is the most important quantity, since it is the core feature of the distributor. The result is condensed in Figure 4-10. As shown in Chapter 4.7.1, the base case with RANS model predicted a better distribution than the experiment while the base case LES predicted a huge deviation. This deviation is also seen in the LES at higher grid resolution, although the main deviation gets shifted from outlet 1 and 2 to outlet 2 and 3. The LES with additional pressure drop (+HDF) showed, like the RANS, an almost equal distribution. However, in contrast to the RANS simulation, with the same trend as the base case LES.

The deviation between experiment and simulation could be caused by entrance effects [30], since the inlet manifold was not modelled in CFD. The assumption of a constant fully developed turbulent inlet profile may not be the optimal solution. However, it appears that entrance effects alone cannot explain the huge deviations. Further investigations in the treatment of the near wall region especially the one of the diffusor inlet section should be carried out since this seems crucial for the flow structure. It is also speculated that the grid resolution must be increased even more to get a more realistic distribution when using LES.

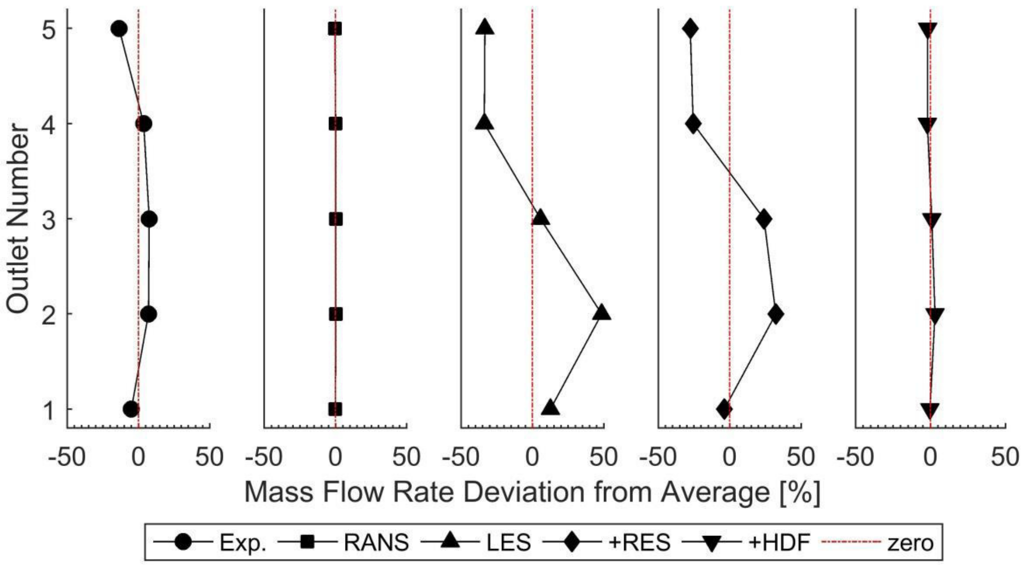

Figure 4-10: Deviation of the outlet mass flow rate from the average. The data represent the experiment (Exp.), the simulation of the base case (RANS) and (LES), LES with the refined mesh (+RES) and additional pressure drop at the outlet (+HDF). All simulations and experiments are carried out at $\overline{Re}_{out} = 1500$ without fibres. The lines are a guide for the eye.

4.7.3. Comparison of the Pressure Drop

The pressure drop of different sections of the distributor, as well as the total pressure loss is investigated. The results are shown in Table 4-2. It is observed that the majority of the pressure drop is caused by the inlet section of the diffusor. This takes up ~83% of the total pressure drop of the apparatus. Also, big differences are observed between the RANS and the LES turbulence model. The difference between the base case LES, the LES with refined simulation grid (+RES) and the LES with additional pressure drop (+HDF) is insignificant (i.e., +7% compared to base case LES).

Since during the experiments only the total pressure drop of the distributor is measured, it is only possible to compare this value with the simulation results. When comparing the experimental results, the RANS simulation predicted a much higher pressure drop (+76%), while the LES predicted a lower pressure drop (-20 %).

The conclusion from the comparison is that neither the LES nor the RANS model could provide a sufficiently accurate prediction for the pressure drop.

Table 4-2: Comparison of pressure drop of different sections of the distributor.

pressure drop Δp **of section [m² s²]**	**Experiment**	**RANS**	**LES**	**+RES**	**+HDF**
inlet	-	1.09	0.52	0.53	0.52
step 1	-	0.03	0.01	0.01	0.01
step 2	-	0.05	0.00	0.00	0.00
step 3	-	0.05	0.02	0.02	0.03
splitter	-	0.10	0.05	0.05	0.08
total	0.75	1.32	0.60	0.61	0.64

5. Conclusion

This work dealt with the development of an apparatus for distributing pulp suspensions. The purpose of the apparatus is to distribute suspension to the Hydrodynamic Fractionation Device (HDF) which will be located downstream. The HDF is a device to fractionate fibres according to their length. The main goal of this work was to design a distributer which provides an equal mass flow at each outlet without pre-fractionating the suspension. In order to reduce later operational costs, the pressure drop has to be kept as low as possible. Therefore, the approach of a forward distributor was chosen. The design of the distributor was based on the known inlet conditions of the HDF as determined in the prior experiments of König [4].

The biggest issue during the experiments was the blockage of the outlet ports. This unwanted phenomenon is also of utmost importance for later pilot scale experiments, because such a blockage would result in a fatal shutdown of the HDF. Therefore, the mechanisms of blockage formation were analysed in detail. The encountered blockages are categorized in two types which show different characteristics based on their occurrence and the removal of the deposited fibres. The most important result is that it is possible to operate the distributor even at an elevated fibre concentration of $w_{fib} = 0.5\%$ in case the mass flow is adjusted accordingly. Regime maps for the tested geometries were developed to help in deciding which mass flow is necessary to ensure a blockage-free operation. For example, for a pulp consistency of $w_{fib} = 0.5\%$ the outlet Reynolds number should be above 3,500. This is in a feasible range, since optimal fractionation conditions in and HDF are obtained at *Re* of approximately 1,500. The required drop in the Reynolds number between the outlet of the distributor and the HDF inlet can be realized, for example, by changing the cross sectional area.

The core feature of the distributor is the homogeneous mass flow distribution, and this topic was also analysed in very detail. The experimental setup was the worst case scenario for the distributor, because in a later pilot scale plant the additional pressure drop from the HDF will have a positive effect on the mass flow distribution. As it is shown experimentally in the present thesis, the distribution is already homogeneous with an average deviation of ±10%. These results are already very promising, and future investigations that include an HDF channel should yield even lower deviations of the mass flow in each channel.

The measurement of the pressure drop in the apparatus was basic, and should be seen as a rough guidance for future work. Challenges with blockages at the measurement point near the inlet manifold, as well as time-varying water levels caused by the peristaltic pump certainly eroded the measurement accuracy. Despite this drawback the acquired data showed good compliance with a simplified pressure drop model. The pressure drop of the distributor is equivalent to that of approximately 3 ÷ 10 serial HDF channels [4], whereas 10 was defined as goal for pilot scale operations.

Besides the experiments single phase CFD simulations were performed. Simulations with different turbulence models, grid resolutions and modifications of the outlet were performed. Unfortunately, neither the results with a RANS nor with a LES turbulence model are sufficient to represent the measured flow conditions in the apparatus. The results obtained with LES, a refined grid resolution, and an additional outlet pressure indicated the most promising results. However, they were still not accurately representative of the experiment data, with a deviation of the pressure drop in the order of 20%. For a first rough estimate of new distributor geometries only LES is an option, since RANS predicted a much too optimistic (i.e., an almost perfect) mass flow distribution. Due to the lack of agreement between experiment and simulation, it is vital for further geometrical variations to execute experiments to investigate the functionality of the distributor. Foremost because the influence of the fibres is neglected in the single phase simulation, experiments are necessary especially for fibre concentrations above 0.1% which are of industrial interest. Hence, more advanced CFD simulations, e.g., similar to those of Hämäläinen [31] would be necessary for a prior *in silico* evaluation of the distributor performance considering such consistencies.

6. Outlook

The findings of this thesis showed that a future development of the forward distributor should be carried out to further investigate the influence of the step size of the diffusor, as well as the geometry of the splitter. According to the simulations the majority of the pressure drop is caused at the inlet section of the step diffusor. Thus, changing the size of the inlet cross section and reducing the step height in the diffusor should lead to a reduction of the pressure drop.

Before carrying out further experiments with the distributor, it is recommended to redesign the pressure measuring point to prevent blockages and install proper digital pressure sensors (i.e. IP65, measuring range 0 – 10 kPa) at the inlet. Blockage detection could also be implemented by placing pressure sensors between every splitter spike. The blockage can be detected by observing increased static pressure levels compared to the normal operation.

Another aspect regard further numbering up of outlets is the mass flow measurement. With further increase of outlet ports it won't be possible to do these simultaneous measurements by hand. Different solutions like a jib-arm with timing triggered by light barriers or pressure switches should be considered. As next best solution the measurement could be done progressively which bears the possibility of measuring time dependant fluctuations.

The next step towards a pilot scale plant must be the investigation of the influence of the distributor on the HDF. Furthermore, an automatic backwashing device (e.g., based on a magnetic valve that triggers a pressure pulse) should be installed to remove blockages from the outlet port. Another aspect for pilot scale application should be the change from a rectangular to circular cross section of the HDF channels. While visual observations will become much more difficult, this allows for an easier manufacturing at larger numbers and increased reliability.

Finally, implementation of a cross flow distributor instead of a forward distributor should also be looked into because it is the state of the art technology in paper machines. Although the pressure drop is expected to be much higher, the homogeneity of the mass flow distribution should increase according to experts from paper machine manufacturers [9]. However, investigations with basic CFD simulations carried out during this thesis could not support this argument for the comparably low-Reynolds-number operating conditions relevant for HDFs. Clearly, using a cross flow distributor would also necessitate significant testing to operate it properly and without blockage.

7. References

[1] “Bio-Based Industries Joint Undertaking.” [Online]. Available: https://bbi-europe.eu/about/about-bbi. [Accessed: 11-Aug-2017].

[2] M. Mayr *et al.*, “Flippr°-an industrial research project in Austria,” *TAPPI J.*, vol. 14, no. 3, pp. 209–212, 2015.

[3] R. S. Seth, “The measurement and significance of fines,” *Pulp Pap. Canada*, vol. 104, no. 2, pp. 41–44, 2003.

[4] J. König, “Experimental Study of Separation of Fines from Fiber Suspensions with Hydrodynamic Filtration,” M.S. thesis, Graz University of Technology, 2016.

[5] T. Timmel, “Flippr2 - Future Lignin and Pulp Processing Research.” [Online]. Available: http://www.flippr.at/jart/prj3/flippr/main.jart. [Accessed: 11-Aug-2017].

[6] H. Heinzmann, “Headbox for distributing pulp suspension and additives,” European Patent EP 0 985 762 B1, 2003.

[7] E. Weisshuhn, “Headbox apparatus for papermaking maschine,” U.S. Patent 4 897 158, 1990.

[8] R. Hegbert, “A Headbox Apparatus,” International Patent WO 93/09286, 1993.

[9] M. Wiltsche, “Personal Communication”, Graz University of Technology, 13-Dez-2016.

[10] M. Wiltsche, *Lecture Notes: Papier- und Kartonherstellung*. Graz University of Technology, 2007.

[11] S. G. Mason, “The Flocculation of Cellulose Fibre Suspensions,” *Pulp Pap. Canada*, pp. 99–104, 1948.

[12] R. Kerekes, “Rheology of fibre suspensions in papermaking: An overview of recent research,” *Nord. Pulp Pap. Res. J.*, vol. 21, no. 5, pp. 598–612, 2006.

[13] S. . Kao and S. G. Mason, “Dispersion of particles by shear,” *Nature*, vol. 253, pp. 619–621, 1975.

[14] L. H. Switzer and D. J. Klingenberg, “Rheology of sheared flexible fiber suspensions via fiber-level simulations,” *J. Rheol. (N. Y. N. Y).*, vol. 47, no. 3, p. 759, 2003.

[15] H. J. Youn and H. L. Lee, “A numerical study of flow behaviour in the turbulence generator of headboxes,” *Appita J.*, vol. 58, no. 3, pp. 196–201, 2005.

[16] Anwar-ul-Haque, F. Ahmad, S. Yamada, and S. R. Chaudhry, “Assessment of Turbulence Models for Turbulent Flow over Backward Facing Step,” *World Congr. Eng. 2007*, vol. II, pp. 1–6, 2007.

[17] R. Eckhart, “Personal Communication”, Graz University of Technology, 07-Aug-2017.

[18] “Fibre Tester Plus User Manual,” *Lorentzen & Wettre*, 2015.

[19] M. Eßl, “Geometry Optimization for Multi Side Channel - Hydrodynamic Fractionation Device.” Construction thesis; Graz University of Technology, 2016.

[20] H. Schade and E. Kunz, *Strömungslehre*, 3rd ed. Berlin, Germany: Walter de Gruyter, 2007.

[21] C. J. Greenshields, “OpenFOAM User Guide 3.x,” *OpenFOAM Found. Ltd*, 2015.

[22] P. Sagaut, *Large Eddy Simulation for Incompressible Flows*, 3rd ed. Berlin, Heidelberg: Springer, 1998.

[23] J. H. Ferziger and M. Perić, *Computational Methods for Fluid Dynamics*, 3rd ed. Berlin, Heidelberg: Springer Berlin Heidelberg, 2002.

[24] F. R. Menter, “Two-Equation Eddy-Eiscosity Turbulence Models for Engineering Applications,” *AIAA J.*, vol. 32, no. 8, pp. 1598–1605, 1994.

[25] W. P. Jones and B. E. Launder, “The Calculation of Low-Reynolds-Number Phenomena with a Two-Equation Model of Turbulence,” *Int. J. Heat Mass Transf.*, vol. 16, pp. 1119–1130, 1973.

[26] D. C. Wilcox, “Reassessment of the Scale-Determining Equation for Advanced Turbulence Models,” vol. 26, no. 11, pp. 1299–1310, 1988.

[27] X. Chai and K. Mahesh, “Dynamic k -equation model for large-eddy simulation of compressible flows,” pp. 385–413, 2012.

[28] M. Saber, J. M. Commenge, and L. Falk, “Rapid design of channel multi-scale networks with minimum flow maldistribution,” *Chem. Eng. Process. Process Intensif.*, vol. 48, no. 3, pp. 723–733, 2009.

[29] H. D. Baehr and K. Stephan, *Wärme-und Stoffübertragung*, 9th ed. Berlin, Heidelberg: Springer Vieweg, 2016.

[30] R. Payri, J. Gimeno, P. Marti-Aldaravi, and G. Bracho, “Study of the influence of the inlet boundary conditions in a LES simulation of internal flow in a diesel injector,” *Math. Comput. Model.*, vol. 57, no. 7–8, pp. 1709–1715, 2013.

[31] T. Hämäläinen, “Modelling of Fibre Orientation and Fibre Flocculation Phenomena in Paper Sheet Forming,” Ph.d. thesis, Tampere University of Technology, 2008.

Appendix A Simulation Results - Extended Forward Distributor

As described in the introduction (see Chapter 1) the distributor with five outlet ports, which was designed and built during this thesis was the first step towards a pilot scale plant. As the next step the geometry G1 is mirrored at the x-y plane. This results in a symmetrical step diffusor with ten outlets, which allows doubling the throughput. This geometry is only investigated via CFD simulations.

A.1 Simulation Setup – Extended Forward Distributor

In order to compare the results of the standard distributor with five outlet ports and the extended one with ten outlets the same boundary condition, initial values and turbulence models are used (see Chapter 4.1, 4.2 and 4.3). Since the cross section of the inlet is also extended the inlet velocity profile was also recalculated. The same procedure as described in Chapter 4.2 was applied to achieve $\overline{Re_{out}} = 1500$ at the outlet ports. The dimensions of the domain are shown in Figure A-1. The simulation domain consists of 2.770.000 hexagonal cells and the same grading pattern as for the standard distributor was applied (i.e. decreased cell size towards the wall in y-direction (height) and towards the steps in x-direction (length)).

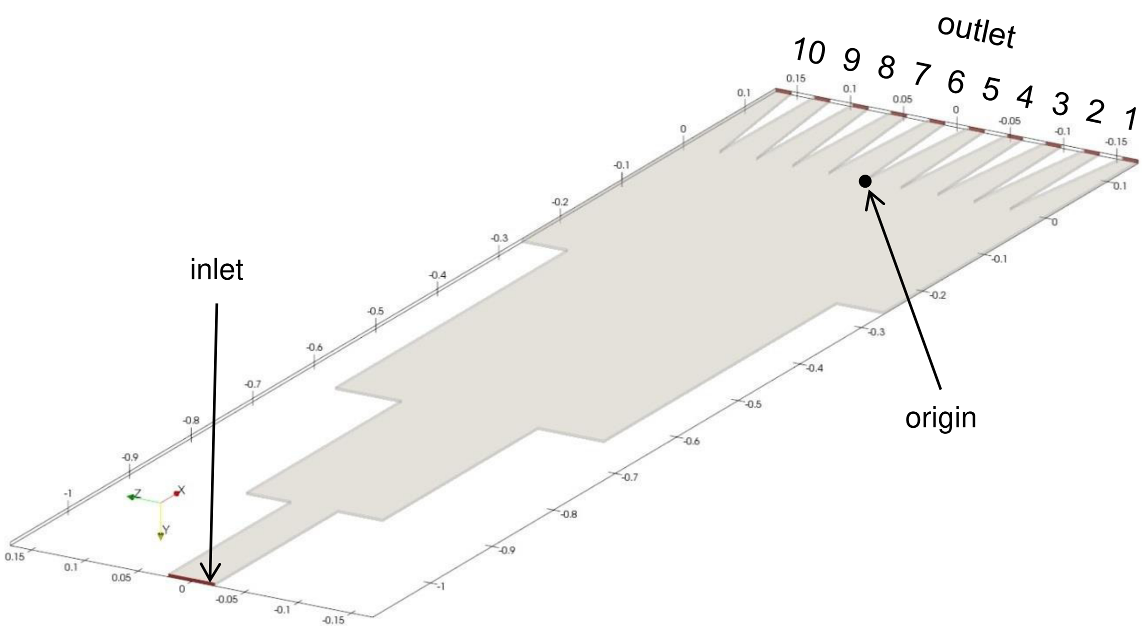

Figure A-1: Dimensions and coordinates of the simulation domain of the extended geometry with ten outlet ports. All inlet and outlet patches are marked in red. All other external faces are walls. The dimensions are given in meters. No geometrical scaling was applied.

A.2 Velocity and Mass Flow Distribution - Extended Forward Distributor

As described in Chapter 4.7.2 the velocity and mass flow distribution is the most important flow quantity of the apparatus. The comparison of velocity distribution for the RANS and LES turbulence model is shown in Figure A-2. For the extended geometry the same flow structure as for the standard geometry is observed. As in the standard geometry the RANS model predicted a perfectly homogeneous distribution at the outlets. The LES model predicted severe inhomogeneity, which in contrast to the standard geometry had an even higher deviation at the centred outlet ports (i.e. outlet 4-7). The deviation of the mass flow rate over the outlet ports in the extended geometry are symmetric at the x-y plane, which was expected. Unfortunately, for this geometry there are no experimental data available to validate the results of the simulations. By taking a close look at the inlet section of the diffusor it was observed that the velocity gradient normal to the wall was much steeper in the RANS simulation than in the LES. These flow conditions were also seen in the simulations with the standard geometry (see Chapter 4.4.2).

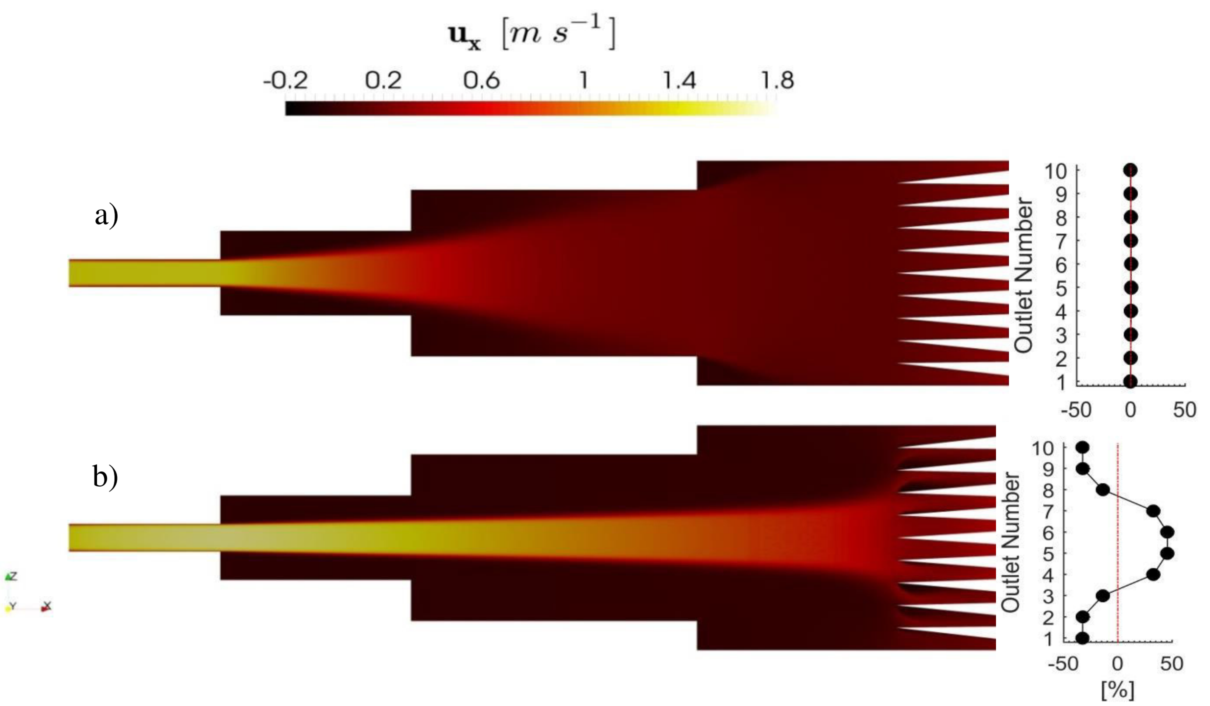

Figure A-2: Comparison of the velocity distribution inside the distributor for the extend geometry at base case settings and $\overline{Re_{out}} = 1500$. The RANS model a) predicted a perfect distribution while the LES model (shown is the time-averaged data) b) shows a free stream-like behaviour. The diagrams represents the relative mass flow deviation from the average in percent. The data shown are in an x-z plane located at the centre of the channel height (i.e., at $y = 0$).

A.3 Pressure Distribution - Extended Forward Distributor

As a second flow quantity, the pressure distribution was investigated. The comparison of pressure distribution for the RANS and LES turbulence model is shown in Figure A-3. As in the standard geometry the pressure loss predicted by the RANS model was twice as high as the one predicted by the LES model (see Chapter 4.4.3). In both models the mayor part of the total pressure drop was caused by the inlet section of the distributor. This was mainly due to the difference in the velocity gradient normal to the wall in this section since the pressure drop is proportional to the gradient (see Chapter 4.4.2). The total pressure drop predicted by the RANS model was lower for the extended geometry compared with the standard one (see Chapter 4.4.3). This was caused by an increased inlet Reynolds number in the extended geometry that had a direct influence on the wall treatment of the RANS model. The inlet Reynolds numbers were different because the hydraulic diameter at the inlet was increased while in order to keep the same outlet mass flow the mean inlet velocity remained unchanged.

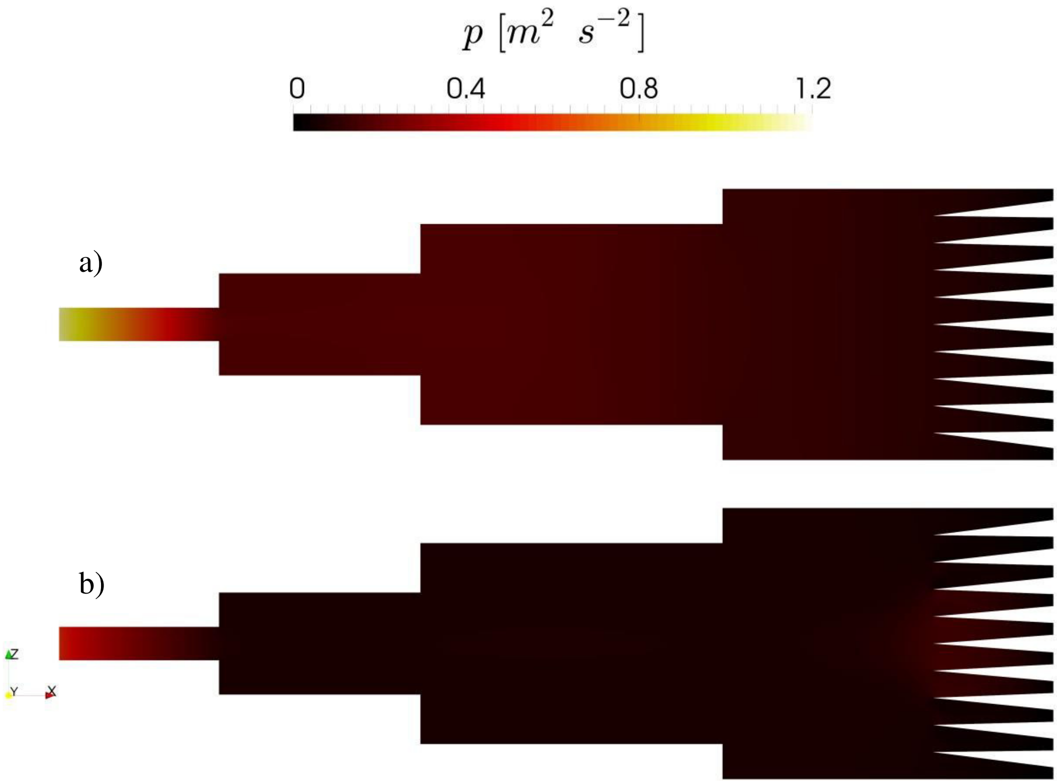

Figure A-3: Comparison of the pressure distribution inside the distributor for the extended geometry at base case settings. The predicted values of the RANS model a) were twice as high as the ones of the LES model b). The data shown are time averages (LES) in an *x-z* plane located at the centre of the channel height (i.e., at $y = 0$)

Appendix B Simulation Results - Cross Flow Distributor

Since the current state of the art for paper machine headboxes is the cross flow distributor, also this topic was briefly looked into. The same concept is also used in heat exchangers. In that case, the cross section of the main channel is mainly constant and an equal mass flow is achieved by tailoring the resistance of each side channel with valves. This option is not favourable for pulp suspensions since the fibres tend to block the valves. The main advantage of the cross flow distributor compared with the forward distributor is the compact design. This geometry is investigated only via CFD simulations.

B.1 Simulation Setup - Cross Flow Distributor

For this simulations the same boundary condition, initial values and turbulence models as in the ones with the forward distributor are used (see Chapter 4.1, 4.2 and 4.3). The recirculation is treated like a normal outlet. For calculation of the inlet velocity profile the same procedure as described in Chapter 4.2 was applied to achieve $\overline{Re}_{out} = 1000$ at the outlet ports. The side channels are aligned against the flow direction in the distributor channel according to the investigations by König [4]. The simulation domain consists of 1.129.000 hexagonal cells. The dimensions of the domain are shown in Figure B-1. For this set of simulations only the RANS turbulence model was used in order to keep the computational effort manageable.

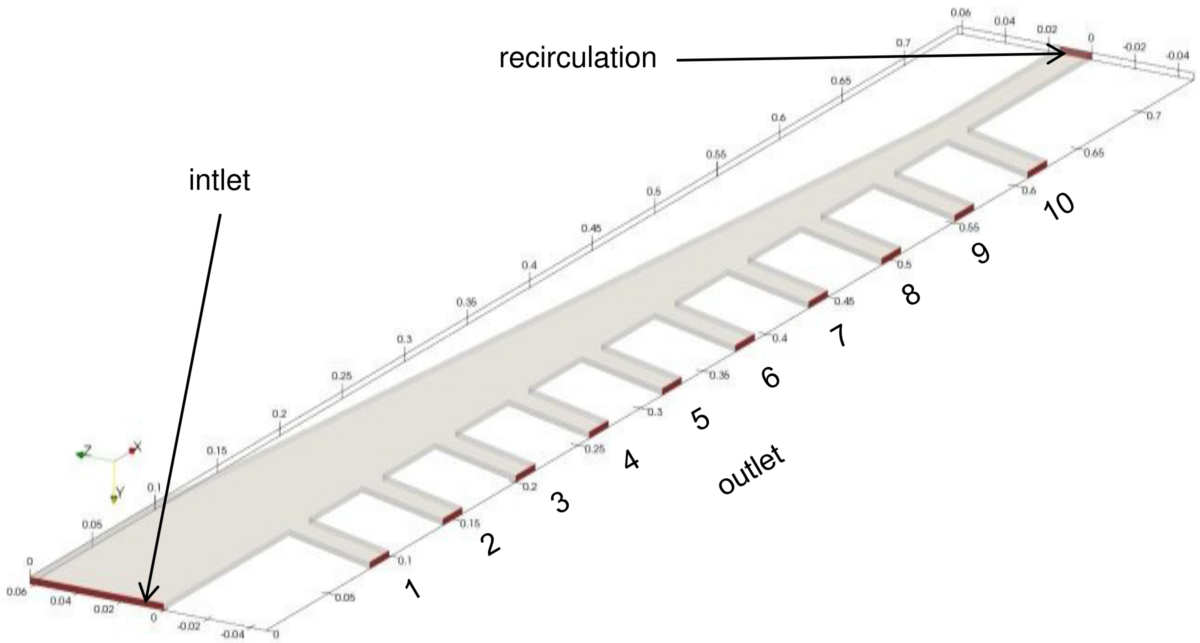

Figure B-1: Dimensions and coordinates of the simulation domain of the cross flow distributor with ten outlet ports. The recirculation is used to avoid ram pressure at outlet 10. All inlet and outlet patches are marked in red. All other external faces are walls. The dimensions are given in meters.

B.2 Velocity and Mass Flow Distribution - Cross Flow Distributor

As first flow quantity, the velocity distribution was looked into. The formation of wakes in the inlet section of the side channels was expected. However, the extent of the recirculation zone was underestimated and in some cases almost reached the outlet, which is unfavourable for the chosen boundary condition. Therefore, the length of the side channels should be increased in further simulations. The simulation showed a severe inhomogeneity in the mass flow distribution. In order to get a more homogeneous distribution an additional pressure drop at the side channels as described in Chapter 4.6 was added. In contrast to the forward distributor, the additional pressure drop had to be doubled to reach a homogeneous distribution (see Chapter B.3 and Chapter 4.6). The pitch of the main channel is also crucial for the mass flow distribution. Hence, further variations of this parameter should be carried out. The comparison of the velocity and mass flow distribution of the standard cross flow geometry and the one with additional pressure drop is shown in Figure B-2.

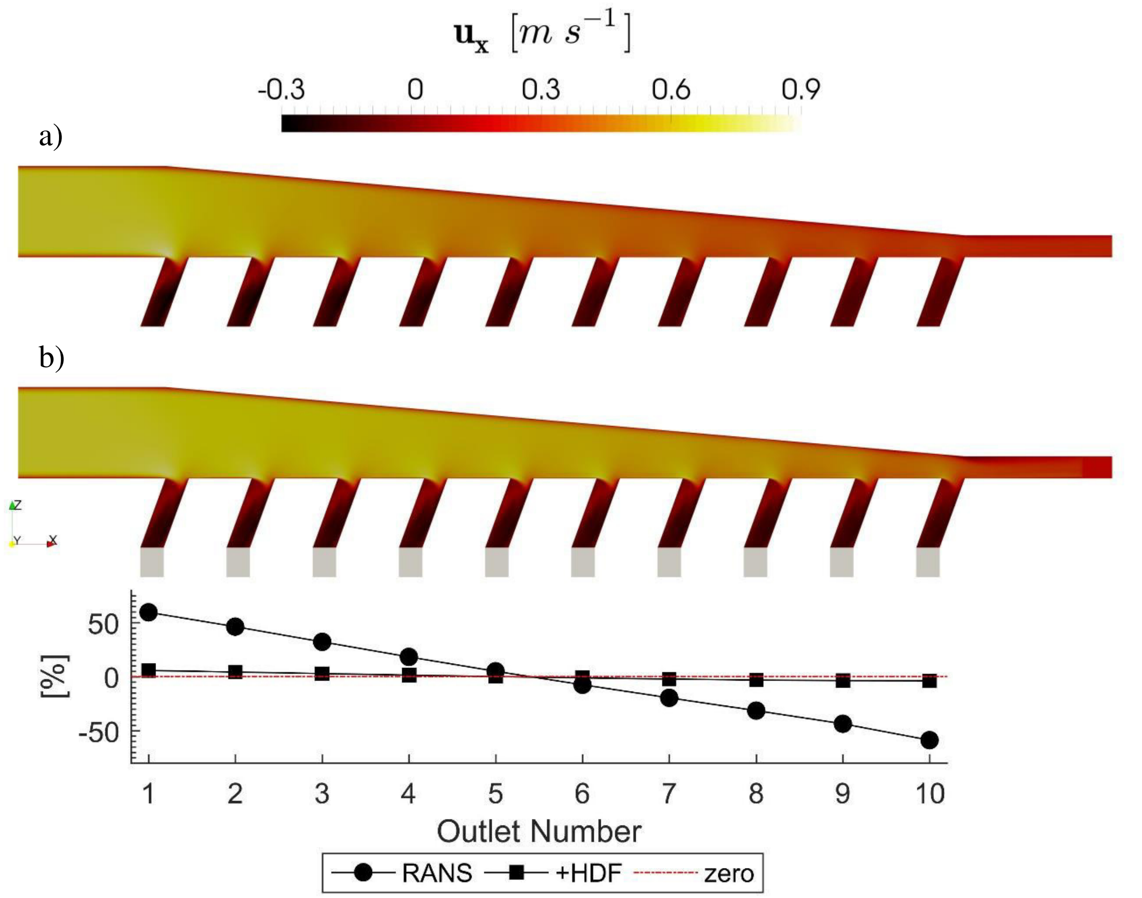

Figure B-2: Comparison of the velocity distribution inside the cross flow distributor at $\overline{Re_{out}} = 1000$. The standard case a) predicted an inhomogeneous distribution compared to the case with additional pressure loss b), which predicts a perfectly homogeneous one. The diagram represents the relative mass flow deviation from the average in percent. The data shown are in an *x*-*z* plane located at the centre of the channel height (i.e., at $y = 0$).

B.3 Pressure Distribution - Cross Flow Distributor

Besides the velocity, also the pressure distribution was investigated. In order to achieve an equal mass flow in the side channels the pressure should be equal at every side channel inlet. As shown in Figure B-3 this is not applicable for the case without additional pressure drop at the side channel outlets. The pitch of the main channel is again the crucial parameter for the equal pressure distribution and depends on the induced and friction losses in the channel. During the design of the geometry it was not possible to calculate these losses with reasonable accuracy in advance, therefore they were neglected. The outlet of the main channel, which is used for recirculation in paper machines, was in these simulations treated like the side channel outlets. Besides the pitch of the main channel, the recirculation is also an important parameter for the pressure distribution. The additional pressure drop was set to an equivalent of 20 serial HDF channels which would be twice as much as it is planned in the pilot scale application. In further investigations this parameter should be varied last and the focus should be on the pitch of the main channel and the recirculation.

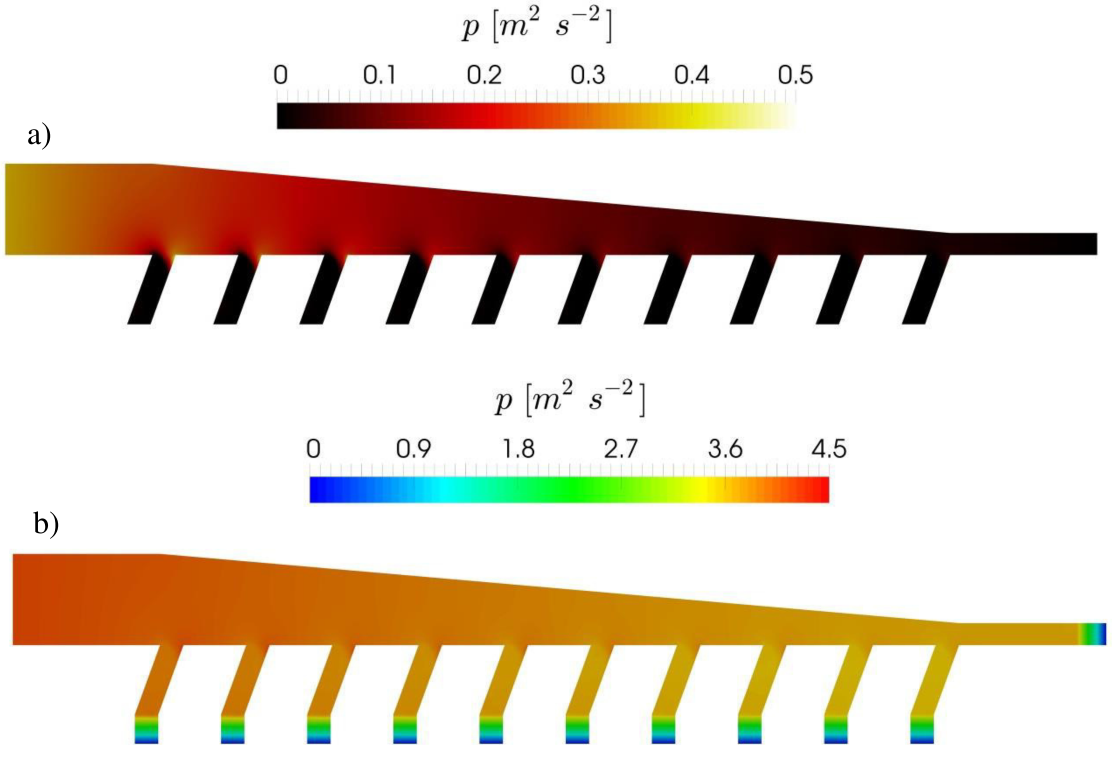

Figure B-3: Comparison of the pressure distribution inside the cross flow distributor at $\overline{Re}_{out} = 1000$. The standard case a) predicted a more inhomogeneous distribution than the case with additional pressure loss b). The additional pressure drop is set to approximately nine times the pressure drop caused by the distributor. The data shown are in an *x*-*z* plane located at the centre of the channel height (i.e., at $y = 0$).

Appendix C Calculation

In this section the pressure drop model used in Chapter 3.4.4 is derived from the Bernoulli equation. In order to support a better understanding a sketch of the whole apparatus is provided in Figure C-1. The variation of the air pressure at the different locations is neglected. Hence, the static pressure is the same at all locations (i.e. $p_0 = p_1 = p_2$).

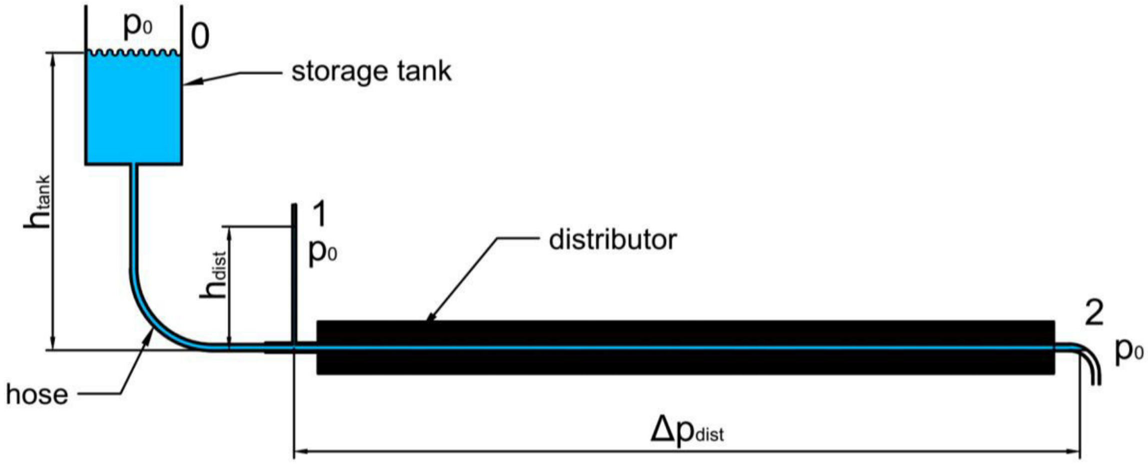

Figure C-1: Sketch for calculation of the pressure drop, the geodesic heights of the storage tank h_{tank} and the inlet manifold h_{dist} are measured during the experiments.

The Bernoulli equation applied from location 0 to 1 is:

$$p_0 + \rho \cdot \frac{w_0^{\,2}}{2} + \rho \cdot g \cdot h_{\text{tank}} = p_1 + \rho \cdot \frac{w_1^{\,2}}{2} + \rho \cdot g \cdot h_{\text{dist}} + \Delta p_{\text{tank}} + \Delta p_{hose} \qquad \textbf{Equation 21}$$

Where w_i is the mean flow velocity, Δp_{tank} is the entrance pressure loss of the storage tank and Δp_{hose} is the pressure loss in the hose that connects the storage tank to the distributor. Assuming that the water level at location 0 and 1 are constant implies $w_0 = w_1 = 0$. Since the static pressure is also the same at these locations (i.e. $p_0 = p_1$) Equation 21 is reduced to:

$$\rho \cdot g \cdot \left(h_{\text{tank}} - h_{\text{dist}}\right) = \Delta p_{\text{tank}} + \Delta p_{hose} \qquad \textbf{Equation 22}$$

The Bernoulli equation applied from location 0 to 2 is:

$$p_0 + \rho \cdot \frac{w_0^{\,2}}{2} + \rho \cdot g \cdot h_{\text{tank}} = p_2 + \rho \cdot \frac{w_2^{\,2}}{2} + \rho \cdot g \cdot h_2 + \Delta p_{\text{tank}} + \Delta p_{hose} + \Delta p_{dist} \qquad \textbf{Equation 23}$$

The geodesic height of the outlet is zero (i.e. $h_2 = 0$). Applying the assumptions that $p_0 = p_2$ and $w_0 = 0$ one gets:

$$\rho \cdot g \cdot h_{\text{tank}} = \rho \cdot \frac{w_2^{\,2}}{2} + \Delta p_{\text{tank}} + \Delta p_{hose} + \Delta p_{dist}$$ **Equation 24**

Combining Equation 22 and Equation 24 results in:

$$\rho \cdot g \cdot h_{\text{dist}} = \rho \cdot \frac{w_2^{\,2}}{2} + \Delta p_{dist}$$ **Equation 25**

Since the Reynolds number is in the transitional regime, the used model to describe the pressure loss in the distributor is a combination of the laminar and turbulent pressure drop model as described in Equation 11.

$$\Delta p_{dist} = \rho \cdot \left(\zeta_{turb} \cdot w_2^{\,2} + \zeta_{lam} \cdot \frac{\nu}{d_h} \cdot w_2 \right)$$ **Equation 26**

Here, ζ_{turb} and ζ_{lam} are the pressure loss coefficients, d_h is the hydraulic diameter of the outlet channel ($d_h = 5\ mm$) and ν is the kinematic viscosity of water at 20°C ($\nu = 1.04 \cdot 10^{-6} m^2 s^{-1}$). Using this model in Equation 25 one gets:

$$\rho \cdot g \cdot h_{\text{dist}} = \rho \cdot \frac{w_2^{\,2}}{2} + \rho \cdot \left(\zeta_{turb} \cdot w_2^{\,2} + \zeta_{lam} \cdot \frac{\nu}{d_h} \cdot w_2 \right)$$ **Equation 27**

Finally the exit loss $\rho \cdot \frac{w_2^{\,2}}{2}$ is also combined with the turbulent (i.e. quadratic) term. This leads to the final correlation of the measured geodesic height (i.e. pressure drop) to the outlet flow rate.

$$\rho \cdot g \cdot h_{\text{dist}} = \rho \cdot \left(\zeta_{turb} \cdot w_2^{\,2} + \zeta_{lam} \cdot \frac{\upsilon}{d_h} \cdot w_2 \right)$$ **Equation 28**

Alternatively, when expressing the velocity by the Reynolds number:

$$\rho \cdot g \cdot h_{\text{dist}} = \rho \cdot \frac{\nu^2}{d_h^{\,2}} \cdot \left(\zeta_{turb} \cdot Re^2 + \zeta_{lam} \cdot Re \right)$$ **Equation 29**

The pressure loss coefficients ζ_{turb} and ζ_{lam} are fitted to the experimental data via the least-squares method. The values are collected in Table 3-1.

Appendix D Technical Drawings

This section contains the technical drawings for the manufacturing of the distributor.

000	Assembly Drawing of Distributor
001	Inlay
002	Top and Bottom Plate
003	Clamp for distributor
004	Clamp for Inlet Manifold
007	Clamp for Outlet
008	Drip Pan

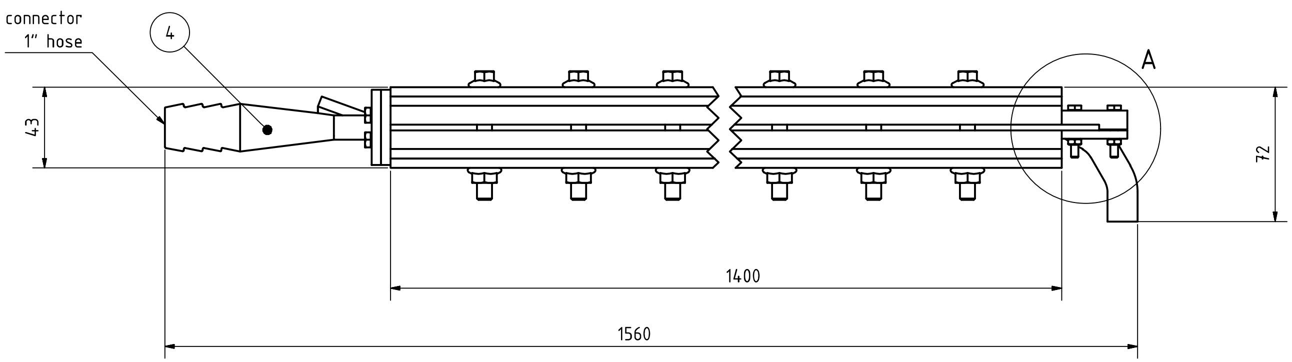

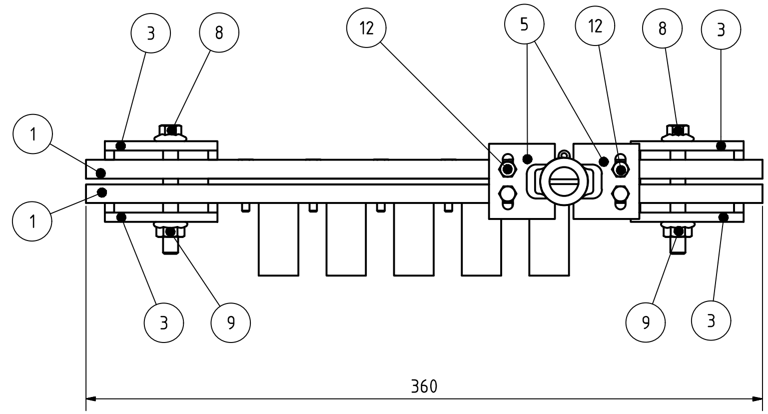

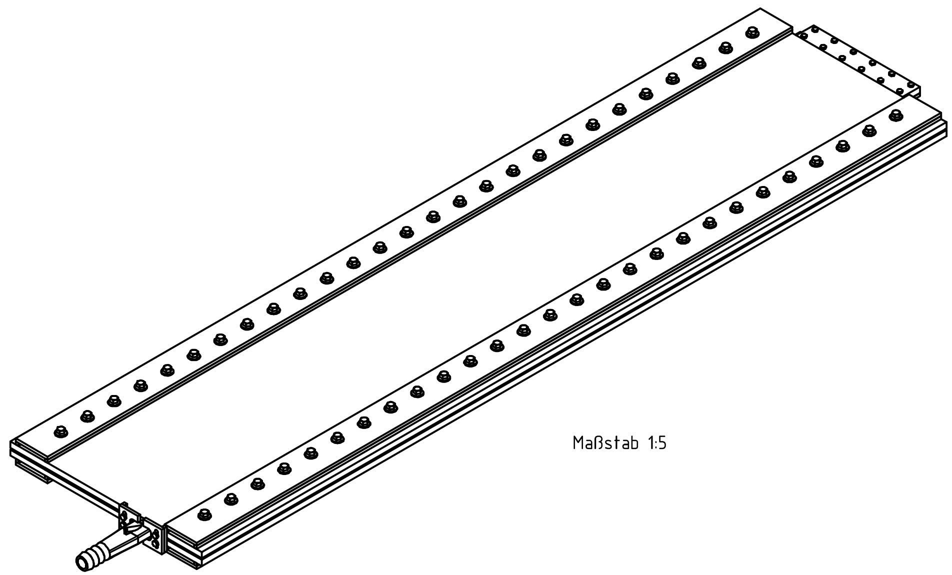

Maßstab 1:5

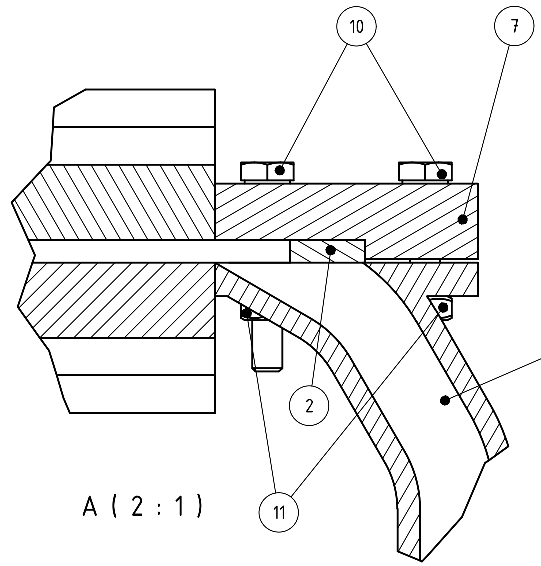

A (2 : 1)

TEILELISTE				
OBJEKT	ANZAHL	BAUTEILNUMMER	MATERIAL	BESCHREIBUNG
1	2	flowDistributor_plate	Polycarbonat, klar	Drawing Nr.: IPPT/T_2_2_2_f/002
2	1	flowDistributor_channel_inlay	ABS-Kunststoff	Drawing Nr.: IPPT/T_2_2_2_f/001
3	4	flowDistributor_klamp	Stahl - S235J0	Drawing Nr.: IPPT/T_2_2_2_f/003
4	1	flowDistributor_manifold	ABS-Kunststoff	
5	2	flowDistributor_manifold_klamp	Stahl, S235J0	Drawing Nr.: IPPT/T_2_2_2_f/004
6	1	flowDistributor_outlet_bottom	ABS-Kunststoff	
7	1	flowDistributor_outlet_clamp	Polycarbonat, klar	Drawing Nr.: IPPT/T_2_2_2_f/007
8	54	ISO 4162 - M8 x 60	Edelstahl	Sechskantschrauben mit Flansch
9	54	ISO 4161 - M8	Edelstahl	Sechskantmuttern mit Flansch
10	12	ISO 4017 - M4 x 25	Edelstahl, 440C	Sechskantschrauben mit Ganzgewinde
11	12	ISO 4032 - M4	Edelstahl, 440C	Sechskantmuttern
12	4	ISO 4017 - M5 x 35	Edelstahl, 440C	Sechskantschrauben mit Ganzgewinde

TU Graz

Allg. Tol.
mk
ISO 2768-1

	Datum	Name
Erstellt	28.11.2016	Michael Eßl
Kontroll.		
Norm		

Maßstab: 1:2
Masse: -
Werkstoff:

Distributor - Assembly

IPPT/T_2_2_2_f/000

1

A2

Status | Änderungen | Datum | Name

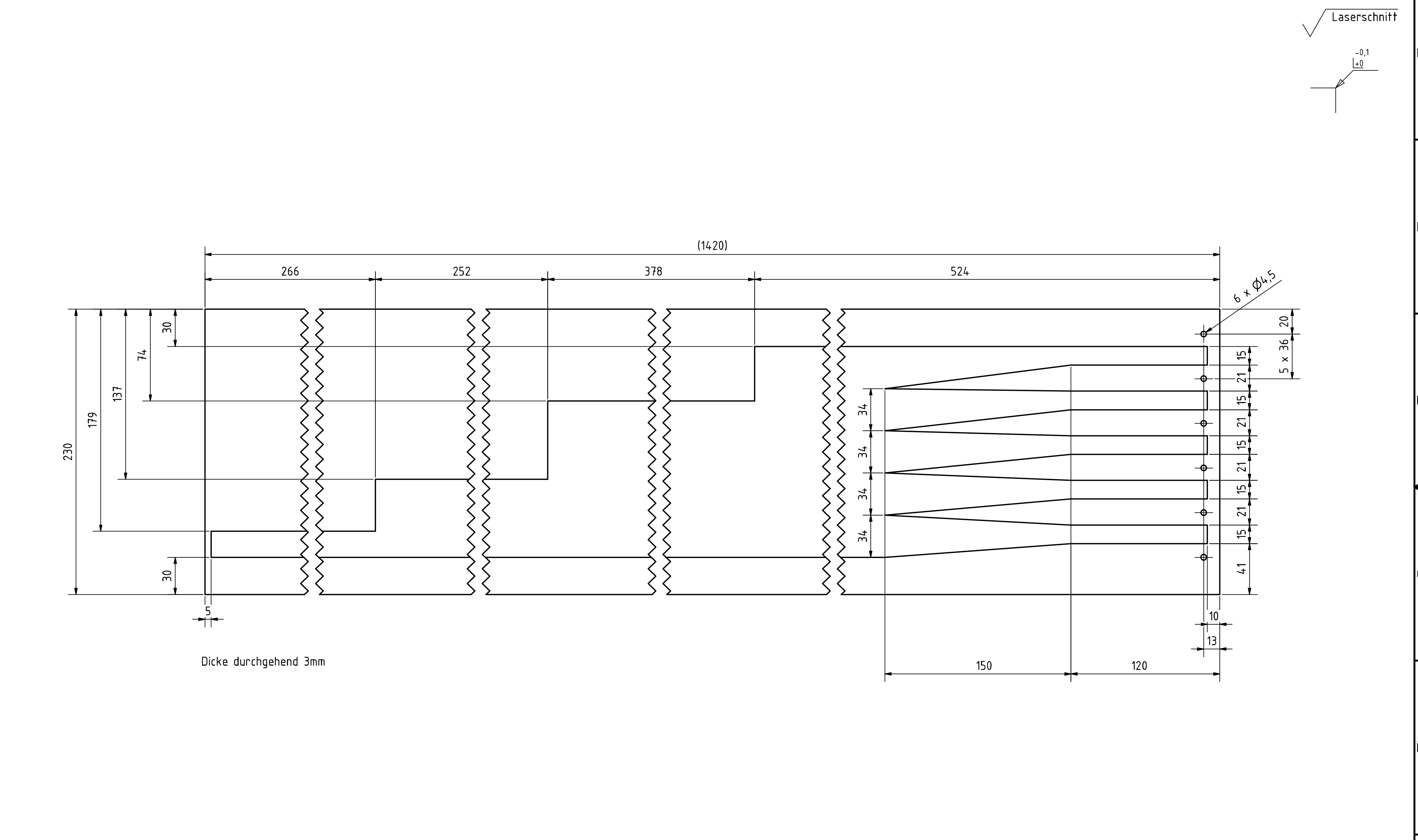

TU Graz	Allg. Tol. mk ISO 2768-1	Maßstab: 1:2	Masse: 0,597 kg
		Werkstoff: ABS-Kunststoff	
	Datum / Name	Channel Inlay	
	Erstellt 28.11.2016 Michael Eßl		
	Kontroll.		
	Norm		
Status / Änderungen / Datum / Name		IPPT/T_2_2_2_f/001	1 A2

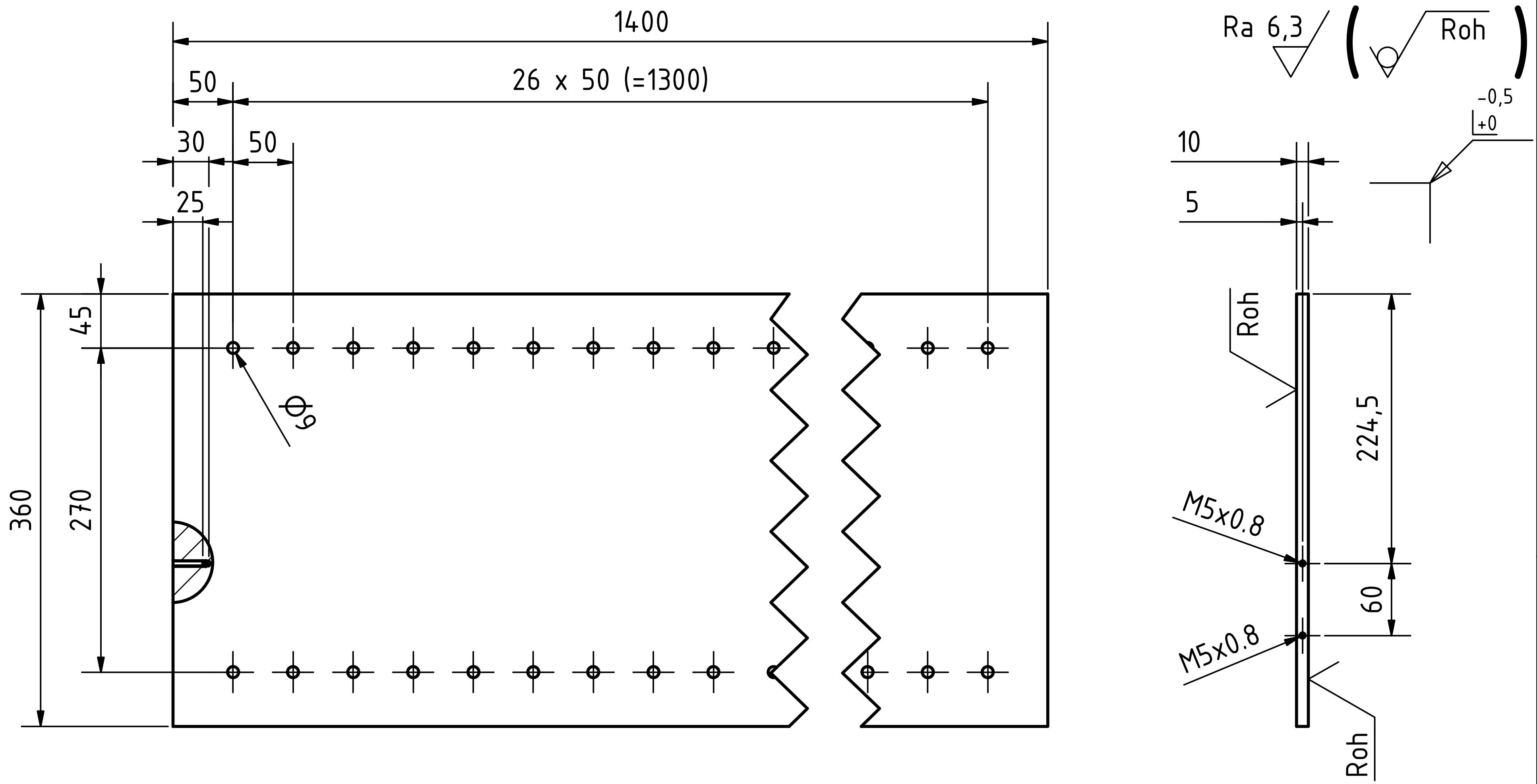

TU Graz

Allg. Tol. mk ISO 2768-1

Maßstab: 1:2

Masse: 6,006 kg

Werkstoff: Polycarbonat, klar

	Datum	Name
Erstellt	28.11.2016	Michael Eßl
Kontroll.		
Norm		

Top-Bottom Plate

IPPT/T_2_2_2_f/002

1

A4

Status	Änderungen	Datum	Name
rev. 1	Durchmesser Löcher	12.12.2016	Eßl

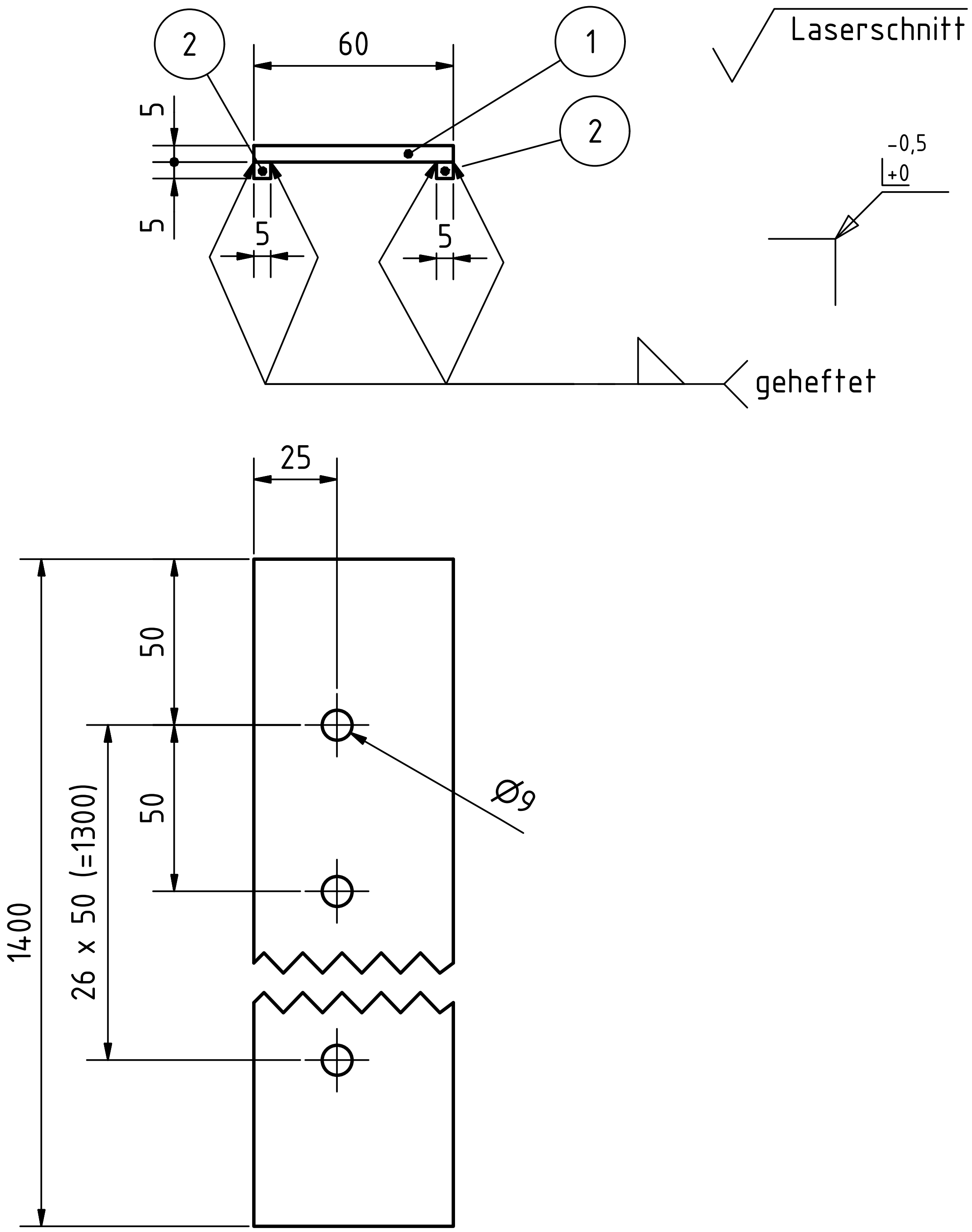

TEILELISTE

OBJEKT	ANZAHL	BAUTEILNUMMER	BESCHREIBUNG
1	1	clamp_top	Rohmaß: 60 x 5 x 1400
2	2	clamp_side	Rohmaß: 5 x 5 x 1400

TU Graz

Allg. Tol. mk ISO 2768-1	
Maßstab:	1:2
Masse:	3,789 kg
Werkstoff:	Stahl - S235J0

	Datum	Name
Erstellt	28.11.2016	Michael Eßl
Kontroll.		
Norm		

Clamp

IPPT/T_2_2_2_f/003

1

A4

Status	Änderungen	Datum	Name
rev.1	Durchmesser Löcher	12.12.2016	Eßl

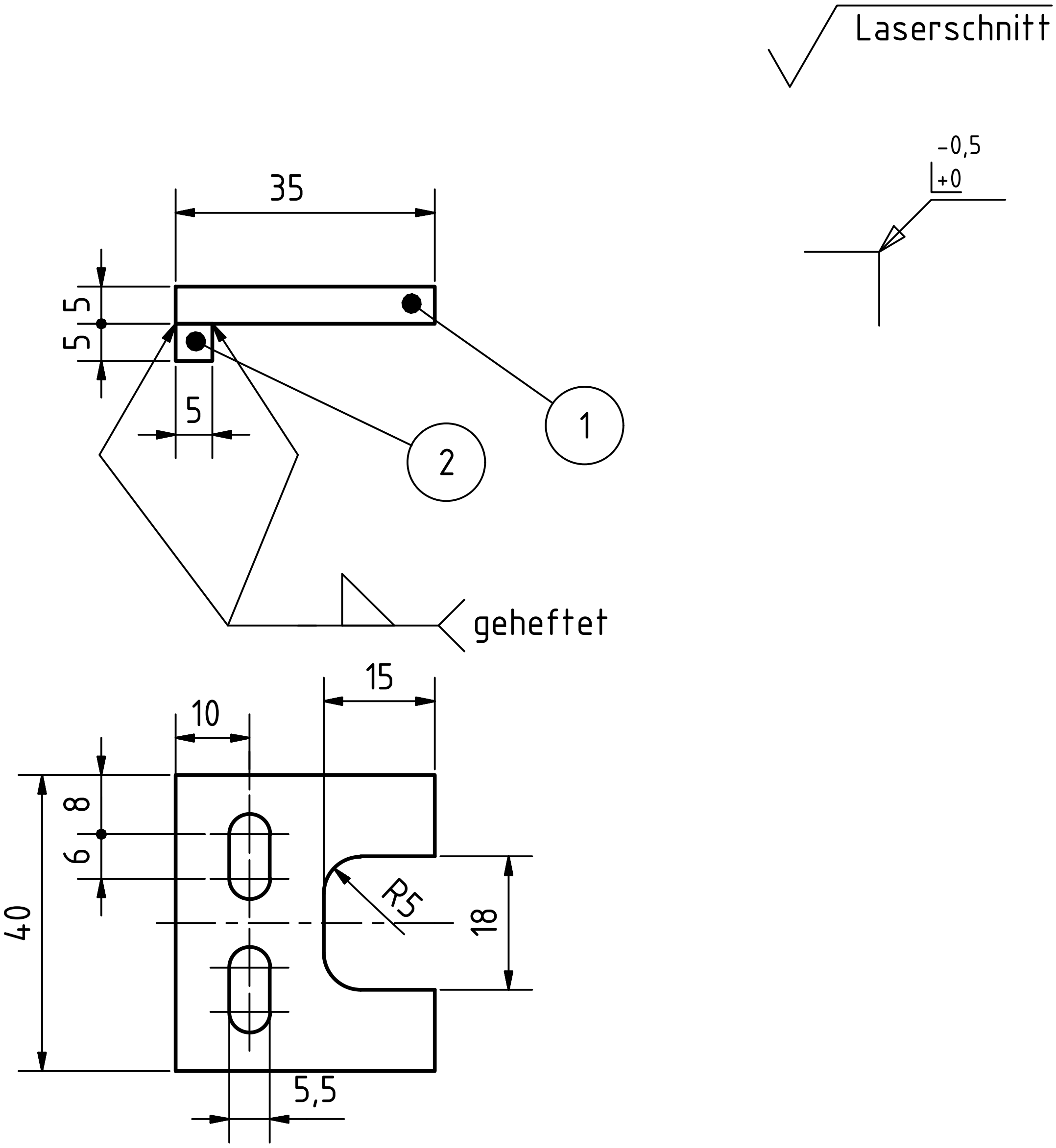

TEILELISTE			
OBJEKT	ANZAHL	BAUTEILNUMMER	BESCHREIBUNG
1	1	manifold_clamp_top	Rohmaß: 35 x 5 x 40
2	1	manifold_clamp_side	Rohmaß: 5 x 5 x 40

TU Graz	Allg. Tol. mk ISO 2768-1	Maßstab: 1:1 · Masse: 0,048 kg
		Werkstoff: Stahl, S235J0

	Datum	Name
Erstellt	28.11.2016	Michael Eßl
Kontroll.		
Norm		

Manifold Clamp

IPPT/T2_2_2_f/004

1

A4

Status	Änderungen	Datum	Name
rev. 1	Breite, Langlöcher	12.12.2016	Eßl

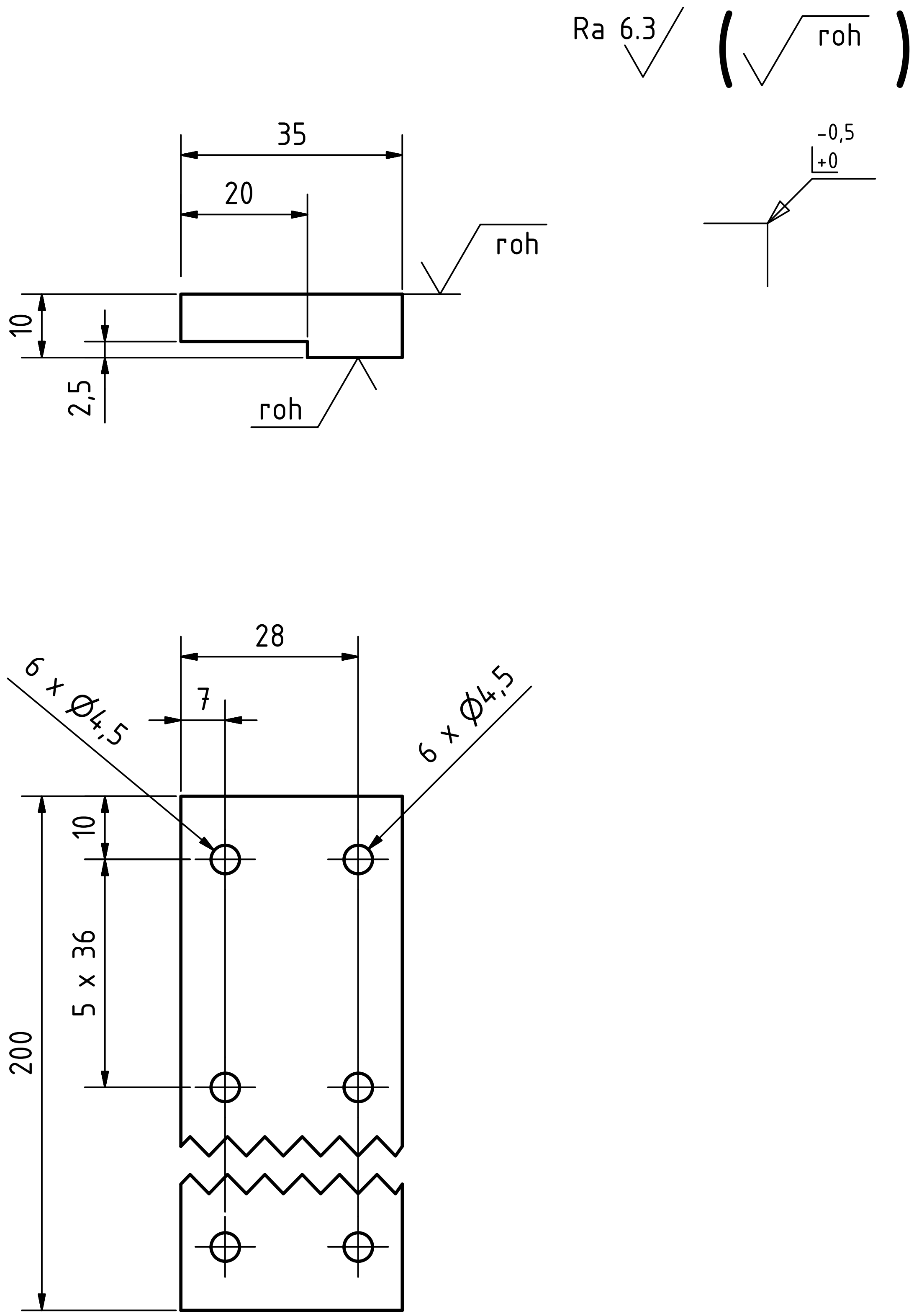

TU Graz	Allg. Tol. mk ISO 2768-1	Maßstab: 1:1	Masse: 0,070 kg
		Werkstoff: Polycarbonat, klar	

	Datum	Name
Erstellt	28.11.2016	Michael Eßl
Kontroll.		
Norm		

Outlet Clamp

IPPT/T_2_2_2_f/007

1

A4

Status	Änderungen	Datum	Name

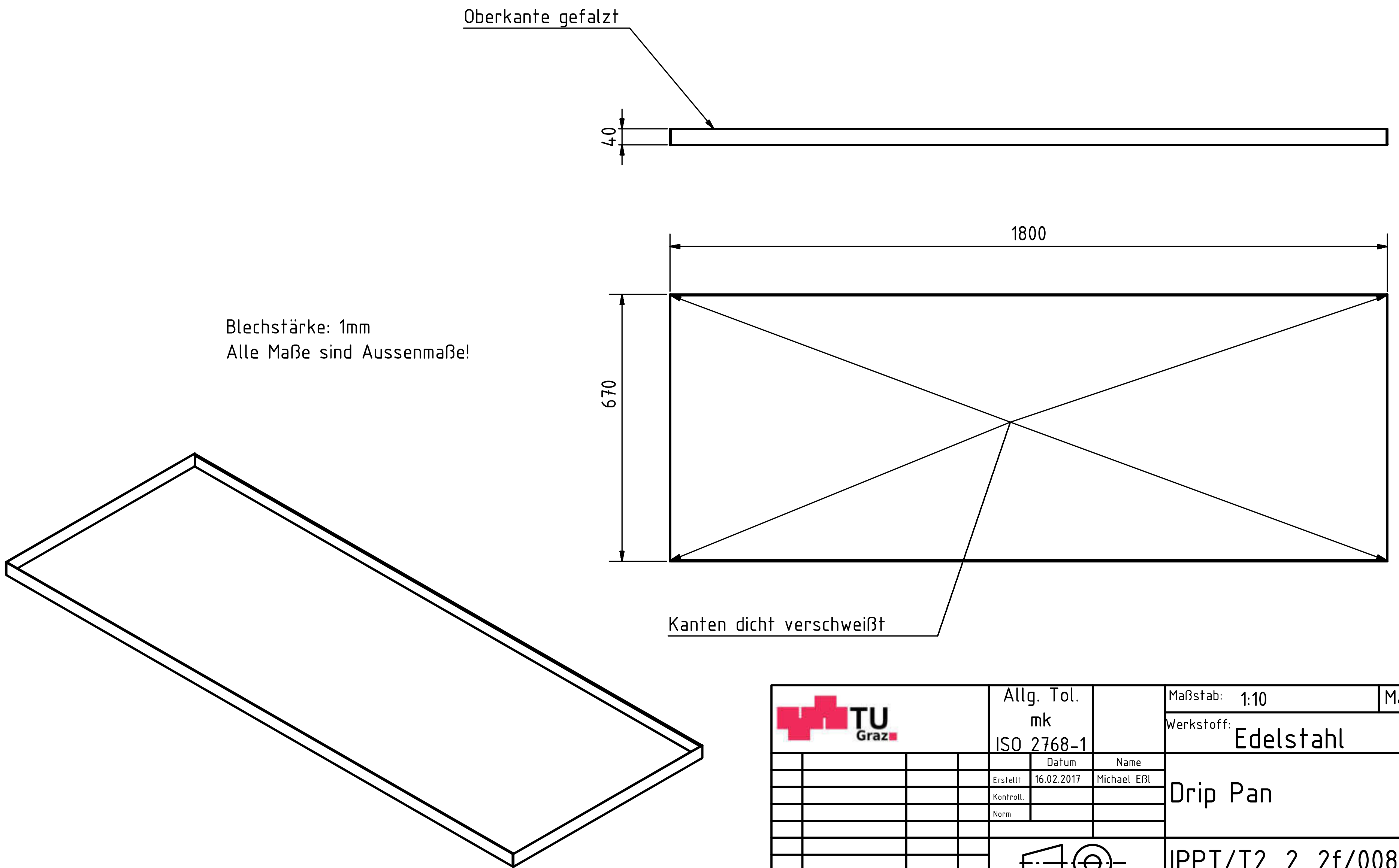

Blechstärke: 1mm
Alle Maße sind Aussenmaße!

TU Graz	Allg. Tol. mk ISO 2768-1	Maßstab: 1:10
		Masse: 11,385 kg
		Werkstoff: Edelstahl
	Datum	Name
Erstellt	16.02.2017	Michael Eßl
Kontroll.		
Norm		

Drip Pan

IPPT/T2_2_2f/008

1

A3

Status	Änderungen	Datum	Name

Appendix E Experimental Data

This section contains the data for the mass flow rates and pressure drop as well as the result of the fibre analysis of the fibre tester.

Geometry: G1 w_fib = 0,00%

time	weighed mass									reattachment length		
t	**m in**	**m out 1**	**m out 2**	**m out 3**	**m out 4**	**m out 5**	**h st**	**h in**	**pump set**	**step1**	**step 2**	**step 3**
[s]	**[g]**	**[g]**	**[g]**	**[g]**	**[g]**	**[g]**	**[mm]**	**[mm]**	**point**	**[mm]**	**[mm]**	**[mm]**
61,28	1349,5	92,0	168,3	181,1	175,1	144,9						
31,45	725,4	158,8	203,0	191,4	188,7	137,5	31	22	17,5			
27,67	622,1	139,8	179,0	168,1	167,6	122,2						
16,06	744,2	164,8	197,2	194,5	187,4	154,3						
16,02	734,3	177,3	190,1	189,0	182,4	150,0	104	51	36,3			
14,78	679,5	162,5	179,1	177,5	171,5	142,4						
12,18	785,5	180,0	198,3	202,0	194,0	166,1						
12,09	775,8	177,1	197,8	197,7	191,5	165,9	180	77	48,5			
14,28	917,9	207,5	227,5	226,5	221,5	189,5						
10,69	899,2	199,7	222,5	223,3	216,8	191,4						
9,43	785,6	180,4	193,9	197,6	194,5	172,9	282	109	60,5			
9,38	790,9	182,0	198,5	199,0	192,1	173,0					not observed	
7,64	819,1	189,2	199,0	207,5	195,1	182,1						
7,39	788,6	175,0	199,6	200,4	190,7	177,1	410	151	68,5			
8,16	854,5	189,5	207,8	214,4	204,2	190,1						
6,50	828,8	187,4	201,1	212,8	201,7	179,7						
6,75	867,3	192,5	213,0	222,2	208,7	185,3	582	196	80			
7,21	916,2	202,8	219,6	231,6	220,7	194,9						
5,19	825,5	183,8	201,5	208,9	203,5	181,2						
5,09	767,6	176,5	187,5	194,1	190,6	173,2	825	260	100			
5,33	819,8	186,6	198,8	205,5	199,5	183,8						

Geometry: G1 w_fib = 0,01%

time	weighed mass									reattachment length		
t	**m in**	**m out 1**	**m out 2**	**m out 3**	**m out 4**	**m out 5**	**h st**	**h in**	**pump set**	**step1**	**step 2**	**step 3**
[s]	**[g]**	**[g]**	**[g]**	**[g]**	**[g]**	**[g]**	**[mm]**	**[mm]**	**point**	**[mm]**	**[mm]**	**[mm]**
33,11	748,40	175,30	184,00	196,60	192,00	154,60	35	23	17,5	240	80	65
14,59	650,90	161,00	170,30	170,60	162,40	141,00	105	52	36,3	245	90	75
11,07	705,10	165,90	184,70	179,50	176,30	153,00	195	83	48,5	260	125	100
9,58	850,70	195,10	211,80	213,10	205,70	180,40	315	132	60,5	-	160	75
7,72	840,80	182,30	210,10	209,80	205,60	187,30	460	177	68,5	-	175	90
6,36	777,70	179,10	193,90	196,10	189,60	173,60	645	211	80	-	185	105
5,51	794,50	187,40	195,70	196,20	191,40	178,70	945	271	100	-	205	130

Geometry: G1 w_fib = 0,05%

time	weighed mass									reattachment length		
t	**m in**	**m out 1**	**m out 2**	**m out 3**	**m out 4**	**m out 5**	**h st**	**h in**	**pump set**	**step1**	**step 2**	**step 3**
[s]	**[g]**	**[g]**	**[g]**	**[g]**	**[g]**	**[g]**	**[mm]**	**[mm]**	**point**	**[mm]**	**[mm]**	**[mm]**
32,78	764,8	202,7	191,4	200,8	165,6	157,8	43	23	17,5	230	90	45
15,38	722,0	174,5	189,0	193,5	167,6	151,4	115	51	36,6	240	100	65
13,44	887,8	211,8	229,5	221,6	204,3	174,0	187	78	48,5	-	130	80
7,63	652,8	154,1	174,4	174,9	163,2	138,8	316	109	60,5	-	145	90
7,80	851,5	184,6	221,5	218,0	204,5	177,1	448	152	68,5	-	170	90
7,00	911,8	202,3	227,3	229,1	213,5	193,9	626	195	80	-	220	100
5,43	845,8	180,4	217,4	212,3	204,9	185,4	807	252	100	-	230	115

Geometry: G1 w_fib = 0,1%

time	weighed mass									reattachment length		
t	**m in**	**m out 1**	**m out 2**	**m out 3**	**m out 4**	**m out 5**	**h st**	**h in**	**pump set**	**step1**	**step 2**	**step 3**
[s]	**[g]**	**[g]**	**[g]**	**[g]**	**[g]**	**[g]**	**[mm]**	**[mm]**	**point**	**[mm]**	**[mm]**	**[mm]**
19,15	898,7	178,5	196,5	202,0	169,9	149,8	126	52	36,6	240	100	65
12,38	830,9	163,2	181,8	170,0	159,4	155,2	219	82	48,5	-	130	80

Geometry: G1 w_fib = 0,5%

time	weighed mass									reattachment length		
t	**m in**	**m out 1**	**m out 2**	**m out 3**	**m out 4**	**m out 5**	**h st**	**h in**	**pump set**	**step1**	**step 2**	**step 3**
[s]	**[g]**	**[g]**	**[g]**	**[g]**	**[g]**	**[g]**	**[mm]**	**[mm]**	**point**	**[mm]**	**[mm]**	**[mm]**
6,46	867,9	219,7	205,2	183,4	211,6	201,6		-	80		not observed	
5,01	740,4	175,5	171,3	150,0	154,8	249,6	944	-	100			

Geometry: G2 w_fib = 0,00%

time				weighed mass						reattachment length		
t	m in	m out 1	m out 2	m out 3	m out 4	m out 5	h st	h in	pump set	step1	step 2	step 3
[s]	[g]	[g]	[g]	[g]	[g]	[g]	[mm]	[mm]	point	[mm]	[mm]	[mm]
35,91	825,0	168,4	208,0	215,3	211,0	176,5						
39,58	904,6	182,3	225,1	233,5	227,4	190,4	56	23	17,5			
32,01	732,3	154,8	187,6	195,4	189,4	159,9						
15,57	731,1	161,3	190,3	189,3	184,9	159,9						
17,26	805,1	172,5	206,6	206,0	200,5	173,5	113	59	36,3			
15,99	757,7	161,8	196,8	196,4	191,4	165,4						
12,68	837,6	179,8	213,7	211,3	208,4	178,4						
10,57	701,3	157,2	184,6	180,1	178,8	153,8	198	91	48,5			
11,91	783,1	172,9	200,8	198,1	196,5	168,5						
8,76	756,5	145,5	213,6	194,0	192,2	164,5					not observed	
8,54	747,9	171,3	192,3	189,1	188,0	161,2	321	140	60,5			
10,07	883,8	194,7	224,1	217,5	217,0	184,9						
8,03	886,4	189,1	222,2	222,3	219,3	186,3						
7,69	838,9	182,5	211,5	211,8	210,5	177,5	476	201	68,5			
7,27	790,1	170,9	201,3	202,3	200,8	169,7						
5,54	728,4	166,7	182,9	188,0	182,5	163,1						
6,39	842,4	189,1	206,6	209,5	207,3	184,3	643	259	80			
7,17	928,3	203,6	224,4	227,5	226,0	201,0						
5,51	870,1	193,0	212,4	218,5	212,9	188,0						
5,20	786,4	177,2	194,2	201,3	194,5	173,2	861	328	100			
5,19	779,0	175,5	192,7	199,1	193,7	172,4						

Geometry: G2 w_fib = 0,01%

time				weighed mass						reattachment length		
t	m in	m out 1	m out 2	m out 3	m out 4	m out 5	h st	h in	pump set	step1	step 2	step 3
[s]	[g]	[g]	[g]	[g]	[g]	[g]	[mm]	[mm]	point	[mm]	[mm]	[mm]
35,97	809,0	162,8	220,8	229,6	210,6	140,0	50	23	17,5	185	85	65
33,74	756,6	153,6	207,8	215,8	199,1	133,5						
18,70	884,3	176,6	223,4	226,6	219,4	192,5	126	55	36,3	220	125	75
14,45	672,0	136,7	178,1	181,1	174,8	155,2						
10,76	725,6	157,8	192,9	190,2	177,8	160,7	211	88	48,5	250	90	90
10,81	709,9	155,1	189,7	188,2	174,0	157,1						
9,21	806,9	179,9	206,7	202,1	201,1	171,9	328	133	60,5	-	120	95
9,20	794,3	177,5	204,1	200,1	196,4	170,1						
5,42	578,7	201,0	143,3	136,7	135,0	116,1	481	174	68,5	-	164	100
5,67	601,0	207,2	147,6	139,5	140,0	120,7						
5,44	699,0	217,5	166,2	166,4	168,4	135,3	686	231	80	-	230	100
5,14	671,8	210,0	161,9	160,1	159,6	134,8						
4,72	723,4	201,0	160,2	216,1	163,1	137,2	987	307	100	-	250	105
5,33	820,2	222,5	174,3	242,8	181,0	153,9						

Geometry: G2 w_fib = 0,05%

time				weighed mass						reattachment length		
t	m in	m out 1	m out 2	m out 3	m out 4	m out 5	h st	h in	pump set	step1	step 2	step 3
[s]	[g]	[g]	[g]	[g]	[g]	[g]	[mm]	[mm]	point	[mm]	[mm]	[mm]
16,61	780,2	176,2	180,6	206,9	198,3	171,5	129	52	36,3	230	100	60
15,53	739,2	167,1	176,4	195,1	191,2	162,8						
12,39	813,9	184,8	182,7	224,2	195,2	181,2	224	99	48,5	270	110	85
10,57	705,5	165,0	160,4	197,1	174,6	161,9						
8,28	716,2	158,9	162,3	196,3	178,9	168,2	0	131	60,5	-	120	90
9,18	797,8	176,5	177,0	221,5	195,3	181,2						
7,29	798,8	173,8	175,5	220,6	194,1	189,7	496	172	68,5	-	160	100
6,81	749,3	167,0	165,2	208,4	182,7	179,7						
5,78	768,7	169,2	168,9	215,8	189,0	179,8	707	263	80	-	200	115
6,01	791,6	171,5	175,6	219,1	195,5	184,1						
4,12	653,0	138,8	140,9	218,5	159,0	149,4	945	295	100	-	270	115
4,34	691,9	146,1	147,0	228,6	166,9	157,1						

Geometry: G2 w_fib = 0,1%

time				weighed mass						reattachment length		
t	m in	m out 1	m out 2	m out 3	m out 4	m out 5	h st	h in	pump set	step1	step 2	step 3
[s]	[g]	[g]	[g]	[g]	[g]	[g]	[mm]	[mm]	point	[mm]	[mm]	[mm]
17,76	856,7	196,2	231,4	217,6	205,2	159,7	135	56	36,3	235	110	50
14,67	699,2	171,3	199,3	181,0	161,3	140,3						
11,20	749,2	165,4	185,8	205,9	196,0	149,3	219	96	48,5	-	130	70
10,28	697,9	156,5	197,9	182,7	175,6	138,4						
8,14	704,2	125,8	195,2	216,6	148,4	170,4	353	135	60,5	-	140	75
8,24	731,0	129,3	200,6	225,0	153,6	176,2						
5,30	565,5	113,3	144,5	228,6	129,6	103,8	505	165	68,5	-	185	80
5,13	554,5	113,3	139,8	224,2	132,3	98,9						
4,22	540,6	112,4	141,3	201,1	129,8	110,9	681	230	80	-	210	90
5,56	718,3	132,7	183,4	250,6	164,4	140,7						
4,50	690,3	180,7	151,2	222,8	150,6	139,1	901	301	100	-	250	100
4,77	722,7	186,3	160,7	230,0	155,4	144,2						

Geometry: G2 w_fib = 0,5%

time				weighed mass						reattachment length		
t	m in	m out 1	m out 2	m out 3	m out 4	m out 5	h st	h in	pump set	step1	step 2	step 3
[s]	[g]	[g]	[g]	[g]	[g]	[g]	[mm]	[mm]	point	[mm]	[mm]	[mm]
5,97	785,0	189,1	87,7	219,4	246,2	195,9	-	-	80			
5,57	840,7	194,1	166,0	222,7	254,7	156,5					not observed	
4,90	754,3	184,7	144,0	208,6	225,7	145,6	932	-	100			

Geometry: G3 w_fib = 0,00%

time	weighed mass									reattachment length		
t [s]	m in [g]	m out 1 [g]	m out 2 [g]	m out 3 [g]	m out 4 [g]	m out 5 [g]	h st [mm]	h in [mm]	pump set point	step1 [mm]	step 2 [mm]	step 3 [mm]
39,54	878,6	188,4	216,5	221,5	212,6	193,9						
35,59	803,2	173,6	203,1	203,5	196,7	197,7	58	34	17,5			
38,29	868,1	183,9	217,2	217,8	210,7	192,4						
21,05	982,1	209,0	245,5	243,1	232,6	204,5						
17,66	833,3	184,4	211,2	211,5	202,3	178,5	130	71	36,3			
20,85	979,5	207,1	245,5	243,3	232,5	205,2						
14,71	942,5	206,1	231,6	232,4	222,4	202,9						
14,10	906,8	197,6	222,6	224,8	214,0	202,6	203	113	48,5			
13,57	882,7	194,4	218,4	218,8	208,4	196,4						
9,63	824,7	189,6	208,1	202,5	193,0	188,9						
10,73	926,0	206,8	230,1	223,3	212,0	207,3	327	169	60,5		not observed	
9,68	823,1	188,4	207,3	202,5	192,0	186,8						
8,51	932,8	208,1	226,7	225,5	215,8	211,3						
9,08	969,7	216,0	233,6	233,3	222,4	218,4	477	241	68,5			
8,09	874,6	195,6	213,6	213,1	204,5	202,0						
6,92	907,4	202,0	222,2	220,8	211,1	207,7						
5,74	756,9	173,4	189,6	189,3	181,5	179,1	670	331	80			
6,01	773,9	175,9	193,3	192,6	184,9	182,5						
4,91	758,8	173,6	190,8	188,9	181,4	178,6						
5,34	827,2	186,1	205,3	203,2	194,3	192,6	915	455	100			
5,26	807,9	182,3	201,5	199,4	190,6	188,2						

Geometry: G3 w_fib = 0,01%

time	weighed mass									reattachment length		
t [s]	m in [g]	m out 1 [g]	m out 2 [g]	m out 3 [g]	m out 4 [g]	m out 5 [g]	h st [mm]	h in [mm]	pump set point	step1 [mm]	step 2 [mm]	step 3 [mm]
37,61	884,0	190,6	235,1	217,9	209,3	185,0	-	-	17,5			
28,45	669,3	152,5	186,7	171,1	165,8	147,4						
18,95	913,3	198,8	226,8	224,7	219,7	197,7	136	63	36,3			
17,26	837,4	183,0	211,5	209,1	202,8	185,2						
12,27	818,8	182,5	205,5	203,1	193,7	188,3	225	124	48,5			
11,84	791,2	177,5	199,5	196,1	189,6	181,6						
9,74	850,4	186,2	209,3	209,3	203,0	196,0	347	175	60,5			
11,18	970,8	209,1	235,1	234,7	227,7	219,9						
8,97	968,0	209,4	233,8	232,3	226,2	220,8	506	241	68,5		not observed	
8,18	885,6	190,9	218,1	215,9	209,1	205,2						
5,10	671,7	145,0	216,2	158,3	156,3	151,3	684	321	80			
6,00	775,2	158,8	243,9	178,3	177,4	171,5						
4,39	676,9	157,8	172,1	172,0	166,7	162,6	937	433	100			
5,03	784,9	177,7	195,3	195,0	189,1	181,4						

Geometry: G3 w_fib = 0,05%

time	weighed mass									reattachment length		
t [s]	m in [g]	m out 1 [g]	m out 2 [g]	m out 3 [g]	m out 4 [g]	m out 5 [g]	h st [mm]	h in [mm]	pump set point	step1 [mm]	step 2 [mm]	step 3 [mm]
40,48	966,8	212,3	243,8	237,7	222,1	203,3	-	-	17,5			
40,61	943,5	213,1	236,1	233,1	216,2	198,3						
19,31	952,2	205,4	238,7	232,5	224,8	205,3	135	56	36,3			
18,84	904,0	194,5	226,9	225,0	214,0	197,7						
12,32	818,8	179,1	202,5	205,5	199,6	186,6	219	96	48,5			
14,73	979,1	209,7	237,0	239,5	230,0	214,9						
8,63	759,5	168,8	192,1	194,3	182,9	175,6	339	117	60,5		not observed	
8,96	788,4	175,9	197,3	199,9	187,4	181,3						
8,60	943,9	201,1	230,1	232,6	219,9	213,9	505	165	68,5			
7,62	834,9	181,7	208,5	208,7	197,9	191,7						
6,26	838,3	178,8	210,7	211,7	197,6	194,7	681	230	80			
5,58	749,6	165,9	190,4	191,3	178,8	177,7						
5,73	914,4	196,5	224,4	224,0	214,7	208,9	901	301	100			
5,21	844,1	182,4	210,1	208,5	200,1	195,7						

Geometry: G3 w_fib = 0,1%

time	weighed mass									reattachment length		
t [s]	m in [g]	m out 1 [g]	m out 2 [g]	m out 3 [g]	m out 4 [g]	m out 5 [g]	h st [mm]	h in [mm]	pump set point	step1 [mm]	step 2 [mm]	step 3 [mm]
35,71	848,5	192,5	211,8	198,4	197,3	202,3	54	25	17,5			
34,67	814,0	200,0	210,5	192,4	173,1	192,1						
16,74	815,0	180,8	203,5	206,7	207,7	169,5	147	75	36,3			
17,86	866,8	185,0	217,5	215,1	208,3	195,2						
12,81	864,6	192,5	218,1	212,2	204,0	191,8	235	105	48,5			
13,47	915,4	203,6	231,3	227,4	203,0	204,3						
10,64	930,4	203,2	229,1	227,6	219,4	204,9	360	175	60,5		not observed	
10,84	946,9	210,5	234,2	229,2	219,7	207,3						
8,58	945,4	202,8	232,9	236,9	219,9	207,1	528	244	68,5			
9,30	1019,9	218,4	248,5	251,3	232,8	223,1						
6,15	818,0	176,9	206,5	207,8	194,3	186,5	732	314	80			
6,51	857,6	184,9	212,7	214,9	204,5	194,9						
5,29	836,6	184,3	207,9	208,8	198,5	191,8	963	420	100			
5,87	938,4	202,3	229,3	230,4	218,7	211,4						

Geometry: G3 w_fib = 0,05%

time	weighed mass									reattachment length		
t [s]	m in [g]	m out 1 [g]	m out 2 [g]	m out 3 [g]	m out 4 [g]	m out 5 [g]	h st [mm]	h in [mm]	pump set point	step1 [mm]	step 2 [mm]	step 3 [mm]
5,19	800,4	137,3	207,2	199,3	218,3	193,0	961	-	100		not observed	
4,76	719,0	116,3	192,3	182,7	213,1	168,1						

Lorentzen & Wettre
A MEMBER OF THE ABB GROUP

Probenname:	links unten 1	Anzahl Fasern	12683 (180020)
Probenart:	IPPT flippr	Anzahl Bilder	3001
Zeit:	2017-02-23 10:37:18	Temperatur	25,3 °C
Anmerkung			

Volumen gewichtet (ISO)

Variable	Wert	Unterschied
Mittlere Länge	2,077 mm	0,057 mm
Mittlere Breite	31,5 µm	0,4 µm
Mittlere Form	81,7 %	0,3 %
Mean fibril area	3,0 %	0,1 %
Mean fibril perimeter	10,2 %	0,1 %
Mean Fines	8,1 %	

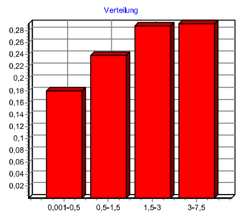

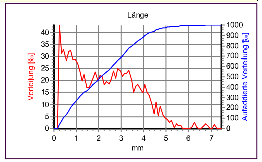

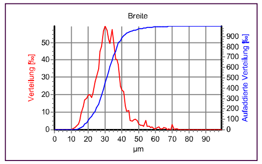

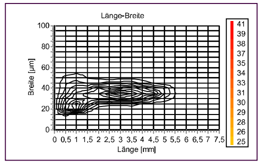

Variable	Gewichtung	Wert
Länge	Länge	1,294 mm
Länge	Breite	0,443 mm
Länge	Fläche	1,856 mm
Länge	Volumen	2,077 mm
Länge	Arithmetik	0,119 mm

Probenname:	links unten 1	Anzahl Fasern	12683 (180020)
Probenart:	IPPT flippr	Anzahl Bilder	3001
Zeit:	2017-02-23 10:37:18	Temperatur	25,3 °C
Anmerkung			

Variable	Gewichtung	Wert
Länge	Länge-Länge	2,887 mm
Breite	Länge	24,7 µm
Breite	Breite	22,4 µm
Breite	Fläche	28,8 µm
Breite	Volumen	31,5 µm
Breite	Arithmetik	16,8 µm
Breite	Länge-Länge	30,3 µm
Form	Länge	83,3 %
Form	Breite	88,5 %
Form	Fläche	82,3 %
Form	Volumen	81,7 %
Form	Arithmetik	89,6 %
Form	Länge-Länge	79,3 %
Feinstoff Grenze	Länge	34,6 %
Feinstoff Grenze	Breite	63,9 %
Feinstoff Grenze	Fläche	13,2 %

Variable	Gewichtung	Wert
Feinstoff Grenze	Volumen	8,1 %
Feinstoff Grenze	Arithmetik	93,0 %
Feinstoff Grenze	Länge-Länge	2,2 %
Anzahl Fasern		12683 (180020)
Anzahl Bilder		3001
Temperatur		25,3 °C
Gesamtlänge		22508 mm
Gesamtfläche		595,7 mm2
Gesamtvolumen		17,42 mm3
Länge pro Bild		8,2 mm
Anzahl Fasern in der Probe		2189763
Mittlerer Knickwinkel		54,9 °
Anzahl Knicke pro mm		0,909 mm-1
Anzahl großer Knicke pro mm		0,312 mm-1
Anzahl Knicke pro Faser		1,248
Anzahl großer Knicke pro Faser		0,428

Lorentzen & Wettre
A MEMBER OF THE ABB GROUP

Probenname:	links unten 2	Anzahl Fasern	12860 (180060)
Probenart:	IPPT flippr	Anzahl Bilder	3004
Zeit:	2017-02-23 10:50:02	Temperatur	25,4 °C
Anmerkung			

Volumen gewichtet (ISO)

Variable	Wert	Unterschied
Mittlere Länge	2,103 mm	0,091 mm
Mittlere Breite	31,3 µm	0,1 µm
Mittlere Form	81,9 %	-0,1 %
Mean fibril area	2,9 %	-0,2 %
Mean fibril perimeter	10,2 %	-0,6 %
Mean Fines	8,5 %	

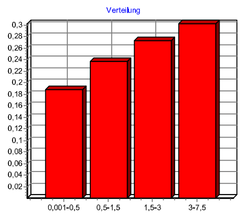

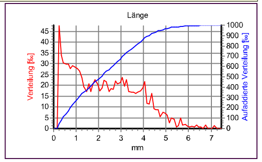

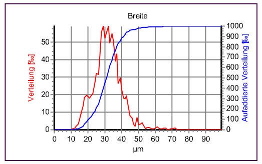

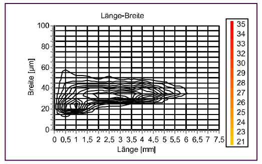

Variable	Gewichtung	Wert
Länge	Länge	1,284 mm
Länge	Breite	0,433 mm
Länge	Fläche	1,866 mm
Länge	Volumen	2,103 mm
Länge	Arithmetik	0,118 mm

Probenname:	links unten 2	Anzahl Fasern	12860 (180060)
Probenart:	IPPT flippr	Anzahl Bilder	3004
Zeit:	2017-02-23 10:50:02	Temperatur	25,4 °C
Anmerkung			

Variable	Gewichtung	Wert
Länge	Länge-Länge	2,955 mm
Breite	Länge	24,6 µm
Breite	Breite	22,3 µm
Breite	Fläche	28,7 µm
Breite	Volumen	31,3 µm
Breite	Arithmetik	17,0 µm
Breite	Länge-Länge	30,4 µm
Form	Länge	83,6 %
Form	Breite	88,7 %
Form	Fläche	82,6 %
Form	Volumen	81,9 %
Form	Arithmetik	89,8 %
Form	Länge-Länge	79,5 %
Feinstoff Grenze	Länge	35,4 %
Feinstoff Grenze	Breite	64,2 %
Feinstoff Grenze	Fläche	13,8 %

Variable	Gewichtung	Wert
Feinstoff Grenze	Volumen	8,5 %
Feinstoff Grenze	Arithmetik	92,9 %
Feinstoff Grenze	Länge-Länge	2,3 %
Anzahl Fasern		12860 (180060)
Anzahl Bilder		3004
Temperatur		25,4 °C
Gesamtlänge		22039 mm
Gesamtfläche		578,2 mm2
Gesamtvolumen		16,80 mm3
Länge pro Bild		8,0 mm
Anzahl Fasern in der Probe		2217899
Mittlerer Knickwinkel		54,7 °
Anzahl Knicke pro mm		0,890 mm-1
Anzahl großer Knicke pro mm		0,309 mm-1
Anzahl Knicke pro Faser		1,217
Anzahl großer Knicke pro Faser		0,423

Lorentzen & Wettre
A MEMBER OF THE ABB GROUP

Probenname:	links unten 3	Anzahl Fasern	12637 (180049)
Probenart:	IPPT flippr	Anzahl Bilder	2956
Zeit:	2017-02-23 11:02:09	Temperatur	25,4 °C
Anmerkung			

Volumen gewichtet (ISO)

Variable	Wert	Unterschied
Mittlere Länge	2,133 mm	-0,017 mm
Mittlere Breite	31,5 µm	0,4 µm
Mittlere Form	81,7 %	0,3 %
Mean fibril area	3,0 %	0,0 %
Mean fibril perimeter	10,4 %	0,0 %
Mean Fines	8,2 %	

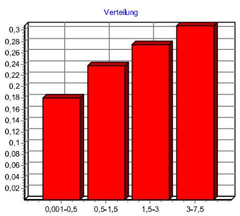

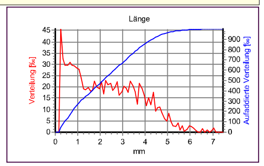

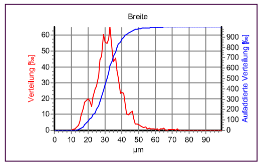

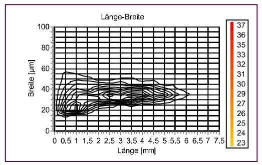

Variable	Gewichtung	Wert
Länge	Länge	1,324 mm
Länge	Breite	0,443 mm
Länge	Fläche	1,906 mm
Länge	Volumen	2,133 mm
Länge	Arithmetik	0,119 mm

Probenname:	links unten 3	Anzahl Fasern	12637 (180049)
Probenart:	IPPT flippr	Anzahl Bilder	2956
Zeit:	2017-02-23 11:02:09	Temperatur	25,4 °C
Anmerkung			

Variable	Gewichtung	Wert
Länge	Länge-Länge	3,004 mm
Breite	Länge	24,8 µm
Breite	Breite	22,4 µm
Breite	Fläche	28,9 µm
Breite	Volumen	31,5 µm
Breite	Arithmetik	16,9 µm
Breite	Länge-Länge	30,4 µm
Form	Länge	83,3 %
Form	Breite	88,5 %
Form	Fläche	82,3 %
Form	Volumen	81,7 %
Form	Arithmetik	89,6 %
Form	Länge-Länge	79,2 %
Feinstoff Grenze	Länge	34,6 %
Feinstoff Grenze	Breite	63,9 %
Feinstoff Grenze	Fläche	13,2 %

Variable	Gewichtung	Wert
Feinstoff Grenze	Volumen	8,2 %
Feinstoff Grenze	Arithmetik	93,0 %
Feinstoff Grenze	Länge-Länge	2,1 %
Anzahl Fasern		12637 (180049)
Anzahl Bilder		2956
Temperatur		25,4 °C
Gesamtlänge		22254 mm
Gesamtfläche		588,0 mm2
Gesamtvolumen		17,16 mm3
Länge pro Bild		8,2 mm
Anzahl Fasern in der Probe		2218185
Mittlerer Knickwinkel		54,9 °
Anzahl Knicke pro mm		0,899 mm-1
Anzahl großer Knicke pro mm		0,306 mm-1
Anzahl Knicke pro Faser		1,228
Anzahl großer Knicke pro Faser		0,418

Lorentzen & Wettre
A MEMBER OF THE ABB GROUP

Probenname:	mitte 1	Anzahl Fasern	13323 (180037)
Probenart:	IPPT flippr	Anzahl Bilder	3070
Zeit:	2017-02-23 09:53:30	Temperatur	25,4 °C
Anmerkung			

Volumen gewichtet (ISO)

Variable	Wert	Unterschied
Mittlere Länge	2,131 mm	0,016 mm
Mittlere Breite	31,3 µm	-0,1 µm
Mittlere Form	81,7 %	0,0 %
Mean fibril area	1,8 %	-0,1 %
Mean fibril perimeter	6,8 %	-0,1 %
Mean Fines	8,1 %	

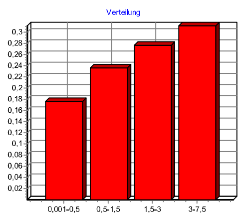

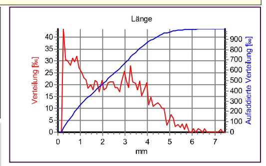

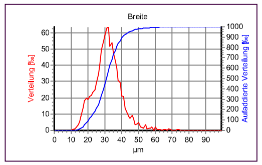

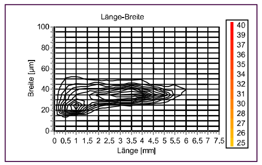

Variable	Gewichtung	Wert
Länge	Länge	1,323 mm
Länge	Breite	0,451 mm
Länge	Fläche	1,895 mm
Länge	Volumen	2,131 mm
Länge	Arithmetik	0,123 mm

Probenname:	mitte 1	Anzahl Fasern	13323 (180037)
Probenart:	IPPT flippr	Anzahl Bilder	3070
Zeit:	2017-02-23 09:53:30	Temperatur	25,4 °C
Anmerkung			

Variable	Gewichtung	Wert
Länge	Länge-Länge	2,937 mm
Breite	Länge	24,7 µm
Breite	Breite	22,3 µm
Breite	Fläche	28,7 µm
Breite	Volumen	31,3 µm
Breite	Arithmetik	17,0 µm
Breite	Länge-Länge	30,4 µm
Form	Länge	83,3 %
Form	Breite	88,4 %
Form	Fläche	82,3 %
Form	Volumen	81,7 %
Form	Arithmetik	89,5 %
Form	Länge-Länge	79,4 %
Feinstoff Grenze	Länge	33,9 %
Feinstoff Grenze	Breite	63,5 %
Feinstoff Grenze	Fläche	13,1 %

Variable	Gewichtung	Wert
Feinstoff Grenze	Volumen	8,1 %
Feinstoff Grenze	Arithmetik	92,6 %
Feinstoff Grenze	Länge-Länge	2,1 %
Anzahl Fasern		13323 (180037)
Anzahl Bilder		3070
Temperatur		25,4 °C
Gesamtlänge		23532 mm
Gesamtfläche		623,5 mm2
Gesamtvolumen		18,24 mm3
Länge pro Bild		8,4 mm
Anzahl Fasern in der Probe		2243859
Mittlerer Knickwinkel		55,1 °
Anzahl Knicke pro mm		0,962 mm-1
Anzahl großer Knicke pro mm		0,334 mm-1
Anzahl Knicke pro Faser		1,324
Anzahl großer Knicke pro Faser		0,461

Lorentzen & Wettre
A MEMBER OF THE ABB GROUP

Probenname: mitte 2
Probenart: IPPT flippr
Zeit: 2017-02-23 10:06:05
Anmerkung

Anzahl Fasern 13160 (180067)
Anzahl Bilder 3142
Temperatur 25,4 °C

Volumen gewichtet (ISO)

Variable	Wert	Unterschied
Mittlere Länge	2,140 mm	-0,025 mm
Mittlere Breite	31,3 µm	0,2 µm
Mittlere Form	81,5 %	0,3 %
Mean fibril area	1,7 %	0,0 %
Mean fibril perimeter	6,7 %	-0,1 %
Mean Fines	8,2 %	

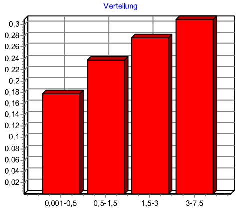

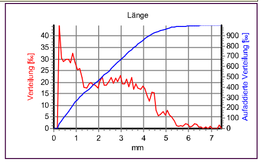

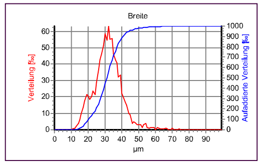

Variable	Gewichtung	Wert
Länge	Länge	1,309 mm
Länge	Breite	0,442 mm
Länge	Fläche	1,895 mm
Länge	Volumen	2,140 mm
Länge	Arithmetik	0,121 mm

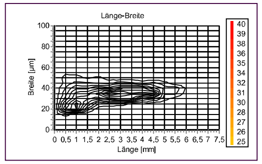

Probenname: mitte 2
Probenart: IPPT flippr
Zeit: 2017-02-23 10:06:05
Anmerkung

Anzahl Fasern 13160 (180067)
Anzahl Bilder 3142
Temperatur 25,4 °C

Variable	Gewichtung	Wert
Länge	Länge-Länge	2,968 mm
Breite	Länge	24,7 µm
Breite	Breite	22,2 µm
Breite	Fläche	28,6 µm
Breite	Volumen	31,3 µm
Breite	Arithmetik	17,0 µm
Breite	Länge-Länge	30,4 µm
Form	Länge	83,3 %
Form	Breite	88,6 %
Form	Fläche	82,2 %
Form	Volumen	81,5 %
Form	Arithmetik	89,7 %
Form	Länge-Länge	79,2 %
Feinstoff Grenze	Länge	34,7 %
Feinstoff Grenze	Breite	64,1 %
Feinstoff Grenze	Fläche	13,5 %

Variable	Gewichtung	Wert
Feinstoff Grenze	Volumen	8,2 %
Feinstoff Grenze	Arithmetik	92,7 %
Feinstoff Grenze	Länge-Länge	2,2 %
Anzahl Fasern		13160 (180067)
Anzahl Bilder		3142
Temperatur		25,4 °C
Gesamtlänge		23302 mm
Gesamtfläche		616,1 mm2
Gesamtvolumen		17,99 mm3
Länge pro Bild		8,1 mm
Anzahl Fasern in der Probe		2161111
Mittlerer Knickwinkel		55,1 °
Anzahl Knicke pro mm		0,950 mm-1
Anzahl großer Knicke pro mm		0,327 mm-1
Anzahl Knicke pro Faser		1,343
Anzahl großer Knicke pro Faser		0,462

Lorentzen & Wettre
A MEMBER OF THE ABB GROUP

Probenname: mitte 3
Probenart: IPPT flippr
Zeit: 2017-02-23 10:18:43
Anmerkung

Anzahl Fasern 12905 (180031)
Anzahl Bilder 3122
Temperatur 25,4 °C

Volumen gewichtet (ISO)

Variable	Wert	Unterschied
Mittlere Länge	2,105 mm	0,076 mm
Mittlere Breite	31,3 µm	0,0 µm
Mittlere Form	81,7 %	-0,4 %
Mean fibril area	1,7 %	-0,1 %
Mean fibril perimeter	6,7 %	-0,4 %
Mean Fines	8,5 %	

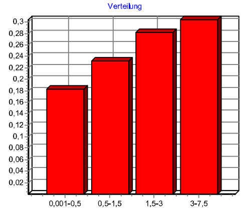

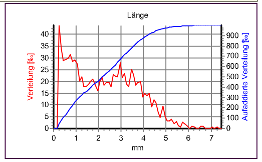

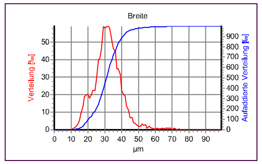

Variable	Gewichtung	Wert
Länge	Länge	1,295 mm
Länge	Breite	0,438 mm
Länge	Fläche	1,873 mm
Länge	Volumen	2,105 mm
Länge	Arithmetik	0,120 mm

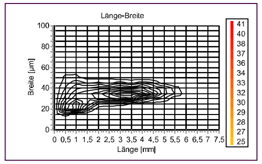

Probenname: mitte 3
Probenart: IPPT flippr
Zeit: 2017-02-23 10:18:43
Anmerkung

Anzahl Fasern 12905 (180031)
Anzahl Bilder 3122
Temperatur 25,4 °C

Variable	Gewichtung	Wert
Länge	Länge-Länge	2,918 mm
Breite	Länge	24,7 µm
Breite	Breite	22,3 µm
Breite	Fläche	28,7 µm
Breite	Volumen	31,3 µm
Breite	Arithmetik	17,1 µm
Breite	Länge-Länge	30,3 µm
Form	Länge	83,3 %
Form	Breite	88,6 %
Form	Fläche	82,3 %
Form	Volumen	81,7 %
Form	Arithmetik	89,7 %
Form	Länge-Länge	79,2 %
Feinstoff Grenze	Länge	35,1 %
Feinstoff Grenze	Breite	64,5 %
Feinstoff Grenze	Fläche	13,7 %

Variable	Gewichtung	Wert
Feinstoff Grenze	Volumen	8,5 %
Feinstoff Grenze	Arithmetik	92,8 %
Feinstoff Grenze	Länge-Länge	2,3 %
Anzahl Fasern		12905 (180031)
Anzahl Bilder		3122
Temperatur		25,4 °C
Gesamtlänge		22493 mm
Gesamtfläche		590,7 mm2
Gesamtvolumen		17,15 mm3
Länge pro Bild		7,8 mm
Anzahl Fasern in der Probe		2134024
Mittlerer Knickwinkel		55,1 °
Anzahl Knicke pro mm		0,975 mm-1
Anzahl großer Knicke pro mm		0,339 mm-1
Anzahl Knicke pro Faser		1,335
Anzahl großer Knicke pro Faser		0,465

Lorentzen & Wettre
A MEMBER OF THE ABB GROUP

Probenname: rechts oben 1
Probenart: IPPT flippr
Zeit: 2017-02-23 08:58:35
Anmerkung

Anzahl Fasern 13201 (180019)
Anzahl Bilder 3655
Temperatur 25,1 °C

Volumen gewichtet (ISO)

Variable	Wert	Unterschied
Mittlere Länge	2,139 mm	0,019 mm
Mittlere Breite	31,3 µm	0,3 µm
Mittlere Form	81,9 %	0,0 %
Mean fibril area	1,6 %	0,1 %
Mean fibril perimeter	6,0 %	0,2 %
Mean Fines	7,4 %	

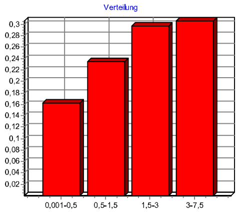

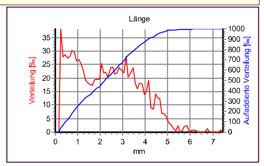

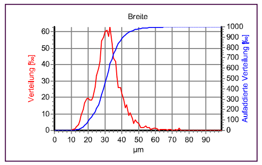

Variable	Gewichtung	Wert
Länge	Länge	1,372 mm
Länge	Breite	0,472 mm
Länge	Fläche	1,927 mm
Länge	Volumen	2,139 mm
Länge	Arithmetik	0,125 mm

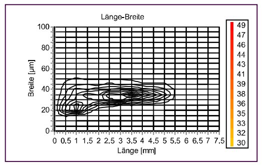

Probenname: rechts oben 1
Probenart: IPPT flippr
Zeit: 2017-02-23 08:58:35
Anmerkung

Anzahl Fasern 13201 (180019)
Anzahl Bilder 3655
Temperatur 25,1 °C

Variable	Gewichtung	Wert
Länge	Länge-Länge	2,911 mm
Breite	Länge	24,9 µm
Breite	Breite	22,3 µm
Breite	Fläche	28,7 µm
Breite	Volumen	31,3 µm
Breite	Arithmetik	16,9 µm
Breite	Länge-Länge	30,1 µm
Form	Länge	83,3 %
Form	Breite	88,4 %
Form	Fläche	82,4 %
Form	Volumen	81,9 %
Form	Arithmetik	89,6 %
Form	Länge-Länge	79,7 %
Feinstoff Grenze	Länge	32,6 %
Feinstoff Grenze	Breite	63,0 %
Feinstoff Grenze	Fläche	12,2 %

Variable	Gewichtung	Wert
Feinstoff Grenze	Volumen	7,4 %
Feinstoff Grenze	Arithmetik	92,7 %
Feinstoff Grenze	Länge-Länge	2,0 %
Anzahl Fasern		13201 (180019)
Anzahl Bilder		3655
Temperatur		25,1 °C
Gesamtlänge		23763 mm
Gesamtfläche		631,3 mm2
Gesamtvolumen		18,49 mm3
Länge pro Bild		7,0 mm
Anzahl Fasern in der Probe		1840658
Mittlerer Knickwinkel		54,7 °
Anzahl Knicke pro mm		0,952 mm-1
Anzahl großer Knicke pro mm		0,325 mm-1
Anzahl Knicke pro Faser		1,348
Anzahl großer Knicke pro Faser		0,460

Lorentzen & Wettre
A MEMBER OF THE ABB GROUP

Probenname: rechts oben 2
Probenart: IPPT flippr
Zeit: 2017-02-23 09:15:11
Anmerkung

Anzahl Fasern 13171 (180050)
Anzahl Bilder 3746
Temperatur 25,3 °C

Volumen gewichtet (ISO)

Variable	Wert	Unterschied
Mittlere Länge	2,152 mm	0,401 mm
Mittlere Breite	31,6 µm	1,2 µm
Mittlere Form	81,7 %	-1,8 %
Mean fibril area	1,6 %	-0,2 %
Mean fibril perimeter	5,8 %	-0,2 %
Mean Fines	7,7 %	

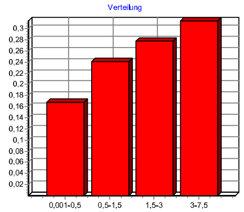

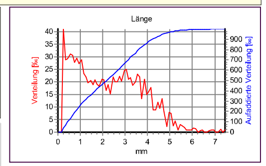

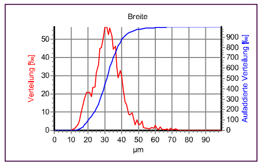

Variable	Gewichtung	Wert
Länge	Länge	1,335 mm
Länge	Breite	0,459 mm
Länge	Fläche	1,911 mm
Länge	Volumen	2,152 mm
Länge	Arithmetik	0,122 mm

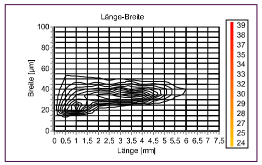

Probenname: rechts oben 2
Probenart: IPPT flippr
Zeit: 2017-02-23 09:15:11
Anmerkung

Anzahl Fasern 13171 (180050)
Anzahl Bilder 3746
Temperatur 25,3 °C

Variable	Gewichtung	Wert
Länge	Länge-Länge	2,935 mm
Breite	Länge	24,8 µm
Breite	Breite	22,3 µm
Breite	Fläche	28,8 µm
Breite	Volumen	31,6 µm
Breite	Arithmetik	16,8 µm
Breite	Länge-Länge	30,5 µm
Form	Länge	83,2 %
Form	Breite	88,6 %
Form	Fläche	82,3 %
Form	Volumen	81,7 %
Form	Arithmetik	89,7 %
Form	Länge-Länge	78,9 %
Feinstoff Grenze	Länge	33,4 %
Feinstoff Grenze	Breite	63,2 %
Feinstoff Grenze	Fläche	12,6 %

Variable	Gewichtung	Wert
Feinstoff Grenze	Volumen	7,7 %
Feinstoff Grenze	Arithmetik	92,7 %
Feinstoff Grenze	Länge-Länge	2,1 %
Anzahl Fasern		13171 (180050)
Anzahl Bilder		3746
Temperatur		25,3 °C
Gesamtlänge		22190 mm
Gesamtfläche		581,6 mm2
Gesamtvolumen		16,92 mm3
Länge pro Bild		6,4 mm
Anzahl Fasern in der Probe		1788590
Mittlerer Knickwinkel		55,6 °
Anzahl Knicke pro mm		0,959 mm-1
Anzahl großer Knicke pro mm		0,346 mm-1
Anzahl Knicke pro Faser		1,315
Anzahl großer Knicke pro Faser		0,474

Lorentzen & Wettre
A MEMBER OF THE ABB GROUP

Probenname:	rechts oben 3	Anzahl Fasern	12924 (180017)
Probenart:	IPPT flippr	Anzahl Bilder	3827
Zeit:	2017-02-23 09:33:03	Temperatur	25,4 °C
Anmerkung			

Volumen gewichtet (ISO)

Variable	Wert	Unterschied
Mittlere Länge	2,273 mm	-0,009 mm
Mittlere Breite	31,6 µm	-0,1 µm
Mittlere Form	81,6 %	-0,3 %
Mean fibril area	1,6 %	0,0 %
Mean fibril perimeter	6,1 %	0,0 %
Mean Fines	7,2 %	

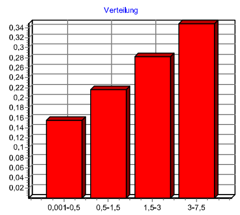

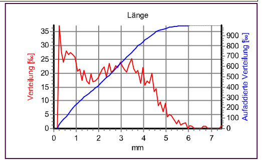

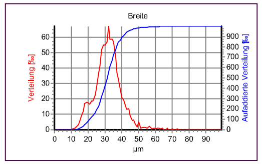

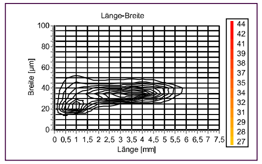

Variable	Gewichtung	Wert
Länge	Länge	1,437 mm
Länge	Breite	0,481 mm
Länge	Fläche	2,035 mm
Länge	Volumen	2,273 mm
Länge	Arithmetik	0,125 mm

Probenname:	rechts oben 3	Anzahl Fasern	12924 (180017)
Probenart:	IPPT flippr	Anzahl Bilder	3827
Zeit:	2017-02-23 09:33:03	Temperatur	25,4 °C
Anmerkung			

Variable	Gewichtung	Wert
Länge	Länge-Länge	3,033 mm
Breite	Länge	25,1 µm
Breite	Breite	22,4 µm
Breite	Fläche	29,1 µm
Breite	Volumen	31,6 µm
Breite	Arithmetik	16,9 µm
Breite	Länge-Länge	30,7 µm
Form	Länge	83,1 %
Form	Breite	88,4 %
Form	Fläche	82,2 %
Form	Volumen	81,6 %
Form	Arithmetik	89,6 %
Form	Länge-Länge	79,5 %
Feinstoff Grenze	Länge	32,5 %
Feinstoff Grenze	Breite	63,4 %
Feinstoff Grenze	Fläche	12,0 %

Variable	Gewichtung	Wert
Feinstoff Grenze	Volumen	7,2 %
Feinstoff Grenze	Arithmetik	92,8 %
Feinstoff Grenze	Länge-Länge	1,8 %
Anzahl Fasern		12924 (180017)
Anzahl Bilder		3827
Temperatur		25,4 °C
Gesamtlänge		22761 mm
Gesamtfläche		602,9 mm2
Gesamtvolumen		17,62 mm3
Länge pro Bild		6,4 mm
Anzahl Fasern in der Probe		1715239
Mittlerer Knickwinkel		54,6 °
Anzahl Knicke pro mm		0,941 mm-1
Anzahl großer Knicke pro mm		0,315 mm-1
Anzahl Knicke pro Faser		1,372
Anzahl großer Knicke pro Faser		0,460

Lorentzen & Wettre
A MEMBER OF THE ABB GROUP

Probenname:	V2 Re 1500 outlet1	Anzahl Fasern	8743 (116106)
Probenart:	IPPT flippr	Anzahl Bilder	5899
Zeit:	2017-05-30 09:45:33	Temperatur	25,3 °C
Anmerkung			

Volumen gewichtet (ISO)

Variable	Wert	Unterschied
Mittlere Länge	2,388 mm	-0,020 mm
Mittlere Breite	31,8 µm	-0,1 µm
Mittlere Form	82,8 %	0,0 %
Mean fibril area	1,2 %	0,0 %
Mean fibril perimeter	4,0 %	0,0 %
Mean Fines	6,1 %	

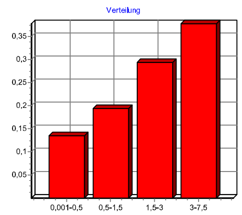

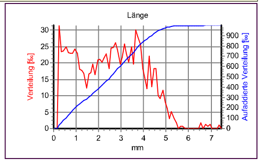

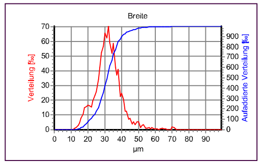

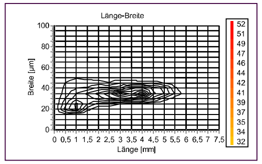

Variable	Gewichtung	Wert
Länge	Länge	1,580 mm
Länge	Breite	0,533 mm
Länge	Fläche	2,166 mm
Länge	Volumen	2,388 mm
Länge	Arithmetik	0,134 mm

Probenname:	V2 Re 1500 outlet1	Anzahl Fasern	8743 (116106)
Probenart:	IPPT flippr	Anzahl Bilder	5899
Zeit:	2017-05-30 09:45:33	Temperatur	25,3 °C
Anmerkung			

Variable	Gewichtung	Wert
Länge	Länge-Länge	3,112 mm
Breite	Länge	25,6 µm
Breite	Breite	22,6 µm
Breite	Fläche	29,4 µm
Breite	Volumen	31,8 µm
Breite	Arithmetik	16,9 µm
Breite	Länge-Länge	30,8 µm
Form	Länge	83,9 %
Form	Breite	88,5 %
Form	Fläche	83,2 %
Form	Volumen	82,8 %
Form	Arithmetik	89,6 %
Form	Länge-Länge	81,2 %
Feinstoff Grenze	Länge	29,6 %
Feinstoff Grenze	Breite	61,7 %
Feinstoff Grenze	Fläche	10,4 %

Variable	Gewichtung	Wert
Feinstoff Grenze	Volumen	6,1 %
Feinstoff Grenze	Arithmetik	92,5 %
Feinstoff Grenze	Länge-Länge	1,5 %
Anzahl Fasern		8743 (116106)
Anzahl Bilder		5899
Temperatur		25,3 °C
Gesamtlänge		14354 mm
Gesamtfläche		377,9 mm2
Gesamtvolumen		11,03 mm3
Länge pro Bild		2,5 mm
Anzahl Fasern in der Probe		734291
Mittlerer Knickwinkel		54,4 °
Anzahl Knicke pro mm		0,828 mm-1
Anzahl großer Knicke pro mm		0,275 mm-1
Anzahl Knicke pro Faser		1,303
Anzahl großer Knicke pro Faser		0,433

Lorentzen & Wettre
A MEMBER OF THE ABB GROUP

Probenname:	V2 Re 1500 outlet2	Anzahl Fasern	10795 (144124)
Probenart:	IPPT flippr	Anzahl Bilder	5896
Zeit:	2017-05-30 10:05:05	Temperatur	25,6 °C
Anmerkung			

Volumen gewichtet (ISO)

Variable	Wert	Unterschied
Mittlere Länge	2,329 mm	0,040 mm
Mittlere Breite	31,6 µm	-0,1 µm
Mittlere Form	82,5 %	0,1 %
Mean fibril area	1,3 %	0,0 %
Mean fibril perimeter	4,5 %	-0,1 %
Mean Fines	6,5 %	

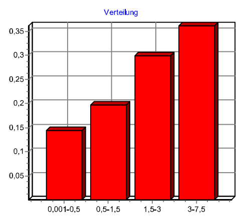

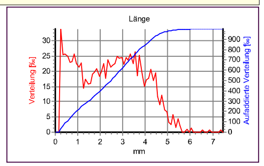

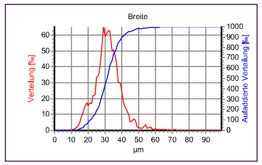

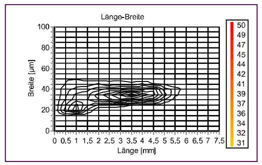

Variable	Gewichtung	Wert
Länge	Länge	1,537 mm
Länge	Breite	0,517 mm
Länge	Fläche	2,114 mm
Länge	Volumen	2,329 mm
Länge	Arithmetik	0,132 mm

Probenname:	V2 Re 1500 outlet2	Anzahl Fasern	10795 (144124)
Probenart:	IPPT flippr	Anzahl Bilder	5896
Zeit:	2017-05-30 10:05:05	Temperatur	25,6 °C
Anmerkung			

Variable	Gewichtung	Wert
Länge	Länge-Länge	3,062 mm
Breite	Länge	25,4 µm
Breite	Breite	22,6 µm
Breite	Fläche	29,2 µm
Breite	Volumen	31,6 µm
Breite	Arithmetik	17,1 µm
Breite	Länge-Länge	30,5 µm
Form	Länge	83,7 %
Form	Breite	88,5 %
Form	Fläche	82,9 %
Form	Volumen	82,5 %
Form	Arithmetik	89,6 %
Form	Länge-Länge	80,8 %
Feinstoff Grenze	Länge	30,3 %
Feinstoff Grenze	Breite	62,2 %
Feinstoff Grenze	Fläche	10,9 %

Variable	Gewichtung	Wert
Feinstoff Grenze	Volumen	6,5 %
Feinstoff Grenze	Arithmetik	92,5 %
Feinstoff Grenze	Länge-Länge	1,6 %
Anzahl Fasern		10795 (144124)
Anzahl Bilder		5896
Temperatur		25,6 °C
Gesamtlänge		18170 mm
Gesamtfläche		478,3 mm2
Gesamtvolumen		13,95 mm3
Länge pro Bild		3,2 mm
Anzahl Fasern in der Probe		907112
Mittlerer Knickwinkel		54,3 °
Anzahl Knicke pro mm		0,857 mm-1
Anzahl großer Knicke pro mm		0,288 mm-1
Anzahl Knicke pro Faser		1,325
Anzahl großer Knicke pro Faser		0,444

Lorentzen & Wettre
A MEMBER OF THE ABB GROUP

Probenname:	V2 Re 1500 outlet3	Anzahl Fasern	13844 (163519)
Probenart:	IPPT flippr	Anzahl Bilder	5886
Zeit:	2017-05-30 10:24:35	Temperatur	25,8 °C
Anmerkung			

Volumen gewichtet (ISO)

Variable	Wert	Unterschied
Mittlere Länge	2,388 mm	0,144 mm
Mittlere Breite	31,7 µm	0,5 µm
Mittlere Form	82,6 %	0,6 %
Mean fibril area	1,3 %	-0,1 %
Mean fibril perimeter	4,7 %	-0,3 %
Mean Fines	6,0 %	

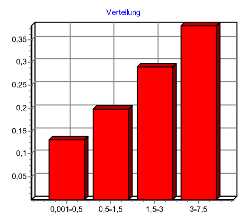

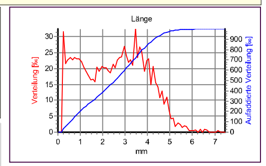

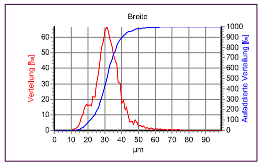

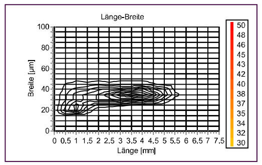

Variable	Gewichtung	Wert
Länge	Länge	1,624 mm
Länge	Breite	0,557 mm
Länge	Fläche	2,177 mm
Länge	Volumen	2,388 mm
Länge	Arithmetik	0,145 mm

Probenname:	V2 Re 1500 outlet3	Anzahl Fasern	13844 (163519)
Probenart:	IPPT flippr	Anzahl Bilder	5886
Zeit:	2017-05-30 10:24:35	Temperatur	25,8 °C
Anmerkung			

Variable	Gewichtung	Wert
Länge	Länge-Länge	3,113 mm
Breite	Länge	25,7 µm
Breite	Breite	22,7 µm
Breite	Fläche	29,3 µm
Breite	Volumen	31,7 µm
Breite	Arithmetik	17,2 µm
Breite	Länge-Länge	30,6 µm
Form	Länge	83,6 %
Form	Breite	88,3 %
Form	Fläche	82,9 %
Form	Volumen	82,6 %
Form	Arithmetik	89,4 %
Form	Länge-Länge	80,9 %
Feinstoff Grenze	Länge	27,9 %
Feinstoff Grenze	Breite	60,1 %
Feinstoff Grenze	Fläche	10,1 %

Variable	Gewichtung	Wert
Feinstoff Grenze	Volumen	6,0 %
Feinstoff Grenze	Arithmetik	91,5 %
Feinstoff Grenze	Länge-Länge	1,4 %
Anzahl Fasern		13844 (163519)
Anzahl Bilder		5886
Temperatur		25,8 °C
Gesamtlänge		24575 mm
Gesamtfläche		662,4 mm2
Gesamtvolumen		19,64 mm3
Länge pro Bild		4,4 mm
Anzahl Fasern in der Probe		1165389
Mittlerer Knickwinkel		54,2 °
Anzahl Knicke pro mm		0,858 mm-1
Anzahl großer Knicke pro mm		0,287 mm-1
Anzahl Knicke pro Faser		1,327
Anzahl großer Knicke pro Faser		0,443

Lorentzen & Wettre
A MEMBER OF THE ABB GROUP

Probenname:	V2 Re 1500 outlet4	Anzahl Fasern	8482 (100040)
Probenart:	IPPT flippr	Anzahl Bilder	3717
Zeit:	2017-05-30 10:44:06	Temperatur	26,0 °C
Anmerkung			

Volumen gewichtet (ISO)

Variable	Wert	Unterschied
Mittlere Länge	2,384 mm	0,157 mm
Mittlere Breite	31,8 µm	0,4 µm
Mittlere Form	82,2 %	-0,4 %
Mean fibril area	1,3 %	-0,1 %
Mean fibril perimeter	4,8 %	-0,2 %
Mean Fines	6,4 %	

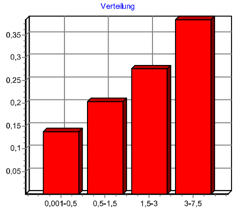

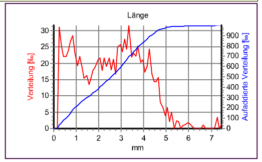

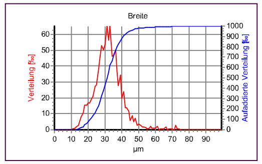

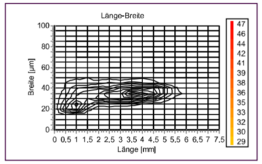

Variable	Gewichtung	Wert
Länge	Länge	1,590 mm
Länge	Breite	0,542 mm
Länge	Fläche	2,156 mm
Länge	Volumen	2,384 mm
Länge	Arithmetik	0,143 mm

Date: 2017-05-30 13:30:11 Instrument number: 260

Probenname:	V2 Re 1500 outlet4	Anzahl Fasern	8482 (100040)
Probenart:	IPPT flippr	Anzahl Bilder	3717
Zeit:	2017-05-30 10:44:06	Temperatur	26,0 °C
Anmerkung			

Variable	Gewichtung	Wert
Länge	Länge-Länge	3,118 mm
Breite	Länge	25,6 µm
Breite	Breite	22,7 µm
Breite	Fläche	29,3 µm
Breite	Volumen	31,8 µm
Breite	Arithmetik	17,3 µm
Breite	Länge-Länge	30,7 µm
Form	Länge	83,5 %
Form	Breite	88,3 %
Form	Fläche	82,7 %
Form	Volumen	82,2 %
Form	Arithmetik	89,4 %
Form	Länge-Länge	80,6 %
Feinstoff Grenze	Länge	28,7 %
Feinstoff Grenze	Breite	60,7 %
Feinstoff Grenze	Fläche	10,6 %

Variable	Gewichtung	Wert
Feinstoff Grenze	Volumen	6,4 %
Feinstoff Grenze	Arithmetik	91,5 %
Feinstoff Grenze	Länge-Länge	1,5 %
Anzahl Fasern		8482 (100040)
Anzahl Bilder		3717
Temperatur		26,0 °C
Gesamtlänge		14677 mm
Gesamtfläche		392,6 mm2
Gesamtvolumen		11,59 mm3
Länge pro Bild		4,2 mm
Anzahl Fasern in der Probe		1161487
Mittlerer Knickwinkel		54,3 °
Anzahl Knicke pro mm		0,865 mm-1
Anzahl großer Knicke pro mm		0,281 mm-1
Anzahl Knicke pro Faser		1,327
Anzahl großer Knicke pro Faser		0,431

Date: 2017-05-30 13:30:11 Instrument number: 260

Lorentzen & Wettre
A MEMBER OF THE ABB GROUP

Probenname:	V2 Re 1500 outlet5	Anzahl Fasern	9875 (100000)
Probenart:	IPPT flippr	Anzahl Bilder	5011
Zeit:	2017-05-30 10:58:02	Temperatur	26,2 °C
Anmerkung			

Volumen gewichtet (ISO)

Variable	Wert	Unterschied
Mittlere Länge	2,466 mm	0,131 mm
Mittlere Breite	31,9 µm	0,7 µm
Mittlere Form	82,8 %	0,1 %
Mean fibril area	1,2 %	-0,1 %
Mean fibril perimeter	4,0 %	-0,4 %
Mean Fines	4,8 %	

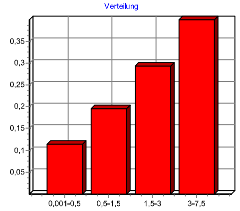

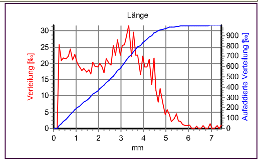

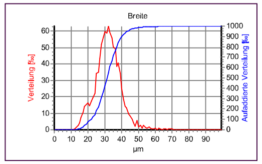

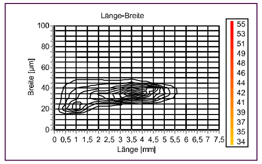

Variable	Gewichtung	Wert
Länge	Länge	1,760 mm
Länge	Breite	0,638 mm
Länge	Fläche	2,269 mm
Länge	Volumen	2,466 mm
Länge	Arithmetik	0,166 mm

Date: 2017-05-30 13:30:22 Instrument number: 260

Probenname:	V2 Re 1500 outlet5	Anzahl Fasern	9875 (100000)
Probenart:	IPPT flippr	Anzahl Bilder	5011
Zeit:	2017-05-30 10:58:02	Temperatur	26,2 °C
Anmerkung			

Variable	Gewichtung	Wert
Länge	Länge-Länge	3,154 mm
Breite	Länge	26,3 µm
Breite	Breite	23,2 µm
Breite	Fläche	29,7 µm
Breite	Volumen	31,9 µm
Breite	Arithmetik	17,3 µm
Breite	Länge-Länge	30,7 µm
Form	Länge	83,5 %
Form	Breite	88,0 %
Form	Fläche	83,0 %
Form	Volumen	82,8 %
Form	Arithmetik	89,1 %
Form	Länge-Länge	81,1 %
Feinstoff Grenze	Länge	23,5 %
Feinstoff Grenze	Breite	55,7 %
Feinstoff Grenze	Fläche	8,2 %

Variable	Gewichtung	Wert
Feinstoff Grenze	Volumen	4,8 %
Feinstoff Grenze	Arithmetik	90,1 %
Feinstoff Grenze	Länge-Länge	1,1 %
Anzahl Fasern		9875 (100000)
Anzahl Bilder		5011
Temperatur		26,2 °C
Gesamtlänge		17443 mm
Gesamtfläche		479,3 mm2
Gesamtvolumen		14,81 mm3
Länge pro Bild		3,7 mm
Anzahl Fasern in der Probe		984247
Mittlerer Knickwinkel		53,7 °
Anzahl Knicke pro mm		0,840 mm-1
Anzahl großer Knicke pro mm		0,269 mm-1
Anzahl Knicke pro Faser		1,340
Anzahl großer Knicke pro Faser		0,428

Date: 2017-05-30 13:30:22 Instrument number: 260

Lorentzen & Wettre
A MEMBER OF THE ABB GROUP

Probenname:	V3 Re 1500 outlet1	Anzahl Fasern	6967 (90599)
Probenart:	IPPT flippr	Anzahl Bilder	5899
Zeit:	2017-05-30 11:24:25	Temperatur	26,4 °C
Anmerkung			

Volumen gewichtet (ISO)

Variable	Wert	Unterschied
Mittlere Länge	2,368 mm	-0,023 mm
Mittlere Breite	31,8 µm	-0,1 µm
Mittlere Form	83,7 %	0,0 %
Mean fibril area	1,3 %	0,0 %
Mean fibril perimeter	4,1 %	-0,1 %
Mean Fines	6,1 %	

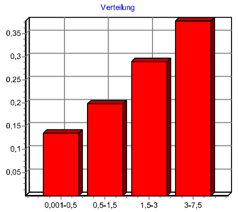

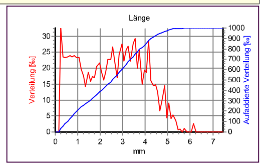

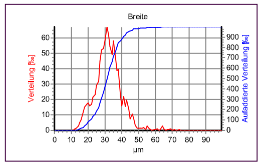

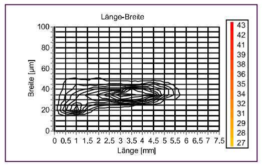

Variable	Gewichtung	Wert
Länge	Länge	1,573 mm
Länge	Breite	0,536 mm
Länge	Fläche	2,147 mm
Länge	Volumen	2,368 mm
Länge	Arithmetik	0,136 mm

Date: 2017-05-30 13:30:33 Instrument number: 260

Probenname:	V3 Re 1500 outlet1	Anzahl Fasern	6967 (90599)
Probenart:	IPPT flippr	Anzahl Bilder	5899
Zeit:	2017-05-30 11:24:25	Temperatur	26,4 °C
Anmerkung			

Variable	Gewichtung	Wert
Länge	Länge-Länge	3,067 mm
Breite	Länge	25,6 µm
Breite	Breite	22,6 µm
Breite	Fläche	29,4 µm
Breite	Volumen	31,8 µm
Breite	Arithmetik	17,0 µm
Breite	Länge-Länge	30,7 µm
Form	Länge	84,5 %
Form	Breite	88,7 %
Form	Fläche	84,0 %
Form	Volumen	83,7 %
Form	Arithmetik	89,7 %
Form	Länge-Länge	82,3 %
Feinstoff Grenze	Länge	29,2 %
Feinstoff Grenze	Breite	61,3 %
Feinstoff Grenze	Fläche	10,3 %

Variable	Gewichtung	Wert
Feinstoff Grenze	Volumen	6,1 %
Feinstoff Grenze	Arithmetik	92,3 %
Feinstoff Grenze	Länge-Länge	1,5 %
Anzahl Fasern		6967 (90599)
Anzahl Bilder		5899
Temperatur		26,4 °C
Gesamtlänge		11194 mm
Gesamtfläche		292,5 mm2
Gesamtvolumen		8,47 mm3
Länge pro Bild		2,0 mm
Anzahl Fasern in der Probe		585131
Mittlerer Knickwinkel		54,2 °
Anzahl Knicke pro mm		0,797 mm-1
Anzahl großer Knicke pro mm		0,261 mm-1
Anzahl Knicke pro Faser		1,218
Anzahl großer Knicke pro Faser		0,399

Date: 2017-05-30 13:30:33 Instrument number: 260

Lorentzen & Wettre
A MEMBER OF THE ABB GROUP

Probenname:	V3 Re 1500 outlet2	Anzahl Fasern	7768 (100028)
Probenart:	IPPT flippr	Anzahl Bilder	5495
Zeit:	2017-05-30 11:48:25	Temperatur	26,6 °C
Anmerkung			

Volumen gewichtet (ISO)

Variable	Wert	Unterschied
Mittlere Länge	2,401 mm	0,006 mm
Mittlere Breite	31,8 µm	0,0 µm
Mittlere Form	82,8 %	-0,2 %
Mean fibril area	1,4 %	0,2 %
Mean fibril perimeter	4,5 %	0,2 %
Mean Fines	5,7 %	

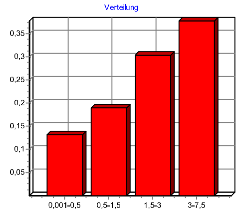

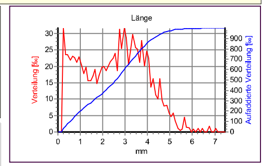

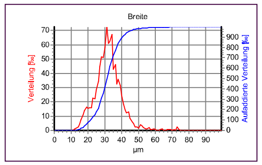

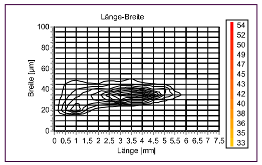

Variable	Gewichtung	Wert
Länge	Länge	1,620 mm
Länge	Breite	0,556 mm
Länge	Fläche	2,188 mm
Länge	Volumen	2,401 mm
Länge	Arithmetik	0,138 mm

Date: 2017-05-30 13:30:42 Instrument number: 260

Probenname:	V3 Re 1500 outlet2	Anzahl Fasern	7768 (100028)
Probenart:	IPPT flippr	Anzahl Bilder	5495
Zeit:	2017-05-30 11:48:25	Temperatur	26,6 °C
Anmerkung			

Variable	Gewichtung	Wert
Länge	Länge-Länge	3,083 mm
Breite	Länge	25,8 µm
Breite	Breite	22,8 µm
Breite	Fläche	29,5 µm
Breite	Volumen	31,8 µm
Breite	Arithmetik	17,0 µm
Breite	Länge-Länge	30,7 µm
Form	Länge	83,8 %
Form	Breite	88,4 %
Form	Fläche	83,2 %
Form	Volumen	82,8 %
Form	Arithmetik	89,4 %
Form	Länge-Länge	81,5 %
Feinstoff Grenze	Länge	28,1 %
Feinstoff Grenze	Breite	60,5 %
Feinstoff Grenze	Fläche	9,7 %

Variable	Gewichtung	Wert
Feinstoff Grenze	Volumen	5,7 %
Feinstoff Grenze	Arithmetik	92,2 %
Feinstoff Grenze	Länge-Länge	1,4 %
Anzahl Fasern		7768 (100028)
Anzahl Bilder		5495
Temperatur		26,6 °C
Gesamtlänge		12666 mm
Gesamtfläche		333,9 mm2
Gesamtvolumen		9,73 mm3
Länge pro Bild		2,4 mm
Anzahl Fasern in der Probe		702714
Mittlerer Knickwinkel		53,9 °
Anzahl Knicke pro mm		0,799 mm-1
Anzahl großer Knicke pro mm		0,255 mm-1
Anzahl Knicke pro Faser		1,254
Anzahl großer Knicke pro Faser		0,400

Date: 2017-05-30 13:30:42 Instrument number: 260

Lorentzen & Wettre
A MEMBER OF THE ABB GROUP

Probenname:	V3 Re 1500 outlet3	Anzahl Fasern	7998 (100018)
Probenart:	IPPT flippr	Anzahl Bilder	5375
Zeit:	2017-05-30 12:06:55	Temperatur	26,7 °C
Anmerkung			

Volumen gewichtet (ISO)

Variable	Wert	Unterschied
Mittlere Länge	2,444 mm	0,057 mm
Mittlere Breite	31,9 µm	0,4 µm
Mittlere Form	82,6 %	-0,4 %
Mean fibril area	1,3 %	0,0 %
Mean fibril perimeter	4,2 %	0,0 %
Mean Fines	5,4 %	

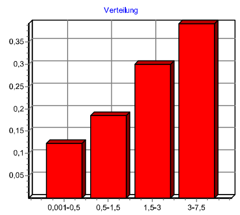

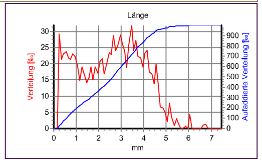

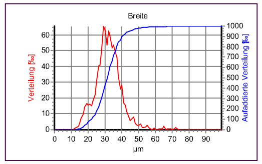

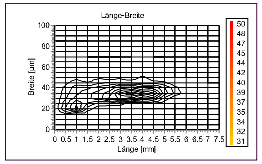

Variable	Gewichtung	Wert
Länge	Länge	1,680 mm
Länge	Breite	0,579 mm
Länge	Fläche	2,238 mm
Länge	Volumen	2,444 mm
Länge	Arithmetik	0,143 mm

Date: 2017-05-30 13:30:55 Instrument number: 260

Probenname:	V3 Re 1500 outlet3	Anzahl Fasern	7998 (100018)
Probenart:	IPPT flippr	Anzahl Bilder	5375
Zeit:	2017-05-30 12:06:55	Temperatur	26,7 °C
Anmerkung			

Variable	Gewichtung	Wert
Länge	Länge-Länge	3,127 mm
Breite	Länge	26,0 µm
Breite	Breite	22,8 µm
Breite	Fläche	29,6 µm
Breite	Volumen	31,9 µm
Breite	Arithmetik	16,9 µm
Breite	Länge-Länge	30,8 µm
Form	Länge	83,6 %
Form	Breite	88,3 %
Form	Fläche	83,0 %
Form	Volumen	82,6 %
Form	Arithmetik	89,4 %
Form	Länge-Länge	81,0 %
Feinstoff Grenze	Länge	27,0 %
Feinstoff Grenze	Breite	59,6 %
Feinstoff Grenze	Fläche	9,3 %

Variable	Gewichtung	Wert
Feinstoff Grenze	Volumen	5,4 %
Feinstoff Grenze	Arithmetik	92,0 %
Feinstoff Grenze	Länge-Länge	1,3 %
Anzahl Fasern		7998 (100018)
Anzahl Bilder		5375
Temperatur		26,7 °C
Gesamtlänge		13669 mm
Gesamtfläche		364,7 mm2
Gesamtvolumen		10,70 mm3
Länge pro Bild		2,7 mm
Anzahl Fasern in der Probe		740481
Mittlerer Knickwinkel		53,7 °
Anzahl Knicke pro mm		0,791 mm-1
Anzahl großer Knicke pro mm		0,249 mm-1
Anzahl Knicke pro Faser		1,265
Anzahl großer Knicke pro Faser		0,398

Date: 2017-05-30 13:30:55 Instrument number: 260

Lorentzen & Wettre
A MEMBER OF THE ABB GROUP

Probenname:	V3 Re 1500 outlet4	Anzahl Fasern	8023 (100001)
Probenart:	IPPT flippr	Anzahl Bilder	5658
Zeit:	2017-05-30 12:25:07	Temperatur	26,8 °C
Anmerkung			

Volumen gewichtet (ISO)

Variable	Wert	Unterschied
Mittlere Länge	2,419 mm	-0,038 mm
Mittlere Breite	31,9 µm	0,0 µm
Mittlere Form	82,8 %	-0,2 %
Mean fibril area	1,3 %	-0,1 %
Mean fibril perimeter	4,3 %	-0,4 %
Mean Fines	5,5 %	

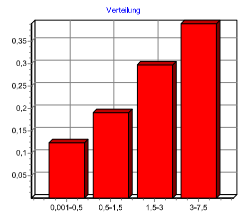

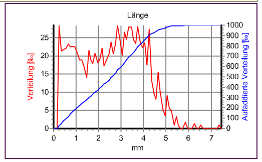

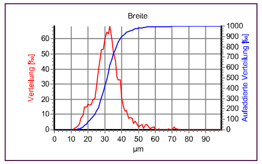

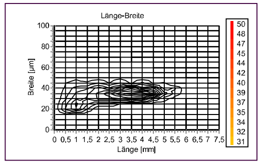

Variable	Gewichtung	Wert
Länge	Länge	1,661 mm
Länge	Breite	0,575 mm
Länge	Fläche	2,213 mm
Länge	Volumen	2,419 mm
Länge	Arithmetik	0,143 mm

Date: 2017-05-30 13:31:03 Instrument number: 260

Probenname:	V3 Re 1500 outlet4	Anzahl Fasern	8023 (100001)
Probenart:	IPPT flippr	Anzahl Bilder	5658
Zeit:	2017-05-30 12:25:07	Temperatur	26,8 °C
Anmerkung			

Variable	Gewichtung	Wert
Länge	Länge-Länge	3,108 mm
Breite	Länge	25,9 µm
Breite	Breite	22,8 µm
Breite	Fläche	29,5 µm
Breite	Volumen	31,9 µm
Breite	Arithmetik	16,9 µm
Breite	Länge-Länge	30,7 µm
Form	Länge	83,6 %
Form	Breite	88,3 %
Form	Fläche	83,0 %
Form	Volumen	82,8 %
Form	Arithmetik	89,3 %
Form	Länge-Länge	81,1 %
Feinstoff Grenze	Länge	27,1 %
Feinstoff Grenze	Breite	59,8 %
Feinstoff Grenze	Fläche	9,4 %

Variable	Gewichtung	Wert
Feinstoff Grenze	Volumen	5,5 %
Feinstoff Grenze	Arithmetik	92,0 %
Feinstoff Grenze	Länge-Länge	1,3 %
Anzahl Fasern		8023 (100001)
Anzahl Bilder		5658
Temperatur		26,8 °C
Gesamtlänge		13581 mm
Gesamtfläche		362,2 mm2
Gesamtvolumen		10,71 mm3
Länge pro Bild		2,5 mm
Anzahl Fasern in der Probe		703882
Mittlerer Knickwinkel		54,4 °
Anzahl Knicke pro mm		0,816 mm-1
Anzahl großer Knicke pro mm		0,272 mm-1
Anzahl Knicke pro Faser		1,296
Anzahl großer Knicke pro Faser		0,432

Date: 2017-05-30 13:31:03 Instrument number: 260

Lorentzen & Wettre
A MEMBER OF THE ABB GROUP

Probenname:	V3 Re 1500 outlet5	Anzahl Fasern	7931 (96718)
Probenart:	IPPT flippr	Anzahl Bilder	5895
Zeit:	2017-05-30 12:44:03	Temperatur	26,9 °C
Anmerkung			

Volumen gewichtet (ISO)

Variable	Wert	Unterschied
Mittlere Länge	2,435 mm	0,081 mm
Mittlere Breite	31,7 µm	-0,2 µm
Mittlere Form	82,8 %	-0,4 %
Mean fibril area	1,3 %	-0,1 %
Mean fibril perimeter	4,2 %	-0,3 %
Mean Fines	5,5 %	

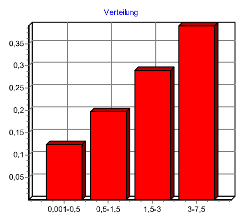

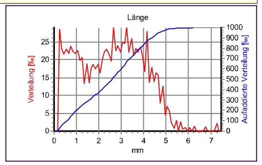

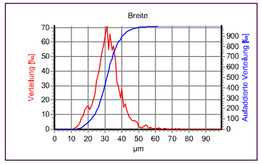

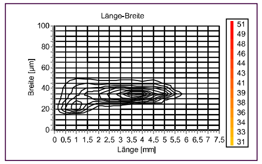

Variable	Gewichtung	Wert
Länge	Länge	1,685 mm
Länge	Breite	0,578 mm
Länge	Fläche	2,236 mm
Länge	Volumen	2,435 mm
Länge	Arithmetik	0,145 mm

Date: 2017-05-30 13:31:12 Instrument number: 260

Probenname:	V3 Re 1500 outlet5	Anzahl Fasern	7931 (96718)
Probenart:	IPPT flippr	Anzahl Bilder	5895
Zeit:	2017-05-30 12:44:03	Temperatur	26,9 °C
Anmerkung			

Variable	Gewichtung	Wert
Länge	Länge-Länge	3,153 mm
Breite	Länge	25,9 µm
Breite	Breite	22,8 µm
Breite	Fläche	29,5 µm
Breite	Volumen	31,7 µm
Breite	Arithmetik	17,0 µm
Breite	Länge-Länge	30,6 µm
Form	Länge	83,7 %
Form	Breite	88,4 %
Form	Fläche	83,1 %
Form	Volumen	82,8 %
Form	Arithmetik	89,4 %
Form	Länge-Länge	81,1 %
Feinstoff Grenze	Länge	26,9 %
Feinstoff Grenze	Breite	59,5 %
Feinstoff Grenze	Fläche	9,4 %

Variable	Gewichtung	Wert
Feinstoff Grenze	Volumen	5,5 %
Feinstoff Grenze	Arithmetik	91,8 %
Feinstoff Grenze	Länge-Länge	1,3 %
Anzahl Fasern		7931 (96718)
Anzahl Bilder		5895
Temperatur		26,9 °C
Gesamtlänge		13229 mm
Gesamtfläche		351,0 mm2
Gesamtvolumen		10,24 mm3
Länge pro Bild		2,3 mm
Anzahl Fasern in der Probe		666566
Mittlerer Knickwinkel		54,1 °
Anzahl Knicke pro mm		0,771 mm-1
Anzahl großer Knicke pro mm		0,250 mm-1
Anzahl Knicke pro Faser		1,253
Anzahl großer Knicke pro Faser		0,406

Date: 2017-05-30 13:31:12 Instrument number: 260

Appendix F Simulation Settings

F.1 LES: dynamic k-Equation Model

For the large eddy simulations (LES) the dynamic k-equation subgrid scale (SGS) model developed by Chai and Mahesh [27] is used. The model is in the category of the one-equation eddy viscosity model where the kinetic energy equation is modelled separately and dynamically closed.

The spatially (Favre) filtered Navier Stokes equation denote as [27]:

$$\frac{\partial\left(\bar{\rho}\tilde{u}_i\right)}{\partial t}=-\frac{\partial}{\partial x_j}\left(\bar{\rho}\tilde{u}_i\tilde{u}_j+\bar{p}\delta_{ij}-2\bar{\mu}\left[\frac{1}{2}\left(\frac{\partial\tilde{u}_i}{\partial x_j}+\frac{\partial\tilde{u}_j}{\partial x_i}\right)-\frac{1}{3}\frac{\partial\tilde{u}_k}{\partial x_k}\delta_{ij}\right]+\bar{\rho}\left(u_iu_j-\tilde{u}_i\tilde{u}_j\right)\right) \quad \textbf{Equation 30}$$

The model constant C_s, which is needed for the calculation of the kinetic subgrid, stresses $\tau_{ij}=\bar{\rho}\left(u_iu_j-\tilde{u}_i\tilde{u}_j\right)$ (see Chapter 4.3.2):

$$C_s\cdot\Delta^2=\frac{1}{2}\cdot\frac{\left\langle L_{ij}^*\cdot M_{ij}^*\right\rangle}{\left\langle M_{ij}^*\cdot M_{ij}^*\right\rangle} \quad \textbf{Equation 31}$$

Here $\langle\ \cdot\ \rangle$ describes the spatial average over homogeneous directions of:

$$L_{ij}^*=L_{ij}-\frac{1}{3}\cdot\delta_{ij}\cdot L_{kk}\quad with\quad L_{ij}=\left(\frac{\overline{\rho\cdot u_i}\cdot\overline{\rho\cdot u_i}}{\rho}\right)-\frac{\overline{\rho\cdot u_i}\cdot\overline{\rho\cdot u_i}}{\bar{\rho}}$$

$$M_{ij}^*=\bar{\rho}\cdot\left|S\cdot\tilde{S}_{ij}^*\right|-\hat{\bar{\rho}}\cdot\left(\frac{\hat{\Delta}}{\Delta}\right)^2\cdot\left|S\right|\hat{\tilde{S}}_{ij}^* \quad \textbf{Equation 32}$$

For this model the conservation equation for the turbulent kinetic energy is:

$$\begin{aligned}\frac{\partial\bar{\rho}k}{\partial t}&=-\frac{\partial\bar{\rho}\tilde{u}_j}{\partial x_j}-\tau_{ij}\tilde{S}_{ij}-2\bar{\mu}\left[S_{ij}^*D_{ij}^*-\tilde{S}_{ij}^*\tilde{D}_{ij}^*\right]-\frac{\partial}{\partial x_j}\left[\frac{5}{3}\left(\bar{\mu}u_j\frac{\partial u_k}{\partial x_k}-\bar{\mu}\tilde{u}_j\frac{\partial\tilde{u}_k}{\partial\tilde{x}_k}\right)\right]\\&+\frac{\partial}{\partial x_j}\left[\tau_{ij}\tilde{u}_i+\bar{\mu}\frac{\partial k}{\partial x_j}+\bar{\mu}\frac{\partial}{\partial x_i}\left(\frac{\tau_{ij}}{\bar{\rho}}\right)+Rq_j\right]-\frac{\partial}{\partial x_j}\left[\frac{1}{2}\bar{\rho}\left(u_iu_iu_j-u_iu_i\tilde{u}_j\right)\right]\\&+\left(\overline{p\frac{\partial u_k}{\partial x_k}}-\bar{p}\frac{\partial\tilde{u}_k}{\partial x_k}\right)\end{aligned} \quad \textbf{Equation 33}$$

Where $\tilde{\bullet}$ denotes the Favre filtered quantities and $\hat{\bullet}$ marks term on which the test filter is applied.

F.2 RANS: k–ω - SST – Model

As described in Chapter 4.3.1 the turbulence is modelled as an increased viscosity. Hence, the Reynolds stresses are written as [23]:

$$-\overline{u_i'u_j'} = \nu_t\left(\frac{\partial \overline{u}_i}{\partial x_j}+\frac{\partial \overline{u}_j}{\partial x_i}\right)-\frac{2}{3}\delta_{ij}k$$ **Equation 34**

Where ν_t is the turbulent viscosity. The turbulence model developed by Menter [24] calculates this kinematic eddy viscosity by:

$$\nu_t = \frac{a_1\cdot k}{\max(a_1\cdot\omega, S\cdot F_2)}$$ **Equation 35**

Where the turbulent kinetic energy is calculated:

$$\frac{\partial k}{\partial t}+U_j\frac{\partial k}{\partial x_j} = P_k-\beta^* k\omega+\frac{\partial}{\partial x_j}\left[\left(\nu+\sigma_k\nu_t\right)\frac{\partial k}{\partial x_j}\right]$$ **Equation 36**

and the specific dissipation rate:

$$\frac{\partial \omega}{\partial t}+U_j\frac{\partial \omega}{\partial x_j} = \alpha S^2-\beta\omega^2+\frac{\partial}{\partial x_j}\left[\left(\nu+\sigma_\omega\nu_t\right)\frac{\partial \omega}{\partial x_j}\right]+2\left(1-F_1\right)\sigma_{\omega 2}\frac{1}{\omega}\frac{\partial k}{\partial x_i}\frac{\partial \omega}{\partial x_i}$$ **Equation 37**

The blending functions are defined as:

$$F_1 = \tanh\left\{\left\{\min\left[\max\left(\frac{\sqrt{k}}{\beta^*\omega y}, \frac{500\nu}{y^2\omega}\right), \frac{4\sigma_{\omega 2}k}{CD_{k\omega}y^2}\right]\right\}^4\right\}$$

$$with\ CD_{k\omega} = \max\left(2\rho\sigma_{\omega 2}\frac{1}{\omega}\frac{\partial k}{\partial x_i}\frac{\partial \omega}{\partial x_i}, 10^{-10}\right)$$ **Equation 38**

$$F_2 = \tanh\left\{\left[\max\left(\frac{2\sqrt{k}}{\beta^*\omega y}, \frac{500\nu}{y^2\omega}\right)\right]^2\right\}$$

The production term for the kinetic energy is:

$$P_k = \min\left(\tau_{ij}\frac{\partial U_i}{\partial x_j}, 10\beta^* k\omega\right)$$ **Equation 39**

The model constants are defined as:

$$\alpha = \frac{5}{9}F_1+0.44\left(1-F_1\right)\ ;\ \beta = \frac{3}{40}F_1+0.0828\left(1-F_1\right)\ ;\ \beta^* = \frac{9}{100}$$

$$\sigma_k = 0.85F_1+\left(1-F_1\right)\ ;\ \sigma_\omega = 0.5F_1+0.856\left(1-F_1\right)\ ;\ \sigma_{\omega 2} = 0.856$$ **Equation 40**

F.3 Mesh Generation Routine

Bash script for generating the simulation domain (i.e. mesh) of the base case simulations of the forward distributor with five outlet ports.

```
#Always run this script in your case-directory

## clear old stuff
./clean
rm -v log.*
rm -rv ./processor*
rm -rv ./0/*
#rm -rv ./constant

## Inlet section of splitter
# create 3rd step with blockMesh
rm -r constant/polyMesh/*
cp -v ./mesh/blockMeshDict ./constant/polyMesh/blockMeshDict
blockMesh

################################################
## activate ippt extrude model in control dict ##
################################################

# redefine patch and extrude step 2
topoSet     -dict mesh/inlet_02.topoSet
createPatch -dict mesh/inlet_02.createPatch -overwrite
rm system/extrudeMeshDict
cp -v ./mesh/inlet_02.extrudeMesh ./system/extrudeMeshDict
extrudeMesh

# redefine patch and extrude step 1
topoSet     -dict mesh/inlet_01.topoSet
createPatch -dict mesh/inlet_01.createPatch -overwrite
rm system/extrudeMeshDict
cp -v ./mesh/inlet_01.extrudeMesh ./system/extrudeMeshDict
extrudeMesh

# redefine patch and extrude inlet
topoSet     -dict mesh/inlet_00.topoSet
createPatch -dict mesh/inlet_00.createPatch -overwrite
rm system/extrudeMeshDict
cp -v ./mesh/inlet_00.extrudeMesh ./system/extrudeMeshDict
extrudeMesh

## Inlet section of splitter
# redefine patch and extrude outlet 01
topoSet     -dict mesh/outlet_01.topoSet
createPatch -dict mesh/outlet_01.createPatch -overwrite
rm system/extrudeMeshDict
cp -v ./mesh/outlet_01.extrudeMesh ./system/extrudeMeshDict
extrudeMesh

# redefine patch and extrude outlet 02
topoSet     -dict mesh/outlet_02.topoSet
createPatch -dict mesh/outlet_02.createPatch -overwrite
rm system/extrudeMeshDict
cp -v ./mesh/outlet_02.extrudeMesh ./system/extrudeMeshDict
extrudeMesh
```

```
# redefine patch and extrude outlet 03
topoSet     -dict mesh/outlet_03.topoSet
createPatch -dict mesh/outlet_03.createPatch -overwrite
rm system/extrudeMeshDict
cp -v ./mesh/outlet_03.extrudeMesh ./system/extrudeMeshDict
extrudeMesh

# redefine patch and extrude outlet 04
topoSet     -dict mesh/outlet_04.topoSet
createPatch -dict mesh/outlet_04.createPatch -overwrite
rm system/extrudeMeshDict
cp -v ./mesh/outlet_04.extrudeMesh ./system/extrudeMeshDict
extrudeMesh

# redefine patch and extrude outlet 05
topoSet     -dict mesh/outlet_05.topoSet
createPatch -dict mesh/outlet_05.createPatch -overwrite
rm system/extrudeMeshDict
cp -v ./mesh/outlet_05.extrudeMesh ./system/extrudeMeshDict
extrudeMesh

## redefine and refine
# define a single patch with all wall-patches in it
createPatch -dict ./mesh/allWall.createPatch -overwrite

# renumberMesh (to speed up computing by reducing the matrix size)
renumberMesh -latestTime -overwrite

# copy Initial Conditions from setup to run directory
cp -rv setup/0.org 0/

###################################################
## deactivate ippt extrude model in control dict ##
###################################################

# create internal patches for pressure, velocity and massflow detection
topoSet -dict ./mesh/probeInlet_01.topoSet
topoSet -dict ./mesh/probeInlet_02.topoSet
topoSet -dict ./mesh/probeInlet_03.topoSet

# map (copy) inlet velocity profile fields from another case
mapFields -consistent -sourceTime latestTime ../000_inletProfile_Re1500_rans

#decompose Case
decomposePar -latestTime -force -constant > log.decomposePar

# checkMesh
checkMesh > log.Mesh

#run case
mpirun -np 4 pimpleFoam -parallel > log.run &
```

F.4 Solver, Solution and Stability Control

This section contains the setup files for the simulations:

• U	initial condition of velocity field
• p	initial condition of pressure field
• k	initial condition of turbulent kinetic energy
• nut	initial condition for turbulent viscosity
• nuTilda	initial condition for test filtered turbulent viscosity (LES only)
• omega	initial condition for the specific dissipation rate (RANS only)
• fvSolution	set solver
• fvSchemes	set discretisation schemes
• transportProperties	set viscosity, thermal conductivity, concentration
• turbulenceProperties	specify turbulence model
• controlDict	set step size, start and end time, I/O settings

```
/*--------------------------------*- C++ -*----------------------------------*\
| =========                 |                                                 |
| \\      /  F ield         | OpenFOAM: The Open Source CFD Toolbox           |
|  \\    /   O peration     | Version:  3.0.x                                 |
|   \\  /    A nd           | Web:      www.OpenFOAM.org                      |
|    \\/     M anipulation  |                                                 |
\*---------------------------------------------------------------------------*
/
FoamFile
{
    version     2.0;
    format      ascii;
    class       volVectorField;
    location    "0";
    object      U;
}
// * * * * * * * * * * * * * * * * * * * * * * * * * * * * * * * * * * * * * //
dimensions      [0 1 -1 0 0 0 0];
internalField   uniform (0 0 0);
boundaryField
{
    inlet00
    {
        type            fixedValue;
        value           nonuniform List<vector>
    1302    //Number of faces in the inlet patch1;
    (
    (x y z) //Velocity for all cells of the inlet patch;
    )       //Not shown in order to kept readability;
    }
    outlet01
    {
        type            inletOutlet;
        inletValue      uniform (0 0 0);
        value           uniform (0 0 0);
    }
    outlet02
    {
        $outlet01
    }
    outlet03
    {
        $outlet01
    }
    outlet04
    {
        $outlet01
    }
    outlet05
    {
        $outlet01
    }
    allWall
    {
        type            fixedValue;
        value           uniform (0 0 0);
    }
}
// ************************************************************************* //
```

```
/*--------------------------------*- C++ -*----------------------------------*\
| =========                 |                                                 |
| \\      /  F ield         | OpenFOAM: The Open Source CFD Toolbox           |
|  \\    /   O peration     | Version:  3.0.x                                 |
|   \\  /    A nd           | Web:      www.OpenFOAM.org                      |
|    \\/     M anipulation  |                                                 |
\*---------------------------------------------------------------------------*
/
FoamFile
{
    version     2.0;
    format      ascii;
    class       volScalarField;
    location    "0";
    object      p;
}
// * * * * * * * * * * * * * * * * * * * * * * * * * * * * * * * * * * * * * //

dimensions      [0 2 -2 0 0 0 0];
internalField   uniform 0;

boundaryField
{
    inlet00
    {
        type            zeroGradient;
    }
    outlet01
    {
        type            fixedValue;
        value           uniform 0;
    }
    outlet02
    {
        $outlet01
    }
    outlet03
    {
        $outlet01
    }
    outlet04
    {
        $outlet01
    }
    outlet05
    {
        $outlet01
    }
    allWall
    {
        type            zeroGradient;
    }
}

// ************************************************************************* //
```

```
/*--------------------------------*- C++ -*----------------------------------*\
| =========                 |                                                 |
| \\      /  F ield         | OpenFOAM: The Open Source CFD Toolbox           |
|  \\    /   O peration     | Version:  3.0.x                                 |
|   \\  /    A nd           | Web:      www.OpenFOAM.org                      |
|    \\/     M anipulation  |                                                 |
\*---------------------------------------------------------------------------*/
FoamFile
{
    version     2.0;
    format      ascii;
    class       volScalarField;
    location    "0";
    object      k;
}
// * * * * * * * * * * * * * * * * * * * * * * * * * * * * * * * * * * * * * //

dimensions      [0 2 -2 0 0 0 0];
internalField   uniform 0.02;

boundaryField
{
    inlet00
    {
        type            fixedValue;
        value           $internalField;
    }
    outlet01
    {
        type                inletOutlet;
        inletValue          uniform 0;
        value               uniform 0;
    }
    outlet02
    {
        $outlet01
    }
    outlet03
    {
        $outlet01
    }
    outlet04
    {
        $outlet01
    }
    outlet05
    {
        $outlet01
    }
    allWall
    {
        type            fixedValue;
        value           uniform 0;
    }
}

// ************************************************************************* //
```

```
/*--------------------------------*- C++ -*----------------------------------*\
| =========                 |                                                 |
| \\      /  F ield         | OpenFOAM: The Open Source CFD Toolbox           |
|  \\    /   O peration     | Version:  3.0.x                                 |
|   \\  /    A nd           | Web:      www.OpenFOAM.org                      |
|    \\/     M anipulation  |                                                 |
\*---------------------------------------------------------------------------*/
FoamFile
{
    version     2.0;
    format      ascii;
    class       volScalarField;
    location    "0";
    object      nut;
}
// * * * * * * * * * * * * * * * * * * * * * * * * * * * * * * * * * * * * * //

dimensions      [0 2 -1 0 0 0 0];
internalField   uniform 0;

boundaryField
{
    inlet00
    {
        type            zeroGradient;
    }
    outlet01
    {
        type            zeroGradient;
    }
    outlet02
    {
        $outlet01
    }
    outlet03
    {
        $outlet01
    }
    outlet04
    {
        $outlet01
    }
    outlet05
    {
        $outlet01
    }
    outlet06
    {
        $outlet01
    }
    allWall
    {
        type            zeroGradient;
    }
}

// ************************************************************************* //
```

```
/*--------------------------------*- C++ -*----------------------------------*\
| =========                 |                                                 |
| \\      /  F ield         | OpenFOAM: The Open Source CFD Toolbox           |
|  \\    /   O peration     | Version:  3.0.x                                 |
|   \\  /    A nd           | Web:      www.OpenFOAM.org                      |
|    \\/     M anipulation  |                                                 |
\*---------------------------------------------------------------------------*/
FoamFile
{
    version     2.0;
    format      ascii;
    class       volScalarField;
    location    "0";
    object      nuTilda;
}
// * * * * * * * * * * * * * * * * * * * * * * * * * * * * * * * * * * * * * //

dimensions      [0 2 -1 0 0 0 0];
internalField   uniform 0;

boundaryField
{
    inlet00
    {
        type            fixedValue;
        value           uniform 0;
    }
    outlet01
    {
        type            inletOutlet;
        inletValue      uniform 0;
        value           uniform 0;
    }
    outlet02
    {
        $outlet01
    }
    outlet03
    {
        $outlet01
    }
    outlet04
    {
        $outlet01
    }
    outlet05
    {
        $outlet01
    }
    allWall
    {
        type            fixedValue;
        value           uniform 0;
    }
}

// ************************************************************************* //
```

```
/*--------------------------------*- C++ -*----------------------------------*\
| =========                 |                                                 |
| \\      /  F ield         | OpenFOAM: The Open Source CFD Toolbox           |
|  \\    /   O peration     | Version:  3.0.x                                 |
|   \\  /    A nd           | Web:      www.OpenFOAM.org                      |
|    \\/     M anipulation  |                                                 |
\*---------------------------------------------------------------------------*/
FoamFile
{
    version     2.0;
    format      ascii;
    class       volScalarField;
    location    "0";
    object      omega;
}
// * * * * * * * * * * * * * * * * * * * * * * * * * * * * * * * * * * * * * //

dimensions      [0 0 -1 0 0 0 0];
internalField   uniform 10;

boundaryField
{
    inlet00
    {
        type            fixedValue;
        value           $internalField;
    }
    outlet01
    {
        type            zeroGradient;
    }
    outlet02
    {
        $outlet01
    }
    outlet03
    {
        $outlet01
    }
    outlet04
    {
        $outlet01
    }
    outlet05
    {
        $outlet01
    }
    allWall
    {
        type            omegaWallFunction;
        value           $internalField;
    }
}

// ************************************************************************* //
```

```
/*--------------------------------*- C++ -*----------------------------------*\
| =========                 |                                                 |
| \\      /  F ield         | OpenFOAM: The Open Source CFD Toolbox           |
|  \\    /   O peration     | Version:  3.0.x                                 |
|   \\  /    A nd           | Web:      www.OpenFOAM.org                      |
|    \\/     M anipulation  |                                                 |
\*---------------------------------------------------------------------------*
/
FoamFile
{
    version     2.0;
    format      ascii;
    class       dictionary;
    object      fvSolution;
}
// * * * * * * * * * * * * * * * * * * * * * * * * * * * * * * * * * * * * * //

solvers
{
    p
    {
        solver          GAMG;
        tolerance       1e-6;
        relTol          0.1;
        smoother        GaussSeidel;
        nPreSweeps      0;
        nPostSweeps     2;
        cacheAgglomeration true;
        agglomerator    faceAreaPair;
        nCellsInCoarsestLevel 10;
        mergeLevels     1;
    };

    pFinal
    {
        $p;
        smoother        DICGaussSeidel;
        tolerance       1e-6;
        relTol          0;
    };

    "(U|k|B|nuTilda|omega)"
    {
        solver          smoothSolver;
        smoother        GaussSeidel;
        tolerance       1e-6;
        relTol          0.0;
    };

    "(U|k|B|nuTilda|omega)Final"
    {
        $U;
        tolerance       1e-07;
        relTol          0;
    };

}

PISO    //LES
{
    nCorrectors     3;
    nNonOrthogonalCorrectors 0;
}

SIMPLE  //RANS
{
    nNonOrthogonalCorrectors 0;
    consistent      yes;
    residualControl
    {
        p               1e-3;
        U               1e-4;
        "(k|omega)"     1e-4;
    }
}

relaxationFactors //LES
{
    "U.*"               1;
    "nuTilda.*"         1;
}

relaxationFactors //RANS
{
    p               0.3;
    U               0.5;
    nuTilda         0.5;
}

cache
{
    grad(U);
}

// ************************************************************************* //
```

```
/*--------------------------------*- C++ -*----------------------------------*\
| =========                 |                                                 |
| \\      /  F ield         | OpenFOAM: The Open Source CFD Toolbox           |
|  \\    /   O peration     | Version:  3.0.x                                 |
|   \\  /    A nd           | Web:      www.OpenFOAM.org                      |
|    \\/     M anipulation  |                                                 |
\*---------------------------------------------------------------------------*
/
FoamFile
{
    version     2.0;
    format      ascii;
    class       dictionary;
    object      fvSchemes;
}
// * * * * * * * * * * * * * * * * * * * * * * * * * * * * * * * * * * * * * //

ddtSchemes
{
    default         backward;                       //for LES Simulation
    default         steadyState:                    //for RANS Simulation
}

d2dt2Schemes
{
}

gradSchemes
{
//LES
    default         Gauss linear;
    grad(nuTilda)   cellLimited Gauss linear 1;
    grad(U)         cellLimited Gauss linear 1;

//RANS
    default             Gauss linear;
    //default             leastSquares; a second-order, least squares distance
calculation using all neighbour cells
    //default             Gauss cubic; third-order scheme that appears in the
dnsFoam simulation on a regular mesh.

    //aktivate for case with poor mesh quality (first U than p,k)
    //grad(U)        cellLimited Gauss linear 1;
    //grad(p)        Gauss linear;
    //grad(k)        cellLimited Gauss linear 1;
}

divSchemes
{
//LES and RANS
    default         none;
    div(phi,U)      Gauss LUST grad(U);
    div(phi,k)      Gauss limitedLinear 1;
    div((nuEff*dev2(T(grad(U))))) Gauss linear;
//RANS
    div(phi,omega)  bounded Gauss upwind;
//LES
    div(phi,nuTilda) Gauss limitedLinear 1;
}

laplacianSchemes
{
//LES
    default         Gauss linear corrected;
//RANS
    default         none;
    laplacian(nuEff,U)              Gauss linear corrected;
    laplacian(rAUf,p)               Gauss linear corrected;
    laplacian((1|((1|(1|A(U)))-H(1))),p) Gauss linear corrected;
    laplacian(DomegaEff,omega)      Gauss linear corrected;
    laplacian(DkEff,k)              Gauss linear corrected;
}

interpolationSchemes
{
    default         linear;
}

snGradSchemes
{
    default         corrected;
}

//RANS
wallDist
{
    method meshWave;
}

// ************************************************************************* //
```

```
/*--------------------------------*- C++ -*----------------------------------*\
| =========                 |                                                 |
| \\      /  F ield         | OpenFOAM: The Open Source CFD Toolbox           |
|  \\    /   O peration     | Version:  3.0.x                                 |
|   \\  /    A nd           | Web:      www.OpenFOAM.org                      |
|    \\/     M anipulation  |                                                 |
\*---------------------------------------------------------------------------*
/
FoamFile
{
    version     2.0;
    format      ascii;
    class       dictionary;
    location    "constant";
    object      transportProperties;
}
// * * * * * * * * * * * * * * * * * * * * * * * * * * * * * * * * * * * * * //

transportModel  Newtonian;

nu              nu [ 0 2 -1 0 0 0 0 ] 1.004e-06;
```

```
/*--------------------------------*- C++ -*----------------------------------*\
| =========                 |                                                 |
| \\      /  F ield         | OpenFOAM: The Open Source CFD Toolbox           |
|  \\    /   O peration     | Version:  3.0.x                                 |
|   \\  /    A nd           | Web:      www.OpenFOAM.org                      |
|    \\/     M anipulation  |                                                 |
\*---------------------------------------------------------------------------*/
FoamFile
{
    version     2.0;
    format      ascii;
    class       dictionary;
    location    "constant";
    object      turbulenceProperties;
}
// * * * * * * * * * * * * * * * * * * * * * * * * * * * * * * * * * * * * * //

// RANS Simulations
simulationType RAS;
{
    RASModel        kOmegaSST;
    turbulence      on;
    printCoeffs     on;
}


//LES Simulations
simulationType  LES;
LES
{
    LESModel            dynamicKEqn;
    delta               cubeRootVol;
    printCoeffs         on;
    turbulence          on;

    dynamicKEqnCoeffs
    {
        filter simple;
    }

    cubeRootVolCoeffs
    {
        deltaCoeff      1;
    }
}

// ************************************************************************* //
```

```
/*--------------------------------*- C++ -*----------------------------------*\
| =========                 |                                                 |
| \\      /  F ield         | OpenFOAM: The Open Source CFD Toolbox           |
|  \\    /   O peration     | Version:  3.0.x                                 |
|   \\  /    A nd           | Web:      www.OpenFOAM.org                      |
|    \\/     M anipulation  |                                                 |
\*---------------------------------------------------------------------------*/
FoamFile
{
    version     2.0;
    format      ascii;
    class       dictionary;
    object      controlDict;
}
// * * * * * * * * * * * * * * * * * * * * * * * * * * * * * * * * * * * * * //

libs
(
    "libOpenFOAM.so"
    "libextrudeModelIPPT.so"
    "libsimpleFunctionObjects.so"
    "libsimpleSwakFunctionObjects.so"
);

application     pisoFoam;       //Set solver

startFrom       latestTime;     //Set methode for simulation start
startTime       0;              //Set time step to start from (method 'startTime')

stopAt          endTime;        //Set methode for simulation end
endTime         10;             //Set time step to end simualtion

deltaT          1e-4;           //Set time step size

writeControl    timeStep;       //Set methode of data writing
writeInterval   500;            //Set time step interval of data writing
purgeWrite      0;              //Set number of data set to keep (0 = keep all)
writeFormat     ascii;          //Set write format
writePrecision  6;              //Set precision for data U,p,k,omega,nut,nuTilda
writeCompression off;           //Switch write compression on/off

timeFormat      general;        //Set time format
timePrecision   6;              //Set time precision

runTimeModifiable true;         //Switch run time modification of controlDict,
                                //fvSchemes, fvSolution on/off

// Define function for Mass Flow and Pressure Drop
functions
{
outMode timeStep;           //Define methode for output
outInt  50;                 //Set write interval
```

```
// Mass Flow Functions
    //Inlet Mass Flow
    fluxIn
    {
        enabled             true;
        log                 true;
        outputControlMode   $outMode;
        outputInterval      $outInt;
        type                swakExpression;
        valueType           patch;
        patchName           inlet00;
        verbose             true;
        autoInterpolate     false;
        warnAutoInterpolate true;
        expression          "phi";
        accumulations
        (
            sum
        );
    }

    //Outlet Mass flow
    fluxOut01
    {
        $fluxIn;
        patchName          outlet01;
    }

    fluxOut02
    {
        $fluxIn
        patchName          outlet02;
    }

    fluxOut03
    {
        $fluxIn;
        patchName          outlet03;
    }

    fluxOut04
    {
        $fluxIn;
        patchName          outlet04;
    }

    fluxOut05
    {
        $fluxIn;
        patchName          outlet05;
    }
```

```
// Pressure Functions - area averaged pressure at patch
    //Pressure at Inlet of distributor
    p_inlet00
    {
        enabled true;
        log true;
        outputControlMode   $outMode;
        outputInterval      $outInt;
        type                swakExpression;
        valueType           patch;
        patchName           inlet00;
        expression          "sum(p*area())/sum(area())";
        verbose             true;
        autoInterpolate     true;
        warnAutoInterpolate false;
        accumulations
        (
            average
            min
            max
        );
    }
    //Pressure at Inlet of first step
    p_inlet01
    {
        $p_inlet00;
        valueType           faceSet;
        setName             probeInlet01fSet;
    }
    //Pressure at Inlet of second step
    p_inlet02
    {
        $p_inlet00;
        valueType           faceSet;
        setName             probeInlet02fSet;
    }
    //Pressure at Inlet of third step
    p_inlet03
    {
        $p_inlet00;
        valueType           faceSet;
        setName             probeInlet03fSet;
    }

    //Pressure Difference between Inlet and Outlet (any outlet because pout = 0)

    dp_in00-out01
    {
        $p_inlet00;
        patchName           inlet00;
        variables           ("p2{patch'outlet01}=sum(p*area())/sum(area());");
        expression          "sum(p*area())/sum(area()) - p2";
    }
}

// ************************************************************************* //
```

Appendix G MATLAB Routines

G.1 Fibre Distribution

The structure of the routine for the analysis of the fibre distribution is shown in Figure G-1.

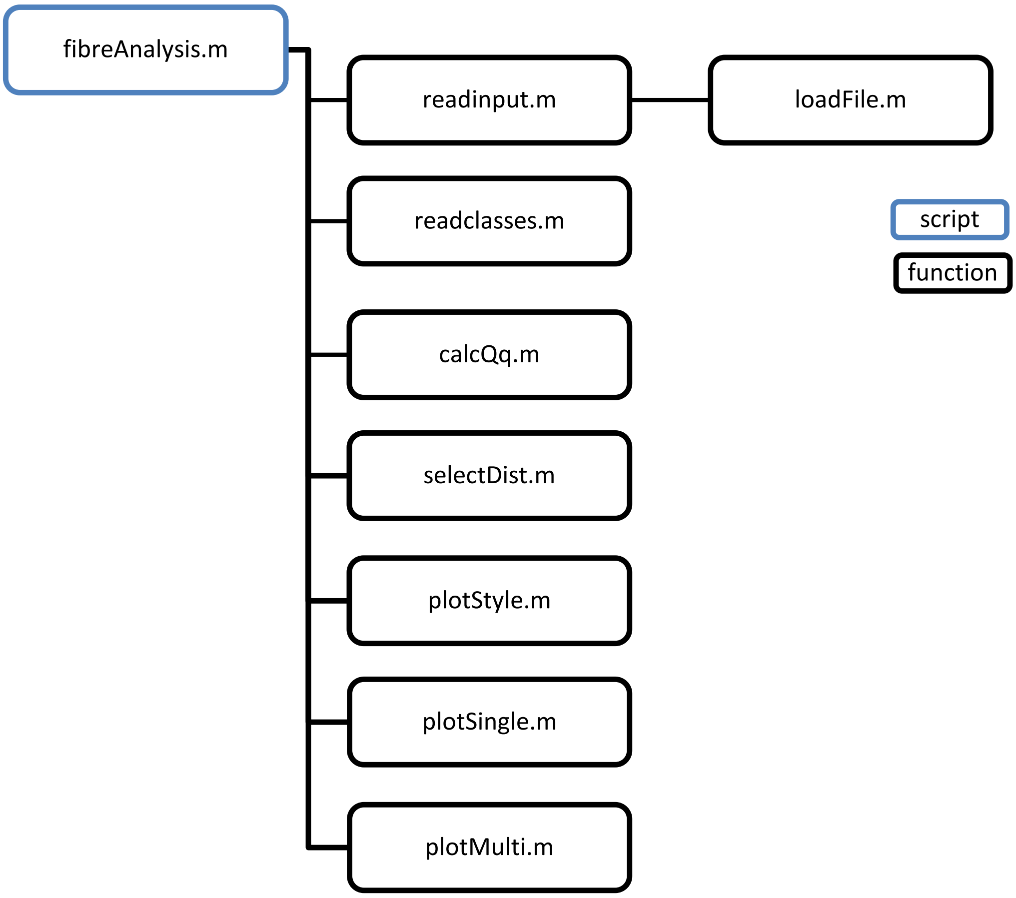

Figure G-1: Structure of the analysis routine for the fibre distribution.

G.2 Blockage Evaluation

This routine creates the regime maps for the blockage of the outlet port

G.3 Pressure Evaluation

This script evaluates the measured geodesic height and calculates the pressure loss.

G.4 Mass Flow Evaluation

This script evaluates the mass flow rates based on the measurements in the experiment.

```matlab
%Matlab Skript: runME.m
%Main programm to tun fibre distribution analysis
%Name: Michael Essl
%Datum: 04.08.2017

clc; close all; clear all; fclose('all');

%% Set your current working path here for faster selection
defaultPath = 'G:
\Michael\100_MSc\7_experiments\1_FibreDistribution_Analysis\MatlabCode';

%% read data files
[raw_data,nCase,datFileName] = readinput(defaultPath);
clearvars textdata colheaders data                     %Delete unused variables

%% read classes from file or define classes
[xo, xm] = readclasses(defaultPath);

%% calculate distributions
[Q,q,fib_dlv,fibMinMax] = calcQq(raw_data,xo);
q(:) = q(:).*1000;                                 %scale q from [% um^-1] to [% mm^-
1]

%% select distribution to plot
[dist] = selectDist();
%dist = [1 2 4 0]; % set standard plot

% check selection
if sum(dist > 0) < 1; %nothing selected
    dist(1) = 4;
    disp('You selected no distribution to plot. Setting default on plot Q3')
end

%% plot cases
if nCase == 1
    [style] = plotStyle('single');
    [fig1] = plotSingle(q,Q,xo,style,dist);
else
    combCaseU = input('Do you want to combine the multiple cases to one case or plot
them seperately? C/S [C]: ', 's');
    if isempty(combCaseU) || isnumeric(combCaseU),
        combCase = 'C';  %set default value to 'combine'
    else
        combCase = upper(combCaseU(1));
    end

    % switch procedure according to user input combCaseU
    switch combCase
        case {'C','K'}
            [style] = plotStyle('single');
            [fig1] = plotSingle(q,Q,xo,style,dist);

        case {'S'}
            [style] = plotStyle('multi');
            [fig1] = plotMulti(q,Q,xo,style,dist);

        otherwise
            error('Wrong input. Please use only C ombine or S eperate');
    end
end
```

```matlab
%Matlab Function: readinput.m
%select, load and combine input data files
%Name: Michael Essl
%Datum: 04.08.2017

function [raw_data,n_c,datFileName] = readinput(defaultPath)
% defaultPath = set default path for input data files
% raw_data = cell array of data read from the input file(s)
% n_c = number of processed files

% 1) select file where data of fibres are stored
% 2) the programm recognices how many files were select, if more than one
% file was selected there are two options
% 2a) calculate one distribution for all files (summing up and thus averaging)
% 2b) calculate a distribution for every input file

if nargin < 1
    defaultPath = pwd;
    disp(['defaultPath set to ',defaultPath]);
end

%% load input data from files
% open user interface for selection of data files (multiple selections possible)
[datFileName, datPathName, datFidx] = uigetfile({'*.txt;*.dat;*.mat;', 'Data Files
(*.txt,*.dat,*.mat)';...
   '*.*',  'All Files (*.*)'},'Select your Input Data files. (multiple selction
possible)',defaultPath,'MultiSelect','on');

%initialice the output data variable
raw_data = [];
%% check what the user selected and process input accordingly
if isequal(datFileName,0) || datFidx == 0  %nothing selected
   error('No file selected or user selected Cancel')

elseif ~iscell(datFileName) %one file selected (Char Array)
    n_c = 1;
    path2case = fullfile(datPathName, datFileName);
    disp(['Selected Case: ', path2case])
    %Import Datafile
    [ImpDat]=loadFile(path2case);
    raw_data{1} = ImpDat.data;

elseif iscell(datFileName) %more files selected (Cell Array)
    % number of columns of datFileName (is converted to a cell array if more than
one file was selected)
    n_c = size(datFileName,2);
    raw_data = cell(1,n_c);

    for k = 1:n_c
        path2case = fullfile(datPathName, datFileName{k});
        [ImpDat] = loadFile(path2case);
        raw_data{k} = ImpDat.data;
        disp(['selected Case: ', path2case])
        clear ImpDat data textdata colheaders n2d_c;
    end
else
    error('Problem with file import');
end
```

```matlab
%Matlab Funktion: loadFile.m
%select, load and combine input data files
%Name: Michael Essl
%Datum: 10.04.2017

function [ImpDat]=loadFile(fileToRead)
%function [ImpDat,deli,headLin]=loadFile(fileToRead)
% fileToRead = the full full path and filename pointing to the data file.
% data = contains the data, in this case should be an Array of [n,6] values
% headerlines = contains a cell array with die header of each column

%% correct decimal point (, -> .)
% First a safety copy which is renamed to  '_bkp' is created
% Next all ',' are changed to '.', which is the correct decimal Seperator fo
Matlab

% define file name of safety copy
bkpFileName = strrep(fileToRead,'.txt','_bkp.txt');

% check if backup file already exists, if not copy the original
if fopen(bkpFileName) < 0 % fopen returns -1 if the file doesn't exist
    copyfile(fileToRead, bkpFileName); %copy(source destination), in full pathes
end

% replace all ',' in the original file with '.'
file    = memmapfile(fileToRead,'Writable',true);
comma   = uint8(',');
point   = uint8('.');
file.Data(( file.Data==comma)' ) = point;


%% Import Data
% load data
ImpDat = importdata(fileToRead);

% Create new variables in the base workspace from those fields.
vars = fieldnames(ImpDat);
for i = 1:length(vars)
    assignin('base', vars{i}, ImpDat.(vars{i}));
end

end
```

```matlab
%Matlab Function: readclasses.m
%select, load and combine file for fibre classes
%Name: Michael Essl
%Datum: 04.08.2017

function [classes, xm] = readclasses(defaultPath)
% defaultPath = set default path for input classes files
% classes = two dimensional array of data read from the input file
% xm = number of processes files

% 1) select file where classes of fibres are defined
% 2) read file and sort assending if necessary

%% load classes from files
% open user interface for selection of file (single selection only)
[classFileName, classPathName, datFidx] = uigetfile({'*.txt;*.dat;*.mat;', 'Data Files
(*.txt,*.dat,*.mat)';...
   '*.*',  'All Files (*.*)'},'Select the file for class definition. (single selctio
only)',defaultPath,'MultiSelect','off');

%% check what the user selected and process input accordingly
if isempty(classFileName) == true || datFidx == 0 %nothing selected
   error('No file selected or user selected Cancel')
end

path2class = fullfile(classPathName, classFileName);
disp(['Selected file for classes: ', path2class])

%% Import Datafile
ImpClass = importdata(path2class);
% [ImpClass,delimiter,headLin] = importdata(fileToRead);
% HEADERLINES = 3; DELIMITER = ' '; Use '\t' for tab.
%ImpClass = importdata(fileToRead, DELIMITER, HEADERLINES);

% Create new variables in the base workspace from those fields.
vars = fieldnames(ImpClass);
for i = 1:length(vars)
    assignin('base', vars{i}, ImpClass.(vars{i}));
end

%% rearrange data for output
classes = ImpClass.data(:,2);

%% sort output data if necessary
if ~isvector(classes) || any(classes < 0), error('Classes must be a vector with
positive numbers');end
if ~issorted(classes), classes = sort(classes); disp('Classes are reordered by
ascendig value.'); end

%% calculate xm
xm = (classes(2:end) + classes(1:end-1))./2;
end
```

```matlab
%Matlab Function: calcq3Q3.m
%calculate distributions (Q0 Q1length Q1diameter Q3) from fibre tester data
%Name: Michael Essl
%Datum: 04.08.2017

function [Q,q,fib_dlv,fibMinMax] = calcQq(raw_data,classes)
% raw_data = imported data from file
% classes = vector with fibre classes (length)
% q3 = data for probability density distribution
% Q3 = data for cumulative distribution
% fib_dlv = cell array, where every cell contains the Matrix with the data
% diameter, length volume.

% 1) specify columns of diameter and length in the raw data file
% 2) make smaller matrix with only diameter and lenght and calculate Volume
%     (assume fibres as zylinders)
% 3) calculate total volume of fibres for every classes

%% check input parameters
if nargin < 1 || isempty(raw_data), error('Please check your input in function
calcq3Q3. No data input for '); end
if nargin < 2 || isempty(classes), error('Please check your input in function
calcq3Q3. No fibre classes submitted.'); end

%% check that classes are properly defined, reorder if necessary
if ~isvector(classes) || sum(classes < 0) > 0, error('Classes must be a vector with
positive numbers');end
if ~issorted(classes), classes = sort(classes); disp('Classes are reordered by
ascendig value.'); end

%% extract fibre length and width
% ask user which column is the length column (default = 2)
colLengthU = input('In which columne are the length? 1,2,3,.. [2]');
if isempty(colLengthU),     % Set default to columne 2
    colLength = 2 ;
    disp('Column for diamters set to default [2].');
elseif isnumeric(colLengthU) && colLengthU <= size(raw_data,2),% check if number
is entered
    colLength = colLengthU ;
else
    error('Input is not a number or larger than raw data matrix');
end

% ask user which column is the diameter column (default = 3)
colDiameterU = input('In which columne are the diamerters? 1,2,3,.. [3]');
if isempty(colDiameterU),      % Set default to columne 3
    colDiameter = 3;
    disp('Column for diamters set to default [3].');
elseif isnumeric(colDiameterU) && colDiameterU <= size(raw_data,2),% check if
number is entered
    colDiameter = colDiameterU ;
else
    error('Input is not a number or larger than raw data matrix');
end

%% Initialize variables for loops
nCase = numel(raw_data);        % number of imported cases
nclasses = length(classes)-1;   % number of fiber classes
QL = nan(nclasses,4,nCase);      % Matrix with dimension 1)classes 2)distribution
Q0-Q3 3)cases
fib_dlv = cell(1,nCase);        % cell array containing the diamter length & volume
fibMinMax = nan(nCase,2);       % min / max fibre length 1.column = min, 2.column =
max

%% calculate sum of distribution (Q0 Q1 Q3) for every class
for k = 1:nCase %loop through cases
    % write raw_data from input into new cell array fib_dlv
    fib_dlv{k}(:,1) = raw_data{k}(:,colLength);
    fib_dlv{k}(:,2) = raw_data{k}(:,colDiameter);
    % calculate fiber volume: assumption fiber is a cylinder
    % V = diameter^2 * pi / 4 * Length
    fib_dlv{k}(:,3) = fib_dlv{k}(:,2).^2 .* pi ./ 4 .* fib_dlv{k}(:,1);
    % find min / max fibre length
    fibMinMax(1,k) = min(fib_dlv{k}(:,1));
    fibMinMax(2,k) = sum(fib_dlv{k}(:,1) < min(classes));
    fibMinMax(3,k) = max(fib_dlv{k}(:,1));
    fibMinMax(4,k) = sum(fib_dlv{k}(:,1) > max(classes));

    for j = 1:nclasses, %loop over all fibre classes
        L = fib_dlv{k}(:,1) > classes(j) & fib_dlv{k}(:,1) <= classes(j+1);%
temporary Logical Array for assigning values to classes
        QL(j,1,k) = sum(L);                    %sum for Q0 distribution
        QL(j,2,k) = sum(fib_dlv{k}(L,1));    %sum for Q1(length) distribution
        QL(j,3,k) = sum(fib_dlv{k}(L,2));    %sum for Q1(diameter) distribution
        QL(j,4,k) = sum(fib_dlv{k}(L,3));    %sum for Q3 distribuion
        clearvars L
    end

    %% check if fibres are larger/smaller than classes
    if any(fibMinMax(:,1) < min(classes))
        disp([num2str(fibMinMax(2,k)),' fibres in case ',num2str(k),' are shorter
than the lowest class you defined. These fibres are excluded from analysis'])
    end

    if any(fibMinMax(:,2) > max(classes))
        disp([num2str(fibMinMax(4,k)),' fibres in case ',num2str(k),' are longer
than the highest class you defined. These fibres are excluded from analysis'])
    end

end

%% calculate total sum(Q0 Q1 Q3), fraction dQ(xm), class width dx,
%  and probability density function and cumulative density function

sumQ = sum(QL,1);
dx = diff(classes);

% fraction
dQ = QL./repmat(sumQ,[nclasses,1,1]);

% contains all distribution q0 q1 q3, not just q3.
q = dQ./repmat(dx(:),[1,size(dQ,2),size(dQ,3)]);

% contains all distribution Q0 Q1 Q3, not just Q3.
Q = cumsum(dQ,1);
end
```

```matlab
%Matlab Function: selectDist.m
%ask user which distributions to plot, multiple choice possible
%Name: Michael Essl
%Datum: 04.08.2017

function [dist] = selectDist()
% dist = row vector with order of distribution

% 1) ask user which distribution to process
% 2)

%% initialize variables
k = 1;
dist = [0 0 0 0];
nameDist = {'Q0','Q1','Q1','Q3'};

while k <= numel(dist)
%% Select distribution Typ
% ask user which distribution to plot 1=Q0 (number), 2=Q1(length), 3=Q1(diameter),
% 4=Q3 (volume) or q to quit selection
disttypU = input('Select distribution 1=Q0, 2=Q1(length), 3=Q1(diameter), 4=Q3 o
q=exit [4]: ','s');
if disttypU == 'q'; break; else disttypU = str2num(disttypU); end;
if isempty(disttypU),     % Set default to 4
    disttyp = 4 ;
elseif isnumeric(disttypU) && disttypU <= 4,% check if number is entered
    disttyp = round(disttypU);
else
    error('Input is not a number or not [1,2,3 or 4]');
end

%% set choise in variable dist and display choice
dist(k) = disttyp;
disp(['Distribution in plot',num2str(k),' set to ',nameDist{disttyp},'.']);

%% continue with loop
k = k + 1;
end

end
```

```matlab
%Matlab Function: plotStyle.m
%select and modify line and marker style for plots
%Name: Michael Essl
%Datum: 04.08.2017

function [style] = plotStyle(plotTyp)
% plotTyp = set style for plot Typ, single oder multi line plots

switch plotTyp
    case {'single','s'}
        style = {'-','--';...            % line style
                [0 0 1],[1 0 0];...      % line color
                'o','o',;...             % marker symbol
                 [0 0 1],[1 0 0]};       % marker face color


    case {'multi','m'}
        style = {'-','--','-','--','-','--','-','--','-';...
% line style
                 [0 0 1],[1 0 0],[0 0 0],[0 0 0],[0 0 0],[0 0 0],[0 0 0],[0 0 0],[0 0
0];...    % line color
                 'o','square','^','diamond','+','o','square','^','diamond';...
% marker symbol
                 [0 0 1],[0 0 1],[0 0 1],[0 0
1],'none','none','none','none','none';...        % marker face color q
                 [1 0 0],[1 0 0],[1 0 0],[1 0
0],'none','none','none','none','none';...        % marker face color Q
                 'outlet 1','outlet 2','outlet 3','outlet 4','outlet 5','outlet
6','outlet 7','outlet 8','outlet 9'}; %legend entries
    otherwise
        error('Wrong input for plot style typ');
end
end
```

```matlab
%Matlab Function: plotSingle.m
%calculate average and std from multiple cases
%plot distributions
%Name: Michael Essl
%Datum: 04.08.2017

function [fig1] = plotSingle(q,Q,xo,style,dist)
% q = probability density distribution for all cases
% Q = cumulative distribution for all cases
% 1) ask user if errorbars should be included
% 1a) calculate standard deviation
% 2) plot distribution:
%   left axis: probability density distribution,
%   right axis: cumulative distribution

%% check input parameters
if nargin < 1 || isempty(q), error('Please check your input in function plotSingle. No
data input for q'); end
if nargin < 2 || isempty(Q), error('Please check your input in function plotSingle. No
data input for Q.'); end
if nargin < 3 || isempty(xo), error('Please check your input in function plotSingle.
No data input for xm.'); end
if nargin < 4 || isempty(style), disp('Style set to standard.'); end
if nargin < 5 || isempty(dist), disp('Distribution set to standard'); dist = [4 0 0
0]; end

%% calculate the mean distribution for all cases
meanq = mean(q,3).*100;
meanQ = mean(Q,3).*100;

%% ask for error calculation if more than one cases is submitted
cErrU = input('Do you want to calculate and plot the mean and std error of the
selected cases? Y/N [Y]: ', 's');
if isempty(cErrU) || isnumeric(cErrU),
    cErr = 'Y';  %set default value to 'yes'
else
    cErr = upper(cErrU(1));
end

if cErr == 'Y';
    errq =  std(q,0,3).*100;
    errQ =  std(Q,0,3).*100;
    cErr = true;
else
    cErr = false;
end

%% prepare and define values for plotting
nDist = sum(dist > 0);      % amount of distributions
xo = xo./1000;              % convert xm from um to mm
xm = (xo(2:end) + xo(1:end-1))./2;% calculate mean of each class
axesOf = 0.05;             % define axes limit offset from min / max
styleTyp = [1 2];           % set style for plots
nameDist = {'q0 Q0' 'q1 Q1' 'q1 Q1' 'q3 Q3'};

%% create figure
fig1 = figure;

%% loop for all distributions
for n = 1:nDist;
```

```matlab
%create and format subplot
subPl(n) = subplot(nDist,1,n,'Parent',fig1);
hold(subPl(n),'on');
box(subPl(n),'off');

% format x - axis
set(subPl(n),'XMinorTick','on');
xlabel(subPl(n),'Fibre Length [mm]','FontName','Arial');
xlim([0 ceil(max(xo))]);

% plot q dist on left axis
yyaxis(subPl(n),'left');
if cErr;
    plq(n) = errorbar(xm,meanq(:,dist(n)),errq(:,dist(n)),...
        'lineStyle',style{1,styleTyp(1)},...
        'Color',style{2,styleTyp(1)},...
        'Marker',style{3,styleTyp(1)},...
        'MarkerFaceColor',style{4,styleTyp(1)},...
        'MarkerEdgeColor',[0 0 0],...
        'MarkerSize',6);
else
    plq(n) = plot(xm,meanq(:,dist(n)),'Parent',subPl(n),...
        'lineStyle',style{1,styleTyp(1)},...
        'Color',style{2,styleTyp(1)},...
        'Marker',style{3,styleTyp(1)},...
        'MarkerFaceColor',style{4,styleTyp(1)},...
        'MarkerEdgeColor',[0 0 0],...
        'MarkerSize',6);
end
ylim([0 round(max(meanq(:,dist(n),:)).*(1+axesOf))]);
ylabel('Probability Density [% mm^{-1}]','FontName','Arial');
set(subPl(n),'YColor',style{2,styleTyp(1)},'YDir','normal','YMinorTick','on');

% set subplot properties
title(subPl(n),['Fibre Distribution ',nameDist{dist(n)}],...
      'FontName','Arial','Position',[0 max(ylim)*(1+axesOf)],...
      'HorizontalAlignment','left');

% plot Q dist on right axis
yyaxis(subPl(n),'right');
if cErr;
    plQ(n) = errorbar(xo(2:end),meanQ(:,dist(n)),errQ(:,dist(n)),...
        'lineStyle',style{1,styleTyp(2)},...
        'Color',style{2,styleTyp(2)},...
        'Marker',style{3,styleTyp(2)},...
        'MarkerFaceColor',style{4,styleTyp(2)},...
        'MarkerEdgeColor',[0 0 0],...
        'MarkerSize',6);
else
    plQ(n) = plot(xo(2:end),meanQ(:,dist(n)),'Parent',subPl(n),...
        'lineStyle',style{1,styleTyp(2)},...
        'Color',style{2,styleTyp(2)},...
        'Marker',style{3,styleTyp(2)},...
        'MarkerFaceColor',style{4,styleTyp(2)},...
        'MarkerEdgeColor',[0 0 0],...
        'MarkerSize',6);
end
ylim([0 101]);
ylabel('Cumulative [%]','FontName','Arial');
set(subPl(n),'YColor',style{2,styleTyp(2)},'YDir','normal',...
```

```
        'YMinorTick','on','YTick',[0 10 20 30 40 50 60 70 80 90 100]);
end

x0=0.1;
y0=0.1;
width=16;
height=nDist*12;
set(gcf,'units','centimeter','position',[x0,y0,width,height]);
end
```

```
%Matlab Function: plotSingle.m
%calculate distributions (Q0 Q1length Q1diameter Q3) from fibre tester data
%Name: Michael Essl
%Datum: 04.08.2017

function [fig1] = plotMulti(q,Q,xo,style,dist)
% q = probability density distribution for all cases
% Q = cumulative distribution for all cases
% 1) ask user to import reference plot
% 2) import data
% 2) plot reference data
% 3)plot distributions and cases:
%   left axis: probability density distribution,
%   right axis: cumulative distribution

%% check input parameters
if nargin < 1 || isempty(q), error('Please check your input in function plotSingle. No
data input for q'); end
if nargin < 2 || isempty(Q), error('Please check your input in function plotSingle. No
data input for Q.'); end
if nargin < 3 || isempty(xo), error('Please check your input in function plotSingle
No data input for xm.'); end
if nargin < 4 || isempty(style), disp('Style set to standard.'); end
if nargin < 5 || isempty(dist), disp('Distribution set to standard'); dist = [4 0 0
0]; end

%% scale q Q to %
q = q.*100;
Q = Q.*100;

%% ask for user if a referenze distribution should be loaded
refDiU = input('Load referenz distribution? Y/N [Y]: ', 's');
if isempty(refDiU) || isnumeric(refDiU),
    refDi = 'Y';  %set default value to 'no'
else
    refDi = upper(refDiU(1));
end

if refDi == 'Y';
    %select file
    [datFileName, ~, datFidx] = uigetfile({'*.mat;', 'Data Files (*.mat)';...
        '*.*',  'All Files (*.*)'},'Select your Input Data files. (single selction)',
pwd,'MultiSelect','off');

    % check selection and process input accordingly
    if isequal(datFileName,0) || datFidx == 0 %nothing selected
        disp('No file selected or user selected Cancel')
        refDi = false;
    else

        % Import the file
        newData1 = load('-mat', datFileName);

        % Create new variables in the base workspace from those fields.
        vars = fieldnames(newData1);
        refDist = newData1.(vars{1});
        clearvars newData1 vars datFileName datFidx refDi refDiU
        refDi = true;
    end
else
```

```matlab
    refDi = false;
end

%% prepare and define values for plotting
nDist = sum(dist > 0);    % amount of distributions
kCase = size(Q,3);        % amount of cases to plot
xo = xo./1000;            % convert xm from um to mm
xm = (xo(2:end) + xo(1:end-1))./2; % calculate mean of each class
axesOf = 0.05;            % define axes limit offset from min / max
styleTyp = [1 2];         % set style for plots
nameDist = {'q0 Q0' 'q1 Q1' 'q1 Q1' 'q3 Q3'};

%% create figure
fig1 = figure;

%% loop for all distributions
for n = 1:nDist;

    %create and format subplot
    subPl(n) = subplot(nDist,1,n,'Parent',fig1);
    hold(subPl(n),'on');
    box(subPl(n),'off');

    %% format x - axis
    set(subPl(n),'XMinorTick','on');
    xlabel(subPl(n),'Fibre Length [mm]','FontName','Arial');
    xlim([0 ceil(max(xo))]);

    %% plot referenze distribution if chosen by user
    if refDi;
        yyaxis(subPl(n),'left');
        plqr = errorbar(xm,refDist(:,dist(n),1),refDist(:,dist(n),2),...
            'lineStyle','-',...
            'lineWidth',1,...
            'Color',[0 0 0],...
            'Marker','o',...
            'MarkerFaceColor',[0 0 0],...
            'MarkerEdgeColor',[0 0 0],...
            'MarkerSize',7);

        %% set subplot title and legend
        title(subPl(n),['Fibre Distribution ',nameDist{dist(n)}],...
            'FontName','Arial','Position',[0 max(ylim)*(1+axesOf)],...
            'HorizontalAlignment','left');

        yyaxis(subPl(n),'right');
        plQr = errorbar(xo(2:end),refDist(:,dist(n),3),refDist(:,dist(n),4),...
            'lineStyle','--',...
            'lineWidth',1,...
            'Color',[0 0 0],...
            'Marker','o',...
            'MarkerFaceColor',[0 0 0],...
            'MarkerEdgeColor',[0 0 0],...
            'MarkerSize',7);

    end

    %% loop for all cases
    for k = 1:kCase;
        % plot q dist on left axis
        yyaxis(subPl(n),'left');
        plq(n,k) = plot(xm,q(:,dist(n),k),'Parent',subPl(n),...
            'lineStyle',style{1,styleTyp(1)},...
            'Color',style{2,styleTyp(1)},...
            'Marker',style{3,k},...
            'MarkerFaceColor',style{4,k},...
            'MarkerEdgeColor',style{4,styleTyp(1)},...
            'MarkerSize',6);
        ylim([0 round(max(max(q(:,dist(n),:))).*(1+axesOf))]);
        ylim([0 110]);
        ylabel('Probability Density [% mm^{-1}]','FontName','Arial');
        set(subPl(n),'YColor',style{2,styleTyp(1)},'YDir','normal','YMinorTick','on');

        % set subplot properties
        title(subPl(n),['Fibre Distribution ',nameDist{dist(n)}],...
            'FontName','Arial','Position',[0 max(ylim)*(1+axesOf)],...
            'HorizontalAlignment','left');

        % plot Q dist on right axis
        yyaxis(subPl(n),'right');
        plQ(n,k) = plot(xo(2:end),Q(:,dist(n),k),'Parent',subPl(n),...
            'lineStyle',style{1,styleTyp(2)},...
            'Color',style{2,styleTyp(2)},...
            'Marker',style{3,k},...
            'MarkerFaceColor',style{5,k},...
            'MarkerEdgeColor',style{5,styleTyp(2)},...
            'MarkerSize',6);

        ylim([0 101]);
        ylabel('Cumulative [%]','FontName','Arial');
        set(subPl(n),'YColor',style{2,styleTyp(2)},'YDir','normal',...
            'YMinorTick','on','YTick',[0 10 20 30 40 50 60 70 80 90 100]);
    end

    %% create legend
    ah1 = gca; % Axes handle 1 (this is the visible axes)
    legend1 = legend(ah1,[plQr,plQ(n,:)],'reference',style{6,1:kCase}); % Legend at
axes 1
    legend('boxoff')
    set(legend1,...
        'Position',[0.7 0.32 0.15 0.38],...
        'FontName','Arial',...
        'Orientation','vertical');

    ah2=axes('position',get(gca,'position'), 'visible','off');  % Axes handle 2
(unvisible, only for place the second legend)
    legend2 = legend(ah2,[plqr,plq(n,:)],'','','','','','','','','','','','');  %
Legend at axes 2
    legend('boxoff')
    set(legend2,...
        'Position',[0.61 0.32 0.15 0.38],...
        'FontName','Arial',...
        'Orientation','vertical');

    % plot rectangle for legend
    annotation(fig1,'rectangle',...
        [0.63 0.32 0.22 0.38]);
end
```

```matlab
%% set plot size
x0=0.1;
y0=0.1;
width=16;
height=nDist*12;
set(gcf,'units','centimeter','position',[x0,y0,width,height]);

%% set output directory and write file
outputDir = uigetdir(pwd,'Please select a output directory');
alphabet = 'abcdefghijklmnopqrstuvwxyz';
print(fig1,[outputDir,'\',alphabet(randi(26,1,3)),'_nCases_',num2str(kCase)],'-dpng');
end
```

```matlab
%Matlab Skript: blockageAnalysis.m
%Plot diagramms based on data of outlet port blockage
%Name: Michael Essl
%Datum: 04.08.2017

% Clear workspace and console
clear all;
close all;
clc;

%%ImportData

%% Initialize variables.
filename{1} = 'G:\Michael\100_MSc\7_experiments\2_Blockage_Analysis\BlockageV1↙
txt';
filename{2} = 'G:\Michael\100_MSc\7_experiments\2_Blockage_Analysis\BlockageV2↙
txt';
filename{3} = 'G:\Michael\100_MSc\7_experiments\2_Blockage_Analysis\BlockageV3↙
txt';
delimiter = '\t';
startRow = 3;

%% Read columns of data as strings:
% For more information, see the TEXTSCAN documentation.
formatSpec = '%s%s%s%[^\n\r]';

for k = 1:length(filename)
%% Open the text file.
fileID = fopen(filename{k},'r');

%% Read columns of data according to format string.
% This section is Auto-generated by MATLAB R2016a on 08.04.2017
% This call is based on the structure of the file used to generate this
% code. If an error occurs for a different file, try regenerating the code
% from the Import Tool.
dataArray = textscan(fileID, formatSpec, 'Delimiter', delimiter, 'HeaderLines' ,↙
startRow-1, 'ReturnOnError', false);

% Close the text file.
fclose(fileID);

%% Convert the contents of columns containing numeric strings to numbers.
% This section is Auto-generated by MATLAB R2016a on 08.04.2017
% Replace non-numeric strings with NaN.
raw = repmat({''},length(dataArray{1}),length(dataArray)-1);
for col=1:length(dataArray)-1
    raw(1:length(dataArray{col}),col) = dataArray{col};
end
numericData = NaN(size(dataArray{1},1),size(dataArray,2));

for col=[1,2,3]
    % Converts strings in the input cell array to numbers. Replaced non-numeric
    % strings with NaN.
    rawData = dataArray{col};
    for row=1:size(rawData, 1);
        % Create a regular expression to detect and remove non-numeric prefixes and
        % suffixes.
```

```
        regexstr = '(?<prefix>.*?)(?<numbers>([-]*(\d+[\,]*)+[\.]{0,1}\d*[eEdD]↙
{0,1}[-+]*\d*[i]{0,1})|([-]*(\d+[\,]*)*[\.]{1,1}\d+[eEdD]{0,1}[-+]*\d*[i]{0,1}))(↙
<suffix>.*)';
        try
            result = regexp(rawData{row}, regexstr, 'names');
            numbers = result.numbers;

            % Detected commas in non-thousand locations.
            invalidThousandsSeparator = false;
            if any(numbers==',');
                thousandsRegExp = '^\d+?(\,\d{3})*\.{0,1}\d*$';
                if isempty(regexp(numbers, thousandsRegExp, 'once'));
                    numbers = NaN;
                    invalidThousandsSeparator = true;
                end
            end
            % Convert numeric strings to numbers.
            if ~invalidThousandsSeparator;
                numbers = textscan(strrep(numbers, ',', ''), '%f');
                numericData(row, col) = numbers{1};
                raw{row, col} = numbers{1};
            end
        catch me
        end
    end
end

%% Allocate imported array to column variable names
a(:,k) = cell2mat(raw(:, 1));
b(:,k) = cell2mat(raw(:, 2));
c(:,k) = logical(cell2mat(raw(:, 3)));

end %end for loop




%% plot results

% Create figure
fig1 = figure;

Alphabet = 'abcdefghijklmnopqrstuvwxyzäöüß';

for n = 1:length(filename);
% Create axes
%sub(n) = axes('Parent',fig1,'Position',[0.13 0.1575 0.775 0.7675]);
%hold(sub(n),'on');

% Create first subplot
sub(n) = subplot(2,2,n);
plot(a(c(:,n),n),b(c(:,n),n),'DisplayName','blockage','MarkerFaceColor',[0 0 0],...
    'MarkerSize',8,...
    'Marker','o',...
    'LineWidth',1,...
    'LineStyle','none',...
    'Color',[0 0 0]);
```

```
hold on;

% Create plot
plot(a(~c(:,n),n),b(~c(:,n),n),'DisplayName','no blockage','MarkerFaceColor',[1 1↙
1],...
    'MarkerSize',8,...
    'Marker','o',...
    'LineWidth',1,...
    'LineStyle','none',...
    'Color',[0 0 0]);

% Create xlabel and ylabel
xlabel('Fibre Concentration [kg_{fibre} / kg_{total}]');
ylabel('Reynolds Number (Outlet)');

% Create title
title([Alphabet(n),')'],...
    'HorizontalAlignment','left',...
    'Position',[1 4300],...
    'FontSize',14);

% Set X-limits and Y-limits of the axes
xlim(sub(n),[0.8 4.2]);
ylim(sub(n),[100 4000]);

box(sub(n),'on');
% Set the X-axes Ticks and TickLabels
set(sub(n),'XTick',[1 2 3 4],'XTickLabel',{'0.01%','0.05%','0.1%','0.5%'});

end %end plot loop

% Create legend
legend1 = legend(sub(1),'show');
set(legend1,...
    'Position',[0.5703 0.3962 0.15 0.05],...
    'Orientation','vertical');

%Set size of plot
x0=0.10;
y0=0.10;
width=16;
height=17.1;
set(gcf,'units','centimeter','position',[x0,y0,width,height]);
%{
saveas(gcf,['blockage_graph_',num2str(geover),'.jpg']);
%}
```

```matlab
%Matlab Skript: evalPressure.m
%Load measured data and plot them into diagramms
%Name: Michael Essl
%Datum: 04.08.2017

% Clear workspace and Console
clear all;
close all;
clc;

%% Import mass flow data for flow rate.
filename = cell(4,3);
filename{1} = 'G:\Michael\100_MSc\7_experiments\4_Pressure_Analysis\pV1c00.txt';
filename{2} = 'G:\Michael\100_MSc\7_experiments\4_Pressure_Analysis\pV1c001.txt';
filename{3} = 'G:\Michael\100_MSc\7_experiments\4_Pressure_Analysis\pV1c005.txt';
filename{4} = 'G:\Michael\100_MSc\7_experiments\4_Pressure_Analysis\pV1c01.txt';
filename{5} = 'G:\Michael\100_MSc\7_experiments\4_Pressure_Analysis\pV2c00.txt';
filename{6} = 'G:\Michael\100_MSc\7_experiments\4_Pressure_Analysis\pV2c001.txt';
filename{7} = 'G:\Michael\100_MSc\7_experiments\4_Pressure_Analysis\pV2c005.txt';
filename{8} = 'G:\Michael\100_MSc\7_experiments\4_Pressure_Analysis\pV2c01.txt';
filename{9} = 'G:\Michael\100_MSc\7_experiments\4_Pressure_Analysis\pV3c00.txt';
filename{10} = 'G:\Michael\100_MSc\7_experiments\4_Pressure_Analysis\pV3c001.txt';
filename{11} = 'G:\Michael\100_MSc\7_experiments\4_Pressure_Analysis\pV3c005.txt';
filename{12} = 'G:\Michael\100_MSc\7_experiments\4_Pressure_Analysis\pV3c01.txt';

% Import files
startRow = 2;
endRow = 8;
P = cell(size(filename));
rho = 1000;     % [kg/m³]
grav = 9.81;    % [m/s²]
for geo = 1:size(filename,2) % Loop over geometries
    for con = 1:size(filename,1) % Loop over concentration
        P{con,geo} = importPressure(filename{con,geo}, startRow, endRow);
        %P{con,geo} = rho.*grav.*H{con,geo}./1000;
        P{con,geo}(:,2:3) = rho.*grav.*P{con,geo}(:,2:3)./1000;
    end
end

% Delete import variables
clearvars filename geo con startRow endRow

%% Plot Data
% Create figure
fig1 = figure;

% Define styles for plot, 1.row Marker Form, 2.row Marker Fill, all other
% styles are uniform
style = {[0 0 0],[0 0 0],[0 0 0],[0 0 0],[0 0 0],[0 0 0],[0 0 0],[0 0 0];..
    'o','square','^','diamond','o','square','^','diamond';...
    [0 0 0],[0 0 0],[0 0 0],[0 0 0],'none','none','none','none';...
    6,6,6,6,6,6,6,6};

%% Plot relative mass flow rate deviation
% Loop plot for all geometries
n = 0; %Plot counter
for geo = 1:size(P,2)
    % create subplot
    subPl(geo) = subplot(2,2,geo);
    % hold on
    hold(subPl(geo),'on');
    for con = 1:size(P,1)
        n = n + 1;
        % Plot pressure in storage tank
        plHg(n) = plot(P{con,geo}(:,1),P{con,geo}(:,2),'Parent',subPl(geo),...
            'Color',style{1,con},...
            'Marker',style{2,con},...
            'MarkerFaceColor',style{3,con},...
            'MarkerEdgeColor',[0 0 0],...
            'MarkerSize',style{4,con});

        % Plot pressure in distributor
        plHin(n) = plot(P{con,geo}(:,1),P{con,geo}(:,3),'Parent',subPl(geo),...
            'Color',style{1,4+con},...
            'Marker',style{2,4+con},...
            'MarkerFaceColor',style{3,4+con},...
            'MarkerEdgeColor',[0 0 0],...
            'MarkerSize',style{4,4+con});
    end
    % Set axes limits and properties
    xlim(subPl(geo),[200 3800]);
    ylim(subPl(geo),[0 10000]);
    set(subPl(geo),'XMinorTick','on','YMinorTick','on');
    % Print Box
    box(subPl(geo),'off');
    % hold off
    hold(subPl(geo),'off');
    % Set axes labels
    title(subPl(geo),['\bf Geometry G', num2str
(geo)],'FontName','Arial','FontSize',11);
    xlabel(subPl(geo),'Reynolds Number (Outlet)','FontName','Arial');
    ylabel(subPl(geo),'Pressure [Pa]','FontName','Arial');
end

%% create legend
ah1 = gca; % Axes handle 1 (this is the visible axes)
legend1 = legend(ah1,plHg(1:4),'C = 0%','C = 0.01%','C = 0.05%','C = 0.1%'); %
Legend at axes 1
legend('boxon')
title(legend1,{'storage','tank'})
set(legend1,...
    'Position',[0.56 0.23 0.14 0.22],...
    'FontName','Arial',...
    'Orientation','vertical');

ah2=axes('position',get(gca,'position'), 'visible','off');  % Axes handle 2
(unvisible, only for place the second legend)
legend2 = legend(ah2,plHin(1:4),'C = 0%','C = 0.01%','C = 0.05%','C = 0.1%');  %
Legend at axes 2
legend('boxon')
title(legend2,{'inlet','manifold'})
set(legend2,...
    'Position',[0.75 0.23 0.14 0.22],...
    'FontName','Arial',...
    'Orientation','vertical');
```

```
%Set size of plot
x0=0.1; y0=0.1;
width=20; height=20;
set(gcf,'units','centimeter','position',[x0,y0,width,height]);
```

```
%Matlab Skript: evalMassFlowExpCompare.m
%Load, Average and Compare Mass Flow Data
%Name: Michael Essl
%Datum: 04.08.2017

% Clear workspace and Console
clear all;
close all;
clc;

%% specify text file
filename{1} = 'G:\Michael\100_MSc\7_experiments\3_Massflow_Analysis\V1_Re1000.txt';
filename{2} = 'G:\Michael\100_MSc\7_experiments\3_Massflow_Analysis\V2_Re1000.txt';
filename{3} = 'G:\Michael\100_MSc\7_experiments\3_Massflow_Analysis\V3_Re1000.txt';
% filename{1} = 'G:\Michael\100_MSc\7_experiments\3_Massflow_Analysis\V1_Re1500.
txt';
% filename{2} = 'G:\Michael\100_MSc\7_experiments\3_Massflow_Analysis\V2_Re1500.
txt';
% filename{3} = 'G:\Michael\100_MSc\7_experiments\3_Massflow_Analysis\V3_Re1500.
txt';

%% Import data from text file.
% This section is Auto-generated by MATLAB R2016a on 04.08.2017
% Initialize variables.
delimiter = '\t';
startRow = 2;
nOutlet =5;
nFiles = length(filename);
% Read columns of data as strings:
% For more information, see the TEXTSCAN documentation.
formatSpec = '%s%s%s%s%s%s%[^\n\r]';

for k = 1:nFiles
% Open the text file.
fileID = fopen(filename{k},'r');

% Read columns of data according to format string.
% This call is based on the structure of the file used to generate this
% code. If an error occurs for a different file, try regenerating the code
% from the Import Tool.
dataArray = textscan(fileID, formatSpec, 'Delimiter', delimiter, 'HeaderLines' ,
startRow-1, 'ReturnOnError', false);

% Close the text file.
fclose(fileID);

% Convert the contents of columns containing numeric strings to numbers.
% Replace non-numeric strings with NaN.
raw = repmat({''},length(dataArray{1}),length(dataArray)-1);
for col=1:length(dataArray)-1
    raw(1:length(dataArray{col}),col) = dataArray{col};
end
numericData = NaN(size(dataArray{1},1),size(dataArray,2));

for col=[1,2,3,4,5]
    % Converts strings in the input cell array to numbers. Replaced non-numeric
    % strings with NaN.
    rawData = dataArray{col};
```

```
    for row=1:size(rawData, 1);
        % Create a regular expression to detect and remove non-numeric prefixes and
        % suffixes.
        regexstr = '(?<prefix>.*?)(?<numbers>([-]*(\d+[\,]*)+[\.]{0,1}\d*[eEdD]
{0,1}[-+]*\d*[i]{0,1})|([-]*(\d+[\,]*)*[\.]{1,1}\d+[eEdD]{0,1}[-+]*\d*[i]{0,1}))(
<suffix>.*)';
        try
            result = regexp(rawData{row}, regexstr,'names');
            numbers = result.numbers;

            % Detected commas in non-thousand locations.
            invalidThousandsSeparator = false;
            if any(numbers==',');
                thousandsRegExp = '^\d+?(\,\d{3})*\.{0,1}\d*$';
                if isempty(regexp(numbers, thousandsRegExp, 'once'));
                    numbers = NaN;
                    invalidThousandsSeparator = true;
                end
            end
            % Convert numeric strings to numbers.
            if ~invalidThousandsSeparator;
                numbers = textscan(strrep(numbers, ',', ''), '%f');
                numericData(row, col) = numbers{1};
                raw{row, col} = numbers{1};
            end
        catch me
        end
    end
end

% Create output variable
V1Rel{k} = cell2mat(raw);
% calculate mean mass flow rate
mMF{k} = repmat(mean(V1Rel{k},2),1,nOutlet);
relV1Rel{k} = (V1Rel{k}-mMF{k})./mMF{k}.*100;
% Clear temporary variables
clearvars fileID dataArray ans raw col numericData rawData row regexstr result
numbers invalidThousandsSeparator thousandsRegExp me;
end

% Clear import variables
clearvars filename delimiter startRow formatSpec k;

%% Create figure
fig1 = figure;

% Define styles for plot, 1.row Marker Form, 2.row Marker Fill, all other
% styles are uniform
style = {[0 0 0],[0 0 0],[0 0 0],[0 0 0],[0 0 0],[0 0 0],[0 0 0],[0 0 0];..
        'o','square','^','diamond','o','square','^','diamond';...
        [0 0 0],[0 0 0],[0 0 0],[0 0 0],'none','none','none','none'};
% Create y-axis data
y = [1:nOutlet];
n = 0;
%% Plot relative mass flow rate deviation
% Loop plot for all Re numbers for relative plot
for k = 1:nFiles
    % Determine number of concentrations
    nConc = size(relV1Rel{k},1);
    for j = 1:nConc
        n = n + 1;
        % create subplot
        subPl(n) = subplot(3,4,n);
        % Plot relative mass flow deviation
        pl(n) = plot(relV1Rel{k}(j,:),y,'Parent',subPl(n),...
                'Color',style{1,j},...
                'Marker',style{2,j},...
                'MarkerFaceColor',style{3,j},...
                'MarkerEdgeColor',[0 0 0],...
                'MarkerSize',6);
            hold(subPl(n),'on');
            % Set axes limits and properties
            xlim(subPl(n),[-30 30]);
            ylim([0.8 5.2]);
            set(subPl(n),'YTick',zeros(1,0),'XMinorTick','on');
            % Print Box
            box(subPl(n),'off');
            % Plot zero line
            l(n) = plot([0 0],[min(ylim) max(ylim)],'-.r');
            hold(subPl(n),'off');
    end
    set(subPl(n-3),'YTick',y);
    ylabel(subPl(n-3),{['Geometry G', num2str(k)],'-----------------','Outlet
Number'},'FontName','Arial');
end
% Set axes labels
xlabel(subPl(10),'Mass Flow Rate Deviation from Average [%]','FontName','Arial');

%% create legend
legend1 = legend([pl(1:4),l(1)],'C = 0%','C = 0.01%','C = 0.05%','C =
0.1%','zero');
set(legend1,...
    'Position',[0.11 0.0 0.77 0.03],...
    'FontName','Arial',...
    'Orientation','horizontal');

%Set size of plot
x0=0.1;
y0=0.1;
width=16;
height=16;
set(gcf,'units','centimeter','position',[x0,y0,width,height]);
```